ANL-6965



# Argonne National Laboratory

## REACTOR DEVELOPMENT PROGRAM

## PROGRESS REPORT

## October 1964

Printed in USA. Price $4.00 . Available from the Clearinghouse for Federal Scientific and Technical Information, National Bureau of Standards, U. S. Department of Commerce, Springfield, Virginia

ANL-6965
Reactor Technology
(TID-4500, 35th Ed.)
AEC Research and
Development Report



ARGONNE NATIONAL LABORATORY
9700 South Cass Avenue
Argonne, Illinois 60440

# REACTOR DEVELOPMENT PROGRAM PROGRESS REPORT

October 1964

Albert V. Crewe, Laboratory Director
Stephen Lawroski, Associate Laboratory Director

| Division | Director |
|---|---|
| Chemical Engineering | R. C. Vogel |
| Idaho | M. Novick |
| Metallurgy | F. G. Foote |
| Reactor Engineering | L. J. Koch |
| Reactor Physics | R. Avery |
| Remote Control | R. C. Goertz |

Report Coordinated by
R. M. Adams and A. Glassner

Issued November 15, 1964

Operated by The University of Chicago
under
Contract W-31-109-eng-38
with the
U. S. Atomic Energy Commission

## FOREWORD

The Reactor Development Program Progress Report, issued monthly, is intended to be a means of reporting those items of significant technical progress which have occurred in both the specific reactor projects and the general engineering research and development programs. The report is organized in a way which, it is hoped, gives the clearest, most logical over-all view of progress. The budget classification is followed only in broad outline, and no attempt is made to report separately on each sub-activity number. Further, since the intent is to report only items of significant progress, not all activities are reported each month. In order to issue this report as soon as possible after the end of the month editorial work must necessarily be limited. Also, since this is an informal progress report, the results and data presented should be understood to be preliminary and subject to change unless otherwise stated.

The issuance of these reports is not intended to constitute publication in any sense of the word. Final results either will be submitted for publication in regular professional journals or will be published in the form of ANL topical reports.

The last six reports issued
in this series are:

| | |
|---|---|
| April 1964 | ANL-6885 |
| May 1964 | ANL-6904 |
| June 1964 | ANL-6912 |
| July 1964 | ANL-6923 |
| August 1964 | ANL-6936 |
| September 1964 | ANL-6944 |

TABLE OF CONTENTS


| | | Page |
|---|---|---|
| 5. | Core Instrumentation | 40 |
| 6. | Fuel Slip-fit Experiment | 40 |
| 7. | Fuel Assembly Sodium Flow Test Loop | 40 |
| II. | General Reactor Technology | 42 |
| A. | Experimental Reactor and Nuclear Physics | 42 |
| 1. | Solid-state Neutron Spectrometer | 42 |
| 2. | Design of Excursion Alarm and Recorder | 44 |
| 3. | High-conversion Critical Experiment | 45 |
| B. | Theoretical Reactor Physics | 46 |
| 1. | Control Rod Evaluation | 46 |
| 2. | Resonance Interference | 47 |
| 3. | Total Neutron Cross Sections | 49 |
| 4. | ZPR-VII Data Analysis | 50 |
| 5. | Correction for Resolution Losses of Radiation-counting Equipment | 50 |
| 6. | An Analytical Method for Optimizing Reflector Located Control Vane Thickness | 55 |
| C. | High-temperature Materials Development | 56 |
| 1. | Ceramics | 56 |
| 2. | Corrosion by Liquid Metals | 59 |
| 3. | Thorium-base Fuels | 59 |
| D. | Other Reactor Fuels and Materials Development | 61 |
| 1. | Nondestructive Testing | 61 |
| 2. | Polarization Studies in Liquid Metal Environment | 63 |
| E. | Remote Control Engineering Development | 65 |
| 1. | Electric Master-Slave Manipulator Mark E4 | 65 |
| 2. | Studies of Higher Force Feedback | 66 |
| F. | Heat Engineering | 66 |
| 1. | Two-phase Flow Studies | 66 |
| 2. | Boiling Liquid Metal Technology | 67 |
| 3. | General Heat Transfer | 68 |
| 4. | ANL-AMU Program | 69 |

TABLE OF CONTENTS


| | Page |
|---|---|
| G. Chemical Separations | 74 |
| 1. Fluidization and Volatility Separation Processes | 74 |
| 2. General Chemistry and Chemical Engineering | 77 |
| 3. Chemical-Metallurgical Process Studies | 79 |
| 4. Calorimetry | 80 |
| H. Plutonium Recycle Program | 80 |
| 1. EBWR Plutonium Recycle Experiment | 80 |
| 2. Plutonium Recycle Vessel Surveillance | 80 |
| 3. Plutonium Recycle Fuel | 81 |
| 4. Plutonium Recycle Control Rods | 82 |
| 5. Nondestructive Tests of Components | 82 |
| 6. Physics Calculations | 82 |
| III. Advanced Systems Research and Development | 84 |
| A. Argonne Advanced Research Reactor (AARR) | 84 |
| 1. Core Physics | 84 |
| 2. Critical Experiment | 85 |
| 3. Heat Transfer | 86 |
| 4. Hydraulic Test Loop | 88 |
| B. Magnetohydrodynamics (MHD) | 89 |
| 1. MHD Power Generation - Jet Pump Studies | 89 |
| C. Regenerative Emf Cells | 89 |
| 1. Bimetallic Cells | 89 |
| IV. Nuclear Safety | 91 |
| A. Thermal Reactor Safety Studies | 91 |
| 1. Metal-Water Reactors | 91 |
| 2. Metal Oxidation-Ignition Studies | 94 |
| B. Fast Reactor Safety Studies | 94 |
| 1. Systematics of Pressure Pulse Phenomena | 94 |
| 2. Critical Constants of $UO_2$ | 96 |

TABLE OF CONTENTS


| | Page |
|---|---|
| C. TREAT | 97 |
| 1. Large TREAT Loop | 97 |
| V. Publications | 99 |

# I. LIQUID-METAL-COOLED REACTORS

## A. General Fast Reactor Physics

### 1. ZPR-III

Doppler experiments with Assembly 45 have continued (see Progress Report for September 1964, ANL-6944, pp. 13-15). Inasmuch as attempts to make measurements at 1200°K led to erratic and unreliable results, the upper temperature limit was reduced to 1100°K. This alleviated a problem of blackening of the radiation shield around the Doppler element and made possible better control of temperatures in both the element and adjacent core material over a long period of time.

A comparison was then made between the results for 1/2-in.- and 1-in.-diameter natural $UO_2$ elements at 500 and 1100°K. The elements had, insofar as possible, the same hardware, and were located at the same core position. The zone in which they were tested had the spectrum of a 5000-liter plutonium carbide reactor with the low energy components somewhat augmented by additional graphite. Under these conditions, an 11% decrease in Doppler coefficient was observed for the larger element. This difference is attributed to an increased self-shielding effect in the one-inch element.

### 2. ZPR-VI

a. Physical Parameters. Assembly No. 3 of ZPR-VI is a "pancake" core, i.e., the length-to-diameter (L/D) ratio is approximately one-third. The core composition, the same as that of Assembly No. 2, is given in Table I. The experimental critical mass was found to be 850 kg of $U^{235}$, the critical volume 950 liters, the critical height and diameter 50.8 cm and 155 cm, respectively.

Initially the dual-purpose (safety/control) rods[1] were loaded with five 0.159-cm-thick columns of enriched fuel to assure adequate reactivity control for safe operation. Measurements made after initial criticality showed that the number of fuel columns could safely be reduced to four. This was subsequently done to attain a more uniform distribution of core materials in the vicinity of the dual purpose rods. The rods were recalibrated. Dual-purpose rod No. 5 in the movable half was found to be worth 71.3 Ih and dual purpose rod No. 6 (opposite DP rod No. 1) in the stationary half was found to be worth 77.8 Ih. Calculations showed 451 Ih to be equivalent to 1% $\Delta k/k$.

b. Dependence of Sodium Void Coefficient on Material Arrangement. Measurements of sodium void coefficients were made for various material arrangements within the core drawers. A typical stationary half-drawer loading is shown in Figure 1. The movable half-drawer loading is a mirror

[1] Reactor Development Program Progress Report, ANL-6944 (Sept 1964), p. 16.

image of Figure 1. The measurements were made within a 30-cm diameter region centered at the axial center of the core. The data obtained are being processed.

Table I. Core and Blanket Compositions in ZPR-VI Assembly No. 3

| | Core | | | Blanket | | |
|---|---|---|---|---|---|---|
| | Atom Density, atom/cm$^3$ x $10^{24}$ | Average Density,[a] gm/cm$^3$ | YOM Volume Fraction[b] | Atom Density, atom/cm$^3$ x $10^{24}$ | Average Density, gm/cm$^3$ | YOM Volume Fraction |
| $U^{235}$ | 0.002285 | 0.8915 | 0.04760 | $8.104 \times 10^{-5}$ | 0.03162 | 0.001688 |
| $U^{238}$ | 0.009853 | 3.982 | 0.2052 | 0.03993 | 15.777 | 0.8318 |
| C | 0.01290 | 0.2573 | 0.1540 | - | - | - |
| Na | 0.007910 | 0.3019 | 0.3595 | - | - | - |
| Fe | 0.01038 | 0.9621 | 0.1226 | 0.004223[c] | 0.3916 | 0.04986 |
| | | | | 0.006782 | 0.6289 | 0.08008 |
| Cr | 0.002983 | 0.2575 | 0.03724 | 0.001214 | 0.1048 | 0.01516 |
| | | | | 0.001950 | 0.1683 | 0.02435 |
| Ni | 0.001390 | 0.1355 | 0.01522 | 0.000566 | 0.0552 | 0.0062 |
| | | | | 0.000909 | 0.0887 | 0.0100 |
| SS-304[c,d] | 0.01475 | 1.355 | 0.17506 | 0.006003 | 0.552 | 0.07122 |
| | | | | 0.00965 | 0.8865 | 0.1146 |

[a] Densities were calculated from known weights and volumes.

[b] The YOM volume fractions were obtained by dividing the actual (homogenized) atom densities by the corresponding atom densities used by Yiftah, Okrent, and Moldauer.

[c] Two sets of values are given for the stainless steel content of the blanket because the inner part of the blanket was contained in stainless steel drawers while the outer portions of the blanket were inserted directly into the matrix tubes. For most calculations, the resulting difference is negligible.

[d] The stainless steel is an alternate listing of the Fe, Cr, and Ni, and its atom density is the sum of the atom densities of these elements.

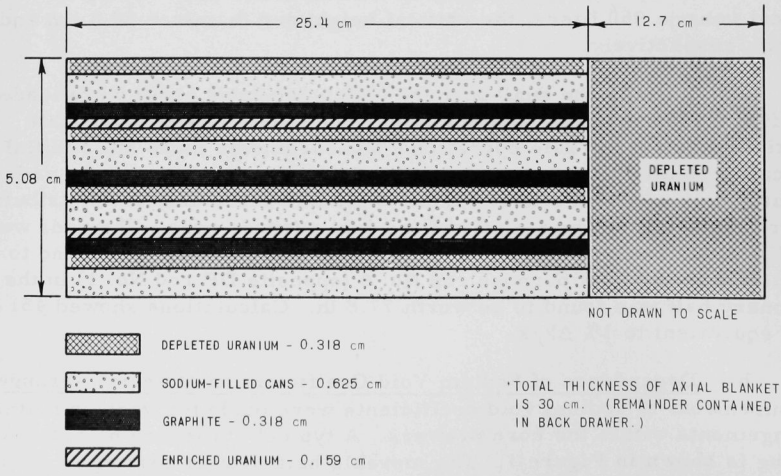


Figure 1. Stationary Half-drawer in Core

The axial dependence of the sodium void coefficient for typical drawer loadings in the center of Assembly No. 3 was determined by removing sodium in different axial locations from a region which had a radius of about 5.5 in. and consisted of 21 drawers in each half. The results are given in Table II.

Table II. Axial Dependence of the Sodium Void Coefficient in the Center of Assembly No. 3

| Voided Region Axial Length,* in. | Mass of the Removed Sodium, kg | Reactivity Change, Ih | Sodium Void Coefficient, Ih/kg |
|---|---|---|---|
| 0 to 3 | 2.83 | -0.5 | -0.2 |
| 3 to 6 | 2.83 | -6.6 | -2.3 |
| 6 to 8 | 1.85 | -9.2 | -5.0 |
| 8 to 10 | 1.85 | -10.8 | -5.8 |

*The distances given are measured from the interface between the two reactor halves.

The radial dependence of the sodium void coefficient near the interface of the halves was measured by removing the sodium from half-rings of different radii in the lower portion of the stationary half. The axial length of these rings was from 0 to 3 in. from the interface. The results are given in Table III.

Table III. Radial Dependence of the Sodium Void Coefficient Near the Interface in Assembly No. 3

| Void Ring Dimensions, in. | | Mass of the Removed Sodium, kg | Reactivity Change, Ih | Sodium Void Coefficient, Ih |
|---|---|---|---|---|
| Inner Radius | Outer Radius | | | |
| 0 | 5.5 | 2.83 | -0.5 | -0.2 |
| (central region) | | | | |
| 9.8 | 14.1 | 2.36 | -2.5 | -1.1 |
| 18.4 | 22.8 | 4.45 | -9.6 | -2.2 |
| 25.0 | 27.1 | 2.22 | -5.0 | -2.3 |
| 29.3 | 31.4 | 2.16 | -4.6 | -2.1 |

3. ZPR-IX

a. Homogeneous Tungsten-Rhenium Cores. Studies of homogeneous tungsten-rhenium-diluted and $U^{235}$-fueled fast reactor cores were completed. The core used in these experiments is identified as No. 4A. Extrapolation of the subcritical measurements led to estimates of the critical composition: 364 kg $U^{235}$, 26.6 kg $U^{238}$, 1541.9 kg W, and 143.5 kg Re. The extrapolated volume, effective radius, and length were 138.2 liters, 56.18 cm, and 27.99 cm, respectively, and the worth of a central drawer (fuel plus diluent) was five times greater than the worth of a peripheral drawer.

A critical configuration was constructed by reducing the rhenium concentration by about 25%. The physical properties of this assembly (Assembly No. 4B) are shown in Table IV.

Table IV. Physical Properties of ZPR-IX Assembly No. 4B

| | Critical Mass:* | | |
|---|---|---|---|
| | (atoms/cm$^3$) x $10^{-24}$ | kg | v/o |
| $U^{235}$ | 0.00674 | 339.8 | 13.84 |
| $U^{238}$ | 0.000486 | 24.9 | 1.02 |
| W | 0.0364 | 1437.6 | 56.29 |
| Re | 0.00247 | 98.7 | 3.73 |
| Al** | 0.00749 | 43.3 | 12.49 |
| Fe | 0.000353 | 4.2 | 0.41 |
| Void | | - | 12.22 |

Volume: 128.8 $\ell$; Length:† 56.18 cm; Effective Radius: 27.015 cm; Reflector Material: Aluminum; Edge Worth of Fuel plus Diluent Relative to Aluminum: 54.48 Ih/drawer; and Central Worth of Fuel plus Diluent Relative to Void: 260.3 Ih/drawer.

*Corrected for excess reactivity only.
**Includes aluminum in matrix, drawer loading, and drawer composition.
†Includes central air and aluminum gap.

Central worths (see Table V) were determined for a number of samples by use of a calibrated rod. To facilitate comparison with the all-tungsten-diluted assembly, the corresponding results for

Assembly No. 4 are listed in the last column. These results indicate a generally harder spectrum and a lower adjoint flux at lower energies for the rhenium-diluted core. In both assemblies, the adjoint flux peaks at about 50 keV, but for Assembly No. 4B it is some 15% lower than for Assembly No. 4 and so the central hydrogen worth changes sign.

Table V. Central Reactivity Worths

| Material | Sample Weight, g | Measured Worth, Ih | Total Worth, Ih/kg | |
|---|---|---|---|---|
| | | | Assembly No. 4B | Assembly No. 4 |
| Li | 28.6 | -2.624 | -917.5 | |
| W | 78.3702 | -0.969 | -12.36 | -12.6 |
| Al | 166.9 | -0.998 | -5.98 | -6.6 |
| Graphite | 103.0 | -1.852 | -17.98 | -22.0 |
| W | 1052.0 | -17.880 | -16.996 | -19.6 |
| $U^{235}$ | 135.40 | +29.608 | +218.7 | +270 |
| $U^{238}$ | 507.0 | -2.644 | -5.215 | -5.5 |
| Re | 1266.9 | -77.030 | -60.80 | -71.7 |
| Au | 1183.6 | -37.799 | -31.94 | -39.3 |
| Hydrogen | 0 to 3 | | -2910.0 | +3350.0 |
| $B^{10}$ | 29.29 | -89.750 | -3065.0 | -3660.0 |

Similar but less extensive measurements of the hydrogen and hydrogen-boron mixture worths were made with Assembly No. 4B as were done with Assembly No. 4. The results for pure hydrogen (Lucite and polyethylene, corrected for carbon) are shown in Figure 2. Also included

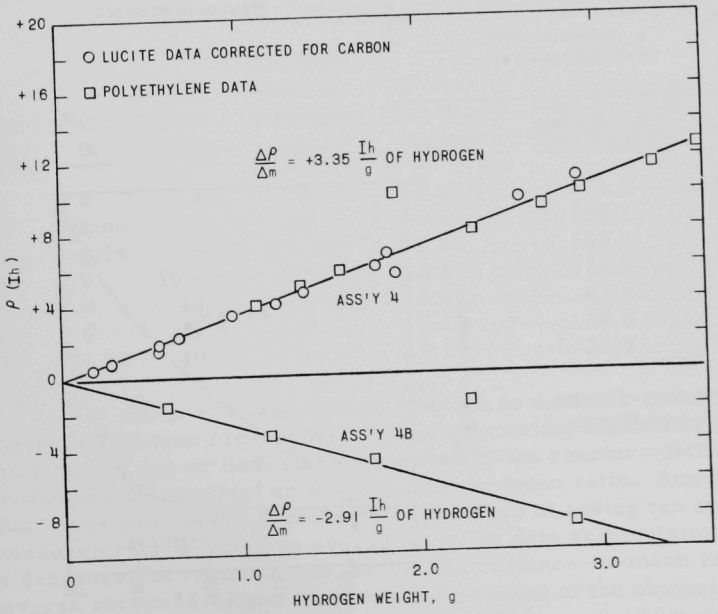


Figure 2

Central Worth of Hydrogen

in Figure 2 are the corresponding results for Assembly No. 4. A correction for oxygen (in Lucite) was determined from the difference in central worth measurements between aluminum and $Al_2O_3$. For these samples, the oxygen correction was less than 0.05 Ih and was neglected.

In an attempt to obtain higher boron concentrations in the boron-Lucite mixtures reported for Assembly No. 4, the boron-Lucite mixture powders were pressed into pellets. A comparison of the 50-50 w/o Lucite-boron mixture in the powdered form to the results of pellet measurements showed that this technique was reliable for boron concentrations of approximately five times greater than the maximum concentration possible with the powders. The change in boron worth in the presence of hydrogen for both Assemblies 4 and 4B are shown in Figure 3; in both assemblies the negative worth of each gram of boron increases exponentially with an increasing hydrogen environment. The worth per gram of sample as a function of Lucite-boron weight fraction is shown in Figure 4 for both assemblies.

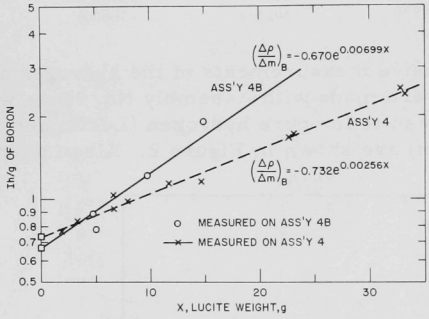


Figure 3

Worth of Boron in Presence of Hydrogen

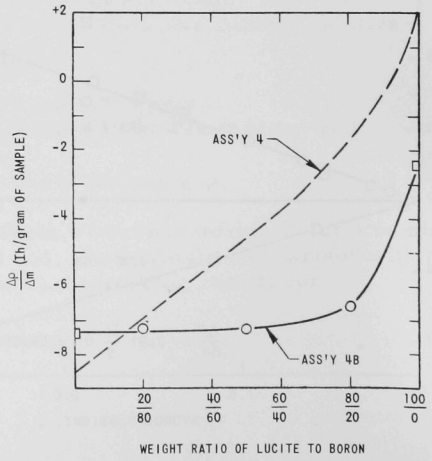


Figure 4

Worth per Gram of Sample of Lucite-boron Mixtures

b. Kinetic Measurements. A number of spatially dependent Rossi-alpha measurements were made. The results of a two-exponential least-squares fit to the data are given in Table VI for the various detector locations.

Table VI. Rossi-alpha Measurements

| Detector Positions* | $\alpha_1 (\times 10^{-6})$ | $\alpha_2 (\times 10^{-4})$ |
|---|---|---|
| 2323-2324 | 0.94 ± 0.34 | 7.00 ± 0.16 |
| 2323-2325 | 3.98 ± 3.00 | 7.31 ± 0.24 |
| 2323-2327 | 1.79 ± 1.02 | 7.17 ± 0.14 |
| 2323-2328 | 1.64 ± 0.50 | 6.96 ± 0.16 |
| 2325-2328 | 0.98 ± 0.50 | 7.10 ± 0.20 |
| 2327-2328 | 0.71 ± 0.50 | 6.75 ± 0.42 |

*Positions given as matrix locations. First number is chamber A (used to start sweep); the second is chamber B (data pulses).

A number of variance and mean measurements were made under varying conditions of $k_{eff}$ and sampling time. These results are listed in Table VII.

Table VII. Variance and Mean Measurements

| Run No. | $k_{ex}$, Ih | Gate Time, msec | Constant Source Strength, n/sec | Power (Arbitrary Units) | Variance, $\sigma^2$ | Mean, $\bar{c}$ | $\frac{\sigma^2}{\bar{c}}$ |
|---|---|---|---|---|---|---|---|
| 1 | 0 | 5 | 0 | 5.65 | 574.5 | 513.6 | 1.12 |
| 2 | -2.66 | 5 | $10^7$ | 5.65 | 550.7 | 505.7 | 1.09 |
| 3 | -5.16 | 5 | $2 \times 10^7$ | 5.65 | 565.2 | 506.6 | 1.12 |
| 4 | 0 | 10 x 5 | 0 | 0.470 | 713.9 | 440.6 | 1.62 |
| 5 | 0 | 40 | 0 | 0.47 | 43.2 | 40.3 | 1.07 |
| 6 | 0 | 8 x 5 | 0 | 0.49 | 39.5 | 38.0 | 1.04 |
| 7 | -21.70 | 40 | 0 | 0.10 | 35.9 | 29.5 | 1.22 |

Runs 1, 2, and 3 were intended to measure the change in the variance-to-mean ratio under slightly subcritical conditions and to evaluate the effect of one or both startup sources in the reactor. Neither condition produced a large effect on the variance-to-mean ratio. Run 4, relative to Run 1, was intended to demonstrate the effect of adding ten separate measurements in which an averaging in the data accumulation would tend to decrease the variance and, hence, the variance-to-mean ratio; the reverse occurred. Runs 5 and 6 were a repeat of the above in which the

difference between the two measurements is in the right direction, but the statistical significance is questionable. Results of Run 7 can be used, together with either Run 1 or 5, to provide a value of $\beta_{eff}$ independent of the prompt-neutron lifetime. This last step has not, as yet, been done since additional data are required to evaluate the statistical reliability of existing data and to explain the reversed behavior of Run 4 relative to the expected behavior of Runs 5 and 6. Analysis of this data is in progress.

## B. General Fast Reactor Fuel Development

### 1. Metallic Fuels

#### a. Uranium-Plutonium-Fizzium Alloys.

(i) Creep of U-10 w/o Pu-10 w/o Fz Alloy. The creep of the U-10 w/o Pu-10 w/o Fz alloy fuel pins for EBR-II was investigated to determine if they would deform under their own weight. Creep tests with a unit stress of 5.9 $g\text{-}mm^{-2}$, which corresponds to the weight of an EBR-II fuel pin, gave the following results: the total creep after one month was 0.08% at 650°C, 0.16% at 750°C, and 0.7% at 850°C. About 90% of the strain occurred within the first 250 hr at 650 and 750°C, but this behavior was not observed for tests at 850°C.

A novel, inexpensive method for studying creep was developed that lends itself to glovebox operation. It consists of loading measured specimens with dead weights and then encapsulating the assemblies in evacuated quartz tubes. These capsules are placed in tube furnaces for various times and then quenched into oil. The specimens are measured with a micrometer to determine change in length.

### 2. Development of Jacket Materials

a. Vanadium Alloys. Jacket materials for the fuel elements of fast reactors must have suitable high-temperature properties, including good strength and integrity, good thermal conductivity, and compatibility with the nuclear fuel and with liquid-metal coolants such as sodium. The jacket materials must also be amenable to fabrication into the desired shapes. Of the various potential jacketing materials that have been considered, vanadium-base alloys are among the more promising, and titanium is the element principally favored for use as an alloying element in the vanadium. Substantial additions of a third element have been tried, but any resulting increases in strength have, up to now, been usually obtained with excessive sacrifices of ductility.

Results to date indicate that, of the binary compositions, those with about 20 w/o of titanium (TV-20 alloy) are probably most suitable. Alloys with higher percentages of titanium have been made, but their

hardness is greater and they are less easy to fabricate; alloys with lesser percentages of titanium are significantly weaker and less resistant to corrosion in oxygen-bearing sodium. The commerical production of TV-20, one of the more compatible compositions, is being encouraged, and the fabrication development and properties of the alloy are being studied. The effects of titanium content in the vanadium and of oxygen content in the sodium are still being investigated.

(i) Creep of V-20 w/o Ti. A creep test of recrystallized V-20 w/o Ti was conducted at a stress level of 35.2 $kg\text{-}mm^{-2}$ and at a temperature of 550°C at $2 \times 10^{-6}$ mm Hg vacuum. The strain rate measured for up to 0.4% strain was $2.6 \times 10^{-9}$ $sec^{-1}$. This rate is lower than would be predicted from the data reported last month (see Progress Report for Sept. 1964, ANL-6944, p. 25) because it was measured by an extensometer on the gauge length. The data reported last month were measured from the crosshead of the tensile machine.

(ii) Corrosion of V-20 w/o Ti by Sodium. Vanadium-20 w/o Ti samples have been exposed to sodium containing 50-100 ppm oxygen for 440 hr at 650°C. The experiment was terminated because of equipment failure. Samples gained 0.96 $mg/cm^2$ as compared with 0.50 $mg/cm^2$ for the same exposure time in sodium containing 10 ppm oxygen. These results show, however, that the increase in corrosion for the same exposure time was not proportional to the increase in oxygen content of the sodium.

(iii) Alloys for Service in Oyxgen-bearing Sodium. Vanadium-titanium alloys containing 0 to 100% titanium (in increments of 10 w/o) have been prepared by levitation melting. An improved (from the point of view of better oxygen-concentration control) apparatus for testing the alloys in sodium is being assembled.

3. Irradiations of Fast Reactor Fuels

a. Transient Irradiations of Thorium-Uranium Alloy. A total of six specimens of Th-22 w/o U alloy, each contained in a graphite-lined stainless steel capsule, were subjected to elevated-temperature transients in the TREAT reactor. The specimens were fabricated by extrusion at 500°C. Reactor and specimen data are tabulated in Table VIII. The specimens, which were sodium bonded in jackets of nominal 0.38-mm-thick Nb-1 w/o Zr or Type 304 stainless steel tubing, had no previous irradiation history.

Post-transient examination revealed that the integrity of the jacketing on all six specimens had been maintained. There were no dimensional or volume changes of jacketed specimens whose temperatures did not rise above the melting point of the uranium phase. When

temperatures above the melting point of the uranium phase occurred, the fuel core was displaced upward inside the jacket, a movement believed to have been caused by pressure of sodium vapor.

Table VIII. Reactor and Specimen Data for Metallurgy TREAT Experiments 5-1 through 5-6 with Th-22 w/o U

| Met. Exp. No. | Transient No. | Specimen No. | Jacket | Reactor Period, sec | Integrated Reactor Power, MW-sec[a] | Maximum Temp, °C[b] |
|---|---|---|---|---|---|---|
| 5-1 | 708 | 152H | Nb-1 w/o Zr | 0.217 | 128 | 999 |
| 5-2 | 709 | 152I | Nb-1 w/o Zr | 0.217 | 86 | 944 |
| 5-3 | 710 | 152K | Nb-1 w/o Zr | 0.217 | 157 | 1434 |
| 5-4 | 711 | 152L | 304 SS | 0.217 | 89 | 745 |
| 5-5 | 712 | 152M | 304 SS | 0.217 | 129 | 923 |
| 5-6 | 713 | 152N | 304 SS | 0.152 | 184 | 1245 |

[a]The specimens were shielded by 0.127-mm cadmium foil.
[b]The temperatures are the maximum recorded temperatures of the jacket surface. Each jacket had two thermocouples attached.

Small dimensional changes were noted in the jacketed specimens subjected to the more severe transients. However, the resultant volume changes were less than 1%.

Metallographic examinations indicate that portions of the Th-22 w/o U fuel core had been molten, but that core-jacket interaction had not occurred to any appreciable extent.

## 4. Radiator-type Fuel Elements

The term "radiator fuel element" has been given to an extended-surface heat-exchanger fuel concept. Such shapes may provide higher heat-exchange rates than from plate- or rod-type fuel elements. The complexity of solid shapes required to fill such elements has so delayed the development of the radiator fuel element that consideration is now being given to the possible use of powder-loaded shapes. The studies reported are directed toward an understanding of the compacting of powdered material and provision of specimens for irradiation.

a. Vibratory Compaction. Binary and ternary systems of angular grit have been vibratorily compacted, and the relationship between packing efficiency and ratio of particle sizes has been determined for the binary. The relationship established for irregularly shaped particles in binary loadings cannot be extended to include ternary loadings, as could be done in the case of the compaction of spherical shapes, presumably because of the very irregular nature of the void in the matrix of angular shapes.

The packing efficiency of a single-component system of angular shapes is a function of the absolute size of the particle loaded. The relationship between packing efficiency and the size of particle is of the form

$Pe = A - (K/d_1) - Be^{-CD/d_1}$, where Pe is the packing efficiency, A is the limiting density of the system, K, B, and C are constants, D is the diameter of the container, and $d_1$ is the "diameter" of the single component. The dependency of the packing efficiency upon the reciprocal of particle "diameter" led to a speculation that surface-to-volume ratio might play a part in the relationship. To test this hypothesis, angular material was ball milled to reduce the angularity and thereby the surface-to-volume ratio. Single-component packing of the ball-milled material was carried out and the packing efficiency was determined. Preliminary analysis of results indicate that the value of K above does indeed decrease with decreasing surface-to-volume ratio. Since, in the system of spheres, the packing efficiency was independent of absolute particle dimension (K = 0), the hypothesis of dependency of packing efficiency upon surface-to-volume ratio may be real.

5. Zero-power Reactor Fuels

a. Fabrication and Jacketing of U-20 w/o Pu-2.5 w/o Mo Fuel Plates. Large numbers of stainless steel-jacketed U-20 w/o Pu-2.5 w/o Mo fuel plates are required for experimental verification of the Southwest Experimental Fast Oxide Reactor (SEFOR) designs in ZPR-III. These elements will eventually be used in the Zero Power Plutonium Reactor (ZPPR). The plates will be fabricated from uranium-base alloy containing 17.9 w/o ($Pu^{239} + Pu^{241}$).

For safe operation, the critical assembly should have a negative temperature coefficient of reactivity. This requires that the jacketed fuel plates show a large positive coefficient of thermal expansion. The jackets must remain leak-tight over several years of handling. The fuel alloy should be oxidation resistant and it must not present a significant fire hazard if a jacket is accidently ruptured in air.

Because the plates are to be commerically fabricated and early delivery is required, the process developed to fabricate the fuel elements should be adaptable to conventional equipment. A minimum of special tooling should be required. Jacket clearances were reduced over the previous zero-power plutonium loadings to meet the requirements for thermal expansion. Assembly of the tight-fitting components without plutonium contamination of the welds required a new jacket design.

Because of difficulties in rolling U-20 w/o Pu-2.5 w/o Mo alloy, precision casting was chosen as the method for making the fuel plates. Both copper and chill molds and graphite "warm" molds were tried. An yttria wash was used to protect the surfaces of both mold materials in test melting, but the final cores were melted in yttria-washed carbon crucibles by vacuum-induction heating. Best results were obtained when the alloys were poured at 1275°C into a carbon mold at 545°C. The cast-plate sizes ranged from 4.493 cm x 6.767 cm x 0.218 cm to 4.514 cm x 14.681 cm x 0.566 cm. The average thickness shrinkage factor was

2.25 percent. The shrinkage factor for length and width was 1.75 percent. Mold replication was excellent. The thickness variations were about 0.4 percent from a given mold. The length and width variations were within 0.1 percent. Corner radii were consistent. Recoating and re-use of the graphite molds is practical. A seven-cavity mold was satisfactorily used to test multiple mold castings.

The sleeve and end-plug jacket design was that previously used for ZPR-III plates. Sufficient clearance was allowed between the core and jacket so that the plutonium core could be inserted in a guard sheath that prevented contamination of the jacket. The guard sheath was removed and a spring was inserted to hold the plate against one side of the jacket. In this design, the large clearances prevented the prompt thermal expansion of the element.

A new close-fitting jacket was designed for the SEFOR critical experiment. It consists of two 0.03-mm-thick stainless steel panels. Each panel has a formed cavity that is about 0.05 percent longer and wider than the dimensions of the core plate. The depth of the cavity in each panel is one-half the core-plate thickness. Each plate has a turned-out rim that provides metal for seal welding.

The fuel element is assembled by placing the core plate in the cavity of one panel and then positioning the second jacket panel over the core plate. Care is taken to prevent plutonium from contaminating the exterior surfaces or the welding rims of the jacket panel. The assembly is sealed by the nonconsumable-electrode, inert-gas, shielded-arch weld method. A special welding machine in a vacuum chamber was constructed for making the welds. This allows the final weld to be made at a pressure of about 400 mb. The side welds are made first; the assembly is then clamped between two copper chills that expose only the edges of the side rims. The rims are fused together by a direct-current arc of about 12 Amp with an electrode traverse rate of about 20 cm/min.

A reinforced bearing shoe was required on each end of the element. Fuel elements were made with various designs of bearing shoes, all of which were objectionable because of cost, decontamination difficulties, or complexities. A weld-cast shoe was developed that overcame these objections. The ends of the fuel elements were closed by means of two 4.78-mm (0.188-in.) diameter cylindrical weld beads, which were subsequently milled flat and parallel to provide the bearing surfaces that transmit the thermal expansion of one element to adjacent elements.

The weld-cast shoes are made from filler strips that are spot welded to either end of the jacket panels. The assembly is clamped between chill molds that support the large weld. Cylindrical, 4.78-mm-diameter stainless steel arc-start and runout bars are provided at each end of the weld joint. The first weld is made at one atmosphere pressure

with an arc current of 120 Amp and an electrode traverse rate of 7.6 cm/min. The second shoe weld is made at a helium pressure of 350 to 400 mb, sealing the fuel element with this internal pressure. The arc current is 135 Amp. When the assembly is removed from the welding chamber, barometric pressure forces the jacket panels into contact with the core plate. (It should be noted that the minimum station pressure recorded at the National Reactor Test Site is about 850 millibars, over twice the internal pressure of the fuel element.) After inspection, the welds are machined. The fuel element is leak detected, gaged and inspected for acceptability. A total of 241 fuel plates were cast and 450 jacket panels were made in the development of these methods. Natural uranium plates were also cast and jacketed for transient excursion dilatometry tests in TREAT.

Specifications were worked out in cooperation with representatives of the General Electric Company, Atomic Power and Equipment Division, the ANL Idaho Division, and the AEC San Francisco office. A contract was awarded by the AEC San Francisco office to the Nuclear Materials and Equipment Company in mid-September for the production of the SEFOR fuel elements.

b. Fabrication of Doppler Test Elements. The fabrication of the Doppler test elements for ZPR-III (see Progress Report for September 1964, ANL-6944, pp. 30-31) has been completed.

Loading was successfully accomplished by attaching the test capsule through the hood wall by means of a soft plastic fitting. The plastic was compressed into the heater helices to form a protective seal. The pellets were loaded into the capsules through a 0.1-mm-thick loading funnel that was cemented at the upper edge to the fitting. In spite of these precautions, all of the capsules loaded showed a surface alpha contamination of several thousand dpm, but they were cleaned to less than 200-dpm direct count and zero wipe count.

The end plug welds were produced by the TIG method. After welding the capsules were again surveyed and decontaminated as required. The final manufacturing operation consisted of evacuating the capsule and backfilling to about 1/8 atm with helium. The evacuation tube was pinched closed and welded. After an additional alpha survey, further decontamination and room temperature leak detection, the capsules were heated to 1000°C and leak detected at operating temperature.

Of sixteen capsules loaded with mixed $UO_2$-$PuO_2$, nine were found to be leak-tight by the helium mass spectrometer at 1000°C, four gave helium signals at temperatures below 600°C, one gave a slight leak indication at 1000°C, one showed current leakage from the heater wire to the capsule sheath, and one had a broken lead wire. Since all capsules

were decontaminated to show less than 200-dpm direct count and less than 25-dpm wipe count and no increase in these levels was detected after testing, the capsules that indicated leaks at temperatures below 1000°C were still considered usable for room-temperature experiments.

Thirteen capsules were loaded with $PuO_2$ pellets and welded closed. Eight of these capsules were found to be leak tight at 1000°C, and two showed excessive current leakage and short-circuited from the lead wire to the sheath. One capsule showed a helium signal and leak indication below 600°C, and one capsule was found to contain a piece of a plastic loading funnel and was deliberately destroyed. One remaining capsule had been designated as a spare and was not tested. All the $PuO_2$ containing capsules were decontaminated to levels below 200-dpm direct count and zero wipe count.

## C. General Fast Reactor Fuel Reprocessing Development

### 1. Skull Reclamation Process

The skull reclamation process will be used for the recovery and purification of fissionable material that remains in the melt refining crucible after a melt-refining operation. This process is being studied on an engineering scale (1.5 kg of uranium per charge).

A major problem in the skull reclamation runs has been foaming of the chloride flux employed. The foaming, which was attributed to water of hydration in the flux, was prevented in the most recent run by pre-treating the flux by contacting it with magnesium at 700°C. This technique will be used in future runs.

Uranium ingots were prepared by retorting the Zn-12 w/o Mg-10 w/o U product solutions from five recent engineering-scale runs. The resulting ingots have been oxidized for sampling and have been analyzed. The results, which are consistent with earlier analyses of the product solutions, indicate a product composition of 91.3 to 95.5 w/o uranium, 0.13 to 0.32 w/o cerium, 0.15 to 0.36 w/o ruthenium, 0.42 to 0.88 w/o molybdenum, 0.54 to 1.4 w/o zirconium, up to 0.27 w/o magnesium, and up to 0.01 w/o beryllium. With the possible exception that zirconium is somewhat high, the product would be satisfactory for realloying in a melt-refining run.

### 2. Materials and Equipment Evaluation

Two runs were conducted to test the corrosion resistance of oxynitride-bonded silicon carbide to Zn-Mg-halide flux systems. In each of these tests, one conducted at 900°C and the other at 800°C, Zn-5 w/o Mg-2 w/o U/$CaCl_2$-$MgCl_2$-$CaF_2$ flux was contained in a carbide crucible. After 48 hr of exposure, it was found that the flux had

penetrated the walls of each crucible and collected in a secondary container. These crucibles thus show no promise for direct use in the skull reclamation process.

3. Advanced Processes

a. Halide Slagging of Uranium-Fissium Fuels. The equilibria of rare earths and plutonium between uranium-plutonium-fissium alloy and salt mixtures is being investigated. Knowledge of the equilibria values will make it possible to extract selectively rare earths and possibly other fission products (such as zirconium) from uranium-plutonium alloys or to extract plutonium from blanket material.

The extraction of zirconium from molten uranium-fissium alloy by a chloride flux containing $MgCl_2$ as an oxidant was investigated. Although the available free energy data indicate that the zirconium should not be oxidized by magnesium chloride at 1200°C, the effect of continuous distillation of $ZrCl_4$, if formed, could not be predicted without experimental data.

The charge material was 16 g of uranium-5 w/o fissium alloy containing 0.68 w/o zirconium and 0.45 w/o cerium. The flux was 3 g of 17 m/o $MgCl_2$-83 m/o $CaCl_2$. The alloy and salt were held in a high-density beryllia crucible at 1200°C for 1 hr under an argon atmosphere and then cooled; next, the phases were analyzed separately. Results indicate that no significant reaction of zirconium with the flux occurred during halide slagging and that about 97% of the cerium was removed from the alloy.

b. Distribution of Californium and Yttrium between Zn-6 w/o Mg and LiCl-$MgCl_2$ Salt. The distribution behavior of yttrium and californium between LiCl-$MgCl_2$ salts of various compositions and zinc-6 w/o magnesium alloy at 800°C has been determined to investigate the potentiality of this salt-metal system for separating rare earths from transplutonium elements. Yttrium, although not a rare earth metal, was used as a representative of this group since it offers the most difficult separation. The results, shown in Figure 5, indicate that a magnesium chloride concentration in the salt between 10 and 20 m/o provides the optimum extraction factor for a practical separation.

c. Phase Diagram of the Plutonium-Magnesium System. A preliminary determination of the liquid immiscibility curve in the plutonium-magnesium system has been completed. The liquid immiscibility region had not been adequately defined in earlier work.

The data were obtained by sampling each of the two liquid phases at various temperatures and analyzing the samples for plutonium.

As shown in Figure 6, the region of liquid immiscibility extends from about 8.5 to 84 a/o magnesium at 625°C. The consolute temperature appears to be about 975°C.

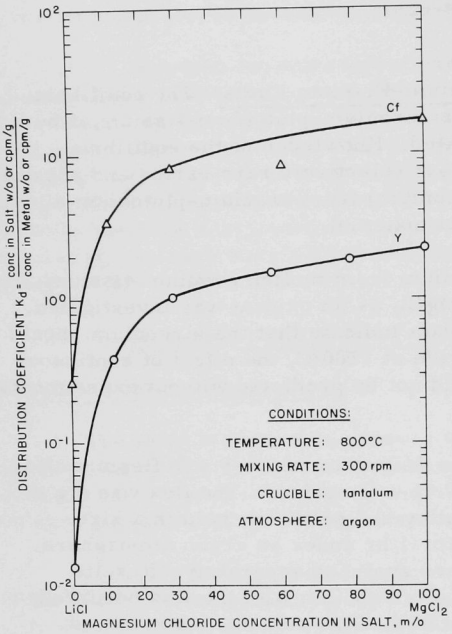


Figure 5

Distribution of Californium and Yttrium between Zn-6 w/o Mg and LiCl-$MgCl_2$ Salt

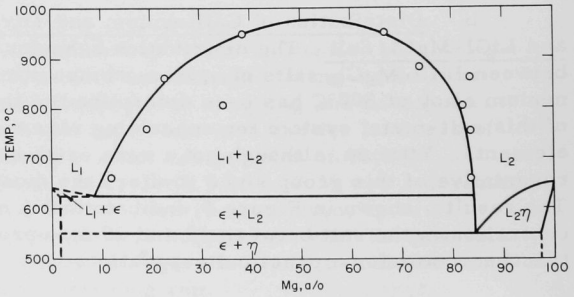


Figure 6

Liquid Immiscibility Gap in the Binary System Magnesium-Plutonium

## 4. Consolidation of Fission Product Wastes in Alloys

A series of exploratory experiments is in progress on the distribution of praseodymium between 30 m/o NaCl-20 m/o KCl-50 m/o $MgCl_2$ and selected alloys of magnesium (see Progress Report for September 1964, ANL-6944, p. 31). The objective of this work is to determine the effect

of various magnesium alloys on the distribution behavior of rare earth fission products, since consolidation of fission products into metallic alloys appears to offer potential advantages both for the storage of radioactive wastes and for possible utilization of fission product decay heat.

Completed results for the distribution of praseodymium between the salt mixture and aluminum-magnesium alloy show a distribution coefficient at 600°C as low as $4.3 \times 10^{-4}$ (conc in salt/conc in metal), which indicates that this alloy would be highly effective for the extraction of rare earths from recycled salt. An antimony-3.2 w/o magnesium alloy also resulted in a relatively low distribution coefficient at 600°C of about $2.5 \times 10^{-3}$ for praseodymium.

Results for the distribution of praseodymium between the salt mixture and copper-magnesium alloy at 600°C showed praseodymium distributing strongly to the salt (distribution coefficient = $10^2$ for the 33 w/o magnesium-copper alloy) instead of to the metal phase. Comparison of these data with the distribution behavior of plutonium in the same system at 600°C indicated that this salt-alloy system may be attractive for the separation of rare earths from plutonium. A plutonium-praseodymium separation factor of at least 240 can be achieved if a copper-magnesium alloy is employed as the liquid metal phase.

5. Decladding Studies for TV-20 Cladding

Study of the removal of vanadium-20 w/o titanium (TV-20) cladding from metallic fuels by chlorination in a molten salt has continued.

In a preliminary laboratory-scale experiment, TV-20 was exposed to 60 v/o $O_2$-40 v/o HF at 550°C and reacted completely. Subsequently, a test was performed in which a small specimen of uranium-fissium alloy partially enclosed in a TV-20 alloy sheath was exposed to 15 v/o $O_2$-85 v/o HF at 500°C for about 2 hr. There was little or no reaction of the TV-20 clad, which split, but extensive oxidation of the uranium alloy. Since oxidation of the uranium alloy is undesirable, this approach has been discontinued.

6. Eddy Current Induction Probe

It has been shown that the new eddy current induction probe (see Progress Report for November 1963, ANL-6808, p. 25) is temperature dependent. The output signals can be corrected for temperature changes by setting a bias voltage in accordance with a predetermined bias-temperature relationship. The maximum error in depth detection attributable to temperature variations is then ±1/8 in.

## D. Sodium Coolant Chemistry

### 1. Cover-gas Impurities

Sodium used as a coolant in thermal and fast reactors may react with contaminants in the cover gas and thereby become impure. To obtain an indication of the reactivity with liquid sodium of various common gaseous species, helium containing traces of hydrogen, methane, nitrogen, oxygen, carbon dioxide, and carbon monoxide has been circulated through liquid sodium at 190, 300, and 385°C. The contaminant concentrations were determined by mass spectrometric analysis. In all cases, oxygen and carbon dioxide reacted completely and rapidly with the sodium. Although the results for carbon monoxide and nitrogen, present simultaneously, are uncertain because both are measured at mass 28, it appears that carbon monoxide reacts rapidly and that nitrogen, as expected, does not react. The methane concentration in the helium did not change, and hydrogen was only partially removed.

### 2. Analysis for Oxygen

Current efforts to develop a method for the analysis of oxygen in sodium utilize the reaction $^{16}O(n,p)^{16}N$. A sodium sample in a 2S aluminum container is irradiated by means of a Cockcroft-Walton generator, and then the sample is transferred to the counting equipment by means of a pneumatic transfer system. A successful series of analyses of sodium and potassium for oxygen has been completed.

## E. EBR-II

### 1. Operations

Late in September, the main fuel gripper and the oscillator drive mechanism were checked out, and the new oscillator rod and thimble assembly installed in the reactor.

Heatup of the primary system from 580°F, by means of electrical and pumping power, was accomplished at the beginning of this month. The steam safety valves were tested and adjusted. During the testing of safety valves, the primary system temperature was held at about 620°F. The temperature was then raised by electrical and pump power to about 645°F, at which time the reactor was operated below 300 kW to expedite plant heatup to 700°F, which was achieved on October 3.

After calibration of primary flow meters versus pump speed, reactor power coefficient measurements were started. These continued until October 7, when both bellows of the steam-bypass-system connection to the turbine condenser were found to be cracked, necessitating immediate

repair. By installing an anchor to restrain movement of the bypass line at the expansion joint, a redesign was achieved so that only one bellows is now required.

During zero-power operation, a pressure gauge was installed on the vent of the primary heat exchanger annulus in preparation for testing argon pressurization of the annulus as a means of reducing temperatures at the top of the heat exchanger well and adjacent primary tank cover areas. Pressurization was started on October 12 and continued at the subsequent power and flow conditions. Argon injection rates up to about 6 std cu ft/hr were tried. Data are being analyzed.

The oscillator rod was calibrated and the reactor was started up for planned 30-MW operation. On October 10, the turbine-generator was synchronized with the NRTS power system. Operation with initial pressure governor control continued until the reactor scrammed on October 19.

Power coefficients were measured on October 10, and thereafter a steady power of 30 MW at 74% coolant flow was initiated. The reactor flow was increased to 100% and power to 37.5 MW on October 13.

During the reactor power run at 37.5 MWt from October 13 through October 19, the generator was in operation at 11.8 MWe, with a net electrical output to the NRTS power system of 8.8 MW. The generator carried the complete NRTS system reactive power load during this period, maintaining a power factor of unity at the Central Facilities substation. Turbine and generator operation was very satisfactory. Integrated reactor power produced during the month was 360 MWd, with an average calculated total burnup of a fuel subassembly in the center of the core of 0.24%.

2. Sticking of Control Rod and Oscillator Drive Mechanisms

Investigation of the scram on October 19 showed that the scram was initiated by a malfunction of a relay and was not due to a scram signal. Two control mechanisms, Nos. 7 and 9, did not drop as called for in a scram. Investigation of the cause was started immediately.

The primary pumps were stopped and compressed air was vented from the scram-assist cylinders so that no forces were imposed upon the control mechanisms except their own weights. The air cylinder was removed from drive mechanism No. 7 to permit tapping the piston with a plastic mallet. A small yoke was placed below the piston to permit lifting with a manual hoist. By alternate upward movement with the hoist and downward movement by tapping, some loosening of the drive was attained. After being exercised in this manner for several hours, the drive moved quite freely under its own weight without air assistance between approximate elevations of 5 and 8 in.

Next, drive mechanism No. 7 was raised to the 13-in. elevation by normal rack movement. A further binding was thereby caused over the entire range from 13 to 0 in. Further exercising as above produced some improvement, but not as marked as before. The mechanism was moved to its lowest position, and the drive was disconnected from the control subassembly. Exercising of the drive alone was attempted, but it was not possible to raise the drive above an elevation of about 4 in. Drive mechanism No. 7 was left in this condition during ensuing work on mechanism No. 9 and the oscillator mechanism, which was also found to be sticking.

The air cylinder was removed from drive mechanism No. 9. A weight of about 200 lb was applied to the piston and, after about 1/4 in. of travel, the assembly fell smoothly under its own weight through the remaining distance.

Next, a plan was prepared to ascertain whether the drives were sticking in the reactor vessel cover or in the small rotating plug. As a preliminary to this plan, which involved raising the reactor vessel cover about 1/8 in., all other control rods were scram-tested and then the control subassemblies were disconnected from their drives. All rod drop times (measured with the control console timer) for scrams from 14 in. with 30 psig scram assist air pressure were satisfactory.

After the control drives had been disconnected from the subassemblies, the reactor vessel cover was raised 1/8 in. Control drive No. 7 rose approximately 3/32 in., and the oscillator holddown tube rose about 1/16 in. All other drives, including No. 9, remained in their "down" positions. This indicated that drive No. 7 and the oscillator holddown tube were sticking in the reactor vessel cover.

Checkout of control assembly No. 9 was continued by operation from the control console. Scrams from elevations of 1, 3, 5, 8, and 10 in., without scram assist air pressure, appeared completely normal.

Next, drive No. 9 was raised in steps from 5 to 14 in. by applying a lifting force of from 350 to 550 lb. When the 11.5-in. elevation was passed, slightly increased friction was observed. At the 14-in. elevation, a slight mallet tap was required to start the assembly moving down. After this the drive could be raised smoothly. It was scrammed several times from the 14-in. elevation. The air cylinder was replaced, and this drive mechanims was scrammed from the 14-in. elevation with 30 psig assist air pressure. Drop time was acceptable.

On October 23, work was started aimed at freeing the oscillator drive mechanism. Control assembly No. 9 was scrammed three more times from the 14-in. elevation; drop times were shorter than previous. The drive was then disconnected from the control subassembly.

The oscillator rod gripper drive shaft was found to be frozen with respect to the guide thimble holddown tube, and the holddown tube sticking in the reactor cover. To determine how tight the holddown tube was in the cover, it was lifted with the oscillator ratchet height adjustment. For the first 1/2 in., the holddown tube came up very freely but would not go down at all. It was raised an additional 1/2 in. with slightly more effort on the ratchet, but still freely. Again it would not move down.

The gripper shaft was moved relative to the holddown in an attempt to free it. The range of movement had increased from about 1/4 in. initially to about 2 in. Further work on this was then suspended.

Special tools were fabricated to free control drive No. 7. These would allow simultaneous rotation and axial movement of the control rod shaft after the drive motor had been removed and the bellows packing seal loosened. This method caused the drive to become free.

3. Reactor Physics

The power coefficient ($\Delta k/k$-MW) of the reactor was measured incrementally over the range from 0 to 30 MW with both increasing and decreasing increments of power. These measurements were performed with two different control rod configurations, and at sodium flows of 100% and 74% of maximum. The results for 100% flow measurement with all rods banked at 11.5 in. are given in Figure 7. The general features of the other measurements were the same. The net loss in reactivity when the power returned to zero was also confirmed in the other runs, and was to be further investigated during the shutdown phases after the 37.5-MW run. Table IX gives the overall results of the four measurements; the power coefficient here is the total value between 0 and 30 MW.

The difference in reactivity measured for the two rod configurations probably can be attributed to effects caused by thermal expansion of the control rod; expansion downward causes an apparent loss of reactivity. The net loss is greater in the case of the fully banked rods (rod configuration No. 2), which is in agreement with the relative rod worths. Further analysis is being carried out.

A measurement of the reactor transfer function was begun at 37.5 MW, 100% flow, but premature scramming of the reactor did not allow the work to be completed. Incomplete results indicate general agreement with previous data.

4. Systems and Components.

a. Steam Safety Valves. Cold and hot testing and setting of the steam safety valves was completed at the beginning of the month. Subsequent experience, however, revealed that for these values hydrostatic

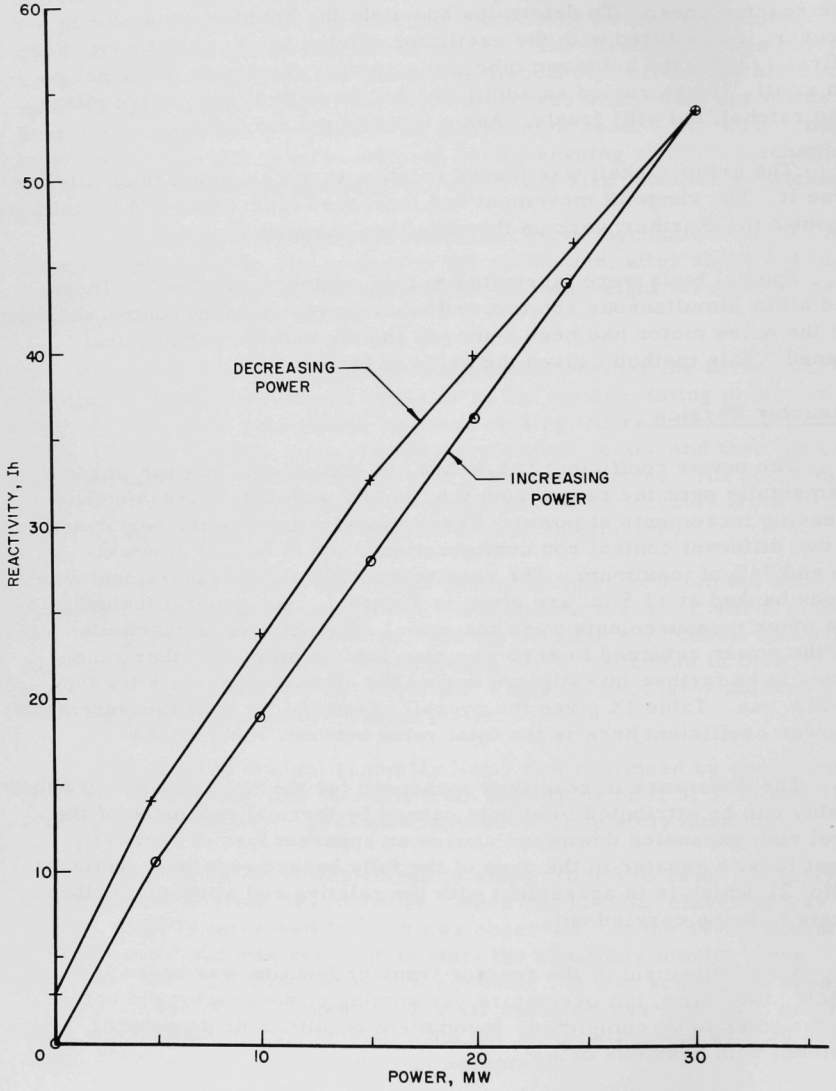


Figure 7. Power Coefficient of EBR-II with 100% Flow and Rods Banked at 11.37 in.

Table IX. Power Coefficient from 0 to 30 MW

| Rod Configuration† | Flow | Reactivity Loss (Ih) | Power Coefficient (Ih/MW) |
|---|---|---|---|
| 1* | 100% | -49 | 1.63 |
| 2** | 100% | -53 | 1.73 |
| 1 | 74% | -64 | 2.13 |
| 2 | 74% | -68 | 2.27 |

*Three rods at 14.0 in., eight rods at 8.35 in.
**Rods banked at 11.4 in.
†Rod No. 3 used for control.

test results have little relationship to relief pressures when operating with steam. Thus, it was necessary to make incremental adjustments in spring tension and to retest until satisfactory relief pressure settings were obtained. Steam drum valves were finally set to relieve at 1400 and 1435 psig, compared with settings of 1390 and 1410 psig during hydrostatic pressure testing. The shell safety valve on feedwater heater No. 4 was set to relieve at 1320 psig.

Also, the superheated steam safety valve had been tested and set the previous month. Although set to relieve at 1340 psig, on two occasions it relieved at 1260 and 1280 psig. The spring tension was again reset this month to relieve at 1320 psig. It is believed that decreased lift pressure may be related to increasing superheat temperature.

b. Steam-bypass System. Power plant operation during the power coefficient measurements (see Sect. 3 above) was hampered somewhat by faulty performance of the large automatic steam-bypass valve. The valve tended to open fully after the stem position reached about half open and also seemed to stick in the full-open position. Acceptable bypass-system operation was achieved by taking sufficient flow through the manual bypass valve so that the opening of the large automatic bypass valve did not exceed about 30%.

A larger pneumatic operator was installed on this valve, but the operation of the valve has not yet been completely tested.

c. Turbine-driven Feedwater Pump. After receipt of new governor valve parts and in the presence of a factory representative, the feedwater pump was brought up to full speed while the reactor was in standby condition. Operation was satisfactory. Checkout of the governor under load will be accomplished during the next operation at power.

d. Turbine Extraction Non-return Valves. The nonreturn valves in the turbine extraction lines were checked out during power operation.

The installation was satisfactory except for setting of the new air-dump valve cam which must be accomplished during shutdown, and further adjustment of the weights on the low pressure extraction line valves when full load is reached. The high-pressure extraction line was placed in service during 37.5-MW operation.

e. Fission Gas Monitor. The charged-wire fission gas monitor was operated on the day shift for initial checkout. Due to partial plugging of the sample piping, it was necessary to install heaters on the shutoff valve and the vapor trap. With the reactor operating at 37.5 MW, a background count rate was obtained. Calibration of the monitor to determine response time and relation to area of fuel exposed remains to be accomplished.

f. Equipment Airlock. The annual leak-rate test of the inner door of the equipment airlock was completed late in September. The leak rate was found to be 2.8 cu ft (36.2 psia at 32°F) per 24 hr. Testing of the shell and outer door of the airlock was completed this month; the leak rate was 19.7 cu ft/24 hr.

Considerable difficulty was encountered in checking the outer door. A neoprene boot, which seals the mechanical interlocks between the two doors, leaked in several places and was repaired.

g. Sodium and Argon Systems. The plugging temperature of the primary sodium remained less than 220°F. The plugging temperature of the secondary sodium was maintained between 250°F and 300°F by intermittent use of the cold trap.

Laboratory analyses of the primary argon indicate about 10 ppm hydrogen and about 1.3% nitrogen. Gamma-spectrometer activity analyses of the cover gas with the reactor at 30 MW showed: $Ar^{41}$ = $1 \times 10^{-3}$ $\mu$C/ml; $Xe^{135}$ = $1.3 \times 10^{-3}$ $\mu$C/ml. Traces of $Kr^{85}$, $Kr^{87}$, and $Kr^{88}$ were identified.

Chemical analyses of the primary sodium made earlier this year showed approximately 1.8 ppm uranium. Calculations were made assuming 1.5 ppm uranium dissolved in the sodium as a contaminant. At 30-MW reactor power, the calculated $Xe^{135}$ level in the cover gas would be $2.7 \times 10^{-3}$ $\mu$C/ml, assuming diffusion of all of it to cover gas.

Considerable trouble was experienced with the gas chromatograph in the secondary argon cover gas system. This has been partially rectified. The hydrogen analyses are believed to be valid, but there is some doubt as to the accuracy of the nitrogen analyses. The hydrogen analyses have been in the 10-30 ppm range, while the nitrogen is probably less than 500 ppm. Efforts are continuing to get this equipment in full operation.

A bellows on the plugging valve in the secondary system plugging meter ruptured. This was replaced, and the plugging meter was returned to operation. Following this, the throttle valve in the plugging meter suffered a ruptured bellows also.

Considerable difficulty was experienced during the month with leaks in the vacuum system for the surge tank on the primary purification system. Work is still in progress to rectify the situation. Progress has been very slow because of the necessity of allowing sodium activity to decay before work can be done.

5. Fuel Cycle Facility

a. Fuel Preparation and Recovery. The fuel element-removal machine, which was developed by the Remote Control Division, is an attachment to the subassembly dismantling machine which provides a semi-automatic method for separating fuel elements from the subassembly. At present, fuel elements are removed individually from the cluster using a model 8 master-slave manipulator (see Progress Report for October 1963, ANL-6801, p. 20). The fuel element removal machine was received, tested in the mockup area, and then remotely installed on the dismantler. Its operability was demonstrated, and it was then removed and transferred again to the mockup area for technician training.

The fuel element-decanning machine has been modified to operate at one-half the original speed to facilitate observing its operation and to reduce the probability of jamming. The reduction in speed does not markedly increase the operating time per assembly. About 50 depleted uranium pins were decanned and chopped without difficulty.

Analytical results from the first melt-refining operation with irradiated uranium are now available. Approximately 99% of the iodine and cerium, greater than 99.9% of the lanthanum and barium, and at least 99.99% of the cesium were removed from the irradiated fuel by melt refining. Some iodine and xenon were found in the vacuum pump oil.

Three fuel elements, representing inside and outside corners, and the central pin of subassembly C-115 were sectioned individually, and the sections were analyzed to obtain vertical and horizontal burnup patterns. Relative burnup was obtained by counting the 1.6-MeV gamma of $La^{140}$ in aliquots of the dissolved pin segments. The maximum-to-average burnup ratio for the three pins was $1.16 \pm 0.01$. Absolute burnup values were obtained by the $La^{139}$ isotopic dilution method. Excellent precision was obtained, and an average burnup of $0.116 \pm 0.002\%$ was obtained from data on four segments of the outside pin. The fast-fission yield of $La^{139}$, on which these numbers are based, was derived from EBR-I, Mark-III fuel $La^{139}$-$Cs^{137}$ ratios and the $Cs^{137}$ fast-fission yield reported by

Kafalas and Crouthamel.[2] Since the later value may be in error, the burnup values given above must carry an uncertainty of ±10%. Burnup estimations based on the $La^{139}$ isotope dilution method for the other two elements are in progress.

The skull from the first melt-refining run with irradiated uranium (see Progress Report for September 1964, ANL-6944, p. 41) has been oxidized and dumped from the crucible. The oxide weight was 750 g from a charge weight of 632 g. A sample of the oxide is being analyzed. Some xenon but no iodine was detected in the offgas from skull oxidation. The level of contamination of the Argon Cell atmosphere, as indicated by the activity level of the bypass filter system, did not change when the oxide was dumped from the crucible, but increased significantly when the crucible was dumped into the waste can.

b. Fuel Fabrication. The 8-kg ingot obtained by melt refining chopped irradiated fuel elements (plus an unirradiated casting heel) from the core assembly discharged after attaining about 0.1% burnup was injection cast to yield about 5 kg of castings. The small charge largely accounts for the smaller than normal casting yield. Helium was again used as the pressurizing and quench gas, but the pressurizing rate was probably higher than desirable, as the top ends of a number of molds were broken off. Of 65 molds containing castings, 36 acceptable pins were obtained. The rejected castings included 11 too short as cast, 2 sheared short, 2 showing porosity, and 10 with dimensions outside the standard diameter limits. Since the rapid pressurization may account for a number of these defects, improvement in yield should be readily accomplished as conditions are refined.

From the rebonding and bond testing of canned fuel elements obtained from the disassembly of various special subassemblies prepared for the EBR-II dry and wet critical tests, 845 acceptable elements have been reclaimed out of 910 processed to date, and 34 are still in process. Seven additional subassemblies have been completed (for a total of nine to date) using the Air Cell assembly and test machines operated in effectively remote fashion, with some machine observations and direct adjustments. Thus far, six core subassemblies, two control subassemblies, and one safety rod subassembly have been manufactured.

Some difficulty has been encountered with overpenetration on one or two of the welds in making core-type subassemblies, although the same welding parameters have produced acceptable welds on control and safety subassemblies. The only discernible difference is that a somewhat larger gap between the hexagonal tube and its mating part exists in the core assemblies than in the control and safety rod hardware. The

[2] P. Kafalas and C. E. Crouthamel, J. Inorg. Nucl. Chem. 4, 239 (1957); see also Errata, ibid., 5, 92 (1957).

welds have been readily corrected, and the subassemblies have been straightened outside the cell. An incell machine is being built to determine deviations from straightness and to straighten subassemblies not meeting the straightness specification.

c. Performance of Process Auxiliaries. Satisfactory performance of the pressure control and purification systems for the Argon Cell atmosphere continued. The typical air in-leakage rate was 0.5 cu ft/hr. The water content of the cell gas averaged about 40 ppm and ranged from 13 to 100 ppm, whereas the oxygen level averaged about 30 ppm and ranged from 15 to 200 ppm. The high moisture level occurred during dryer regeneration, and the high oxygen level after a weekend shutdown of the purification system.

The possibility of removing the small amount of carbon dioxide contained in the cell atmosphere by adsorption on the Linde type 5A molecular sieves, normally used for water removal, after exhaustive regeneration of these agents was considered. In a preliminary test, the apparent carbon dioxide content was reduced from 74 to 36 ppm.

Repairs were continued on the electromechanical manipulator carriage which had been damaged by being dropped. All major components have now been repaired except the telescoping tubes. The vendor indicates that about two months will be required to accomplish this, at the end of which time reassembly of the carriage can commence.

A closed-circuit television camera system has been obtained and placed in operation. Its possible use in the air and transfer cells will be evaluated.

d. Skull Reclamation Process. An additional experiment has been conducted to determine if improved removal of the uranium (from the intermetallic decomposition step) that adheres to the surface of the tungsten crucible would be obtained with two successive hydriding reactions. In a previously reported experiment (see Progress Report for September 1964, ANL-6944, p. 43), only one hydriding conversion step was performed. In the current experiment, the charge was prepared by first simulating the zinc-uranium intermetallic formation and precipitation step of the process, then decomposing the intermetallic compound and subsequently precipitating metallic uranium. The product was metallic uranium dispersed in a zinc-50 w/o magnesium solution. This product was the charge to the tungsten crucible for the two-step hydriding experiment which was conducted in a hydrogen atmosphere at temperatures maintained between 270 and 305°C for $4\frac{1}{2}$ hr. The crucible and its contents were then held under the hydrogen atmosphere overnight at room temperature.

After the first hydriding step, about 41.6 w/o of the original charge to the crucible could be readily poured from the crucible. The

poured material was returned to the tungsten crucible and the crucible contents were then subjected to a second hydriding step. The amount of material that could be easily poured increased to 61 w/o of the original charge to the crucible.

The rest of the material, which adhered to the crucible, was concentrated in that segment of the crucible from which the supernatant zinc-magnesium solution had been decanted during the uranium precipitation step of the charge preparation. This material consisted of two different forms: (1) a brittle material which contained several visible cracks and was located in the crucible bottom, and (2) a continuous metallic phase which covered the brittle material and extended up the sidewall of the crucible. The continuous metallic phase appeared to be zinc-magnesium that was not decanted from the crucible after the uranium-precipitation step of the charge preparation. This continuous metallic phase required considerable force to remove it from the crucible. After it had been loosened, the brittle material was easily freed from the crucible. The brittle material was apparently locked in place by the overlying continuous metallic phase.

On the basis of the results obtained in this run and previous runs (see ANL-6944, pp. 43-44), the degree to which this residual material (precipitated uranium dispersed in zinc-magnesium) can be freed from the surface of a tungsten crucible appears to depend upon the following three factors: (1) the distribution of uranium precipitate in the zinc-magnesium, (2) the thickness of the zinc-magnesium coating surrounding the uranium particles, and (3) the composition of the zinc-magnesium phase. Further work is planned to evaluate the potential application of a hydriding step in the final product consolidation for the skull reclamation process.

Engineering-scale prototype equipment is being developed for the skull recovery process. In order to stir the contents of the crucible in the prototype (M-2) skull oxide reclamation furnace (see Progress Report for July 1964, ANL-6923, pp. 35 and 38), a suitable stuffing box for the rotating shaft of the mixer must be provided in the top of this furnace. The stuffing box must be sufficiently tight to maintain desired pressure and atmosphere conditions within the furnace and must also be able to withstand the furnace operating temperatures.

Tests of various candidate bearing and packing components have been carried out with an experimental stuffing box mounted on the M-1 skull oxide reclamation furnace. The agitator stuffing box assembly shown in Figure 8 was used in these tests. The assembly has an upper and a lower bearing. The upper bearing is a conventional, sealed ball bearing greased with NRRG-159, a radiation-resistant lubricant suitable for temperatures up to 175°C. The lower bearing is a sleeve bearing made of a graphite material, National Carbon Co. TS-574. The stuffing

box was packed with an asbestos packing impregnated with molydisulfide, spaced alternately with a second material made of Fiberfrax, reinforced with Inconel wire and impregnated with molydisulfide. This Fiberfrax material is a very hard packing and acts as a supplementary bearing.

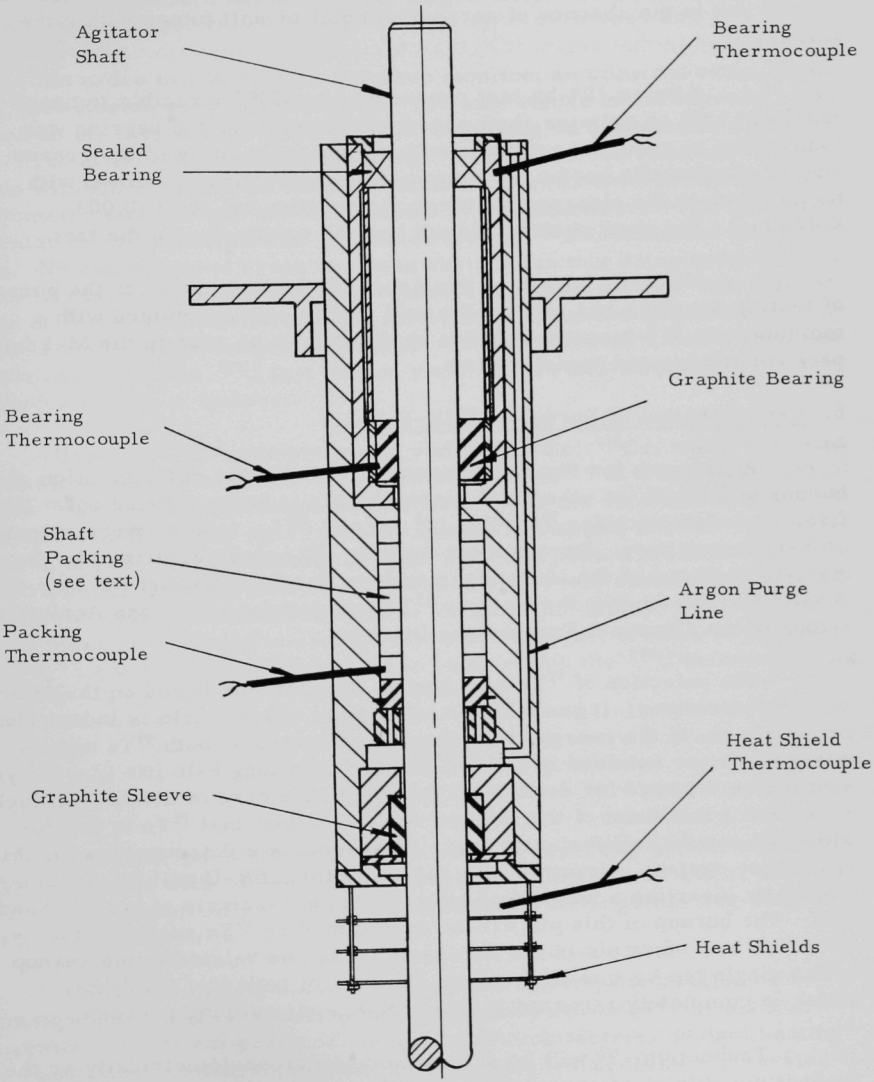


Figure 8. Agitator Stuffing Box Assembly

To simulate the design planned for the M-2 furnace, three stainless steel heat shields were positioned below the packing housing. In the tests, the M-1 furnace was operated at process temperatures and with an argon atmosphere of ~2 psig. However, the impeller shaft (constructed of carbon steel) was tested under no-load conditions (i.e., the crucible was empty) and in the absence of corrosive metal or salt fumes within the furnace.

After a 109-hr test conducted at ~800°C (crucible temperature) and with an agitator shaft speed of 750 rpm, the top bearing was found to be in excellent condition with no loss or melting of the grease. The lower graphite bearing appeared to be in excellent condition with no increase in the clearance between the bearing and shaft (0.003-0.004 in.). The shaft packing did not become brittle during the test.

No further tests of this assembly will be made for the purpose of testing bearings and seals. The unit will now be assembled with a molybdenum-30% tungsten agitator shaft and will be used in the M-1 furnace for mixing and transfer tests.

6. Determination of Burnup of EBR-II Fuel

A program for the development of methods for determination of burnup of EBR-II (or other fast reactor) fuels is being carried out. The fission product nuclides $^{99}Tc$ ($2 \times 10^5$ yr) and $^{139}La$ (stable) were selected as burnup monitors. Development work on $^{139}La$ was performed by the Analytical Group of the Idaho Division (see Progress Report for May 1964, ANL-6904, pp. 49-50); the work on $^{99}Tc$ was carried out by the Analytical Group of the Chemical Engineering Division.

The selection of $^{99}Tc$ as a burnup monitor was based on the following considerations: it has a high fission yield and its yield is independent, or nearly so, of the energy of the fissioning neutrons; both $^{99}Tc$ and its precursors are retained in the fuel at 600°C; its long half-life ($2 \times 10^5$ yr) eliminates the need for decay corrections; in the case of the EBR-II fuel it is not a constituent of the original fuel. The fact that $^{99}Tc$ is not removed in the EBR-II fuel-reprocessing scheme is a disadvantage for this particular system. However, this difficulty for EBR-II will be circumvented by inserting a virgin fuel pin in each subassembly of reprocessed fuel. The burnup of this pin will be determined by $^{99}Tc$ analysis; the burnup of any other pin in the subassembly can be related to the burnup of the virgin pin by a radiochemical analysis of both pins for $^{140}Ba$, which is completely removed in the EBR-II melt refining process.

Technetium-99 will be determined spectrophotometrically as the technetium-dithiol complex[3] after distillation of technetium septoxide

[3]Meyer, R. J., Oldham, R. D., and Larsen, R. P., Separation and Spectrophotometric Determination of Technetium in Fissium, Anal. Chem. 36, 1975 (1964).

from sulfuric acid. Only the distillation must be performed remotely since the radiation level of distillates is low (~25 mr/hr). The precision and accuracy of the method were tested by analyzing inactive uranium-fissium alloys containing known amounts of technetium (equivalent to 1% burnup). The relative standard deviation for a single determination was 0.7% with no detectable bias.

In order to use $^{99}Tc$ as a burnup monitor, an accurate value of its $^{235}U$ fast-fission yield is necessary. The only values in the literature are based on the fast-fission yield of $^{99}Mo$, assuming no independent yield for $^{99}Tc$. A direct determination of the $^{235}U$ fast fission yield of $^{99}Tc$ was made with EBR-I Mark-III fuel. Technetium-99 was determined spectrophotometrically; burnup was determined by radiochemical $^{137}Cs$ analysis. A tentative value of 5.2% was calculated for the $^{235}U$ fast fission yield of $^{99}Tc$. No estimation of error has been assigned to this value because there is reason to believe that the reported value for the $^{235}U$ fast fission yield of $^{137}Cs$ is somewhat low. A series of irradiations is planned in EBR-II which, when completed, will provide material for a more accurate determination of the $^{235}U$ fast fission yield of $^{99}Tc$ and other fission product nuclides of interest.

Uranium-235 thermal-fission yields of $^{99}Tc$, $^{133}Cs$, and $^{137}Cs$ were determined on 47% enriched $U_3O_8$ irradiated in CP-5 to a burnup of 25% of the $^{235}U$. (This information was necessary for the determination of burnup for EBR-II fuel specimens irradiated in thermal reactors.) The number of fissions was calculated from pre- and post-irradiation mass spectrometric uranium analyses. Technetium-99 was determined spectrophotometrically. The concentration of each cesium isotope was determined by the mass spectrometric-isotope dilution technique. Values of 6.07 $\pm$ 0.08, 6.75 $\pm$ 0.07, and 6.32 $\pm$ 0.04 were obtained for the $^{235}U$ thermal fission yields of $^{99}Tc$, $^{133}Cs$ and $^{137}Cs$, respectively.

## F. FARET

### 1. General

The principal activities for the current reporting period continued to be concerned with Title II engineering at the Laboratory and at the architect-engineer offices. Bechtel reported 76% completion for Title II at the end of September.

The Laboratory's review of Bechtel's drawings is continuing. Drawings now being reviewed by the Laboratory cover general plant arrangement, electrical power, structural and architectural design, heating and ventilating, sodium piping, and construction for process and service systems.

Design Package II (Reactor Vessel) has been completed. Design Packages III (Heat Exchangers), IV (Liquid Metal Pumps), and V (Instrumentation) are being reviewed by the Laboratory for final approval.

Bechtel has completed a preliminary analysis of the cell for impact loading. This analysis confirms the feasibility of absorbing impact loads by both elastic and plastic deformation. Bechtel is completing a final design of the cell structure.

The radial biological shield and the radial energy absorption structure have been combined into a single structure serving both purposes. The conceptual design consists of about 4 in. of borated steel and 12 in. of high-temperature concrete surrounded by vertical and circumferential reinforcing steel to absorb radially directed impact energy. This portion of the shield is separated from the cavity liner and surrounding ordinary concrete by at least a 12-in. gas space. The borated steel and high-temperature concrete portion is cooled by a NaK cooling system. Argon gas flows in the 12-in. annular gas space for cooling the ordinary concrete. The concept appears feasible, and Bechtel is proceeding with the detailed design.

Bechtel is currently attempting to select suitable locations for the nuclear instrument thimbles. Several alternatives are available, namely, (1) the instrument thimbles emerge horizontally into the front cell area from the ordinary concrete outside the cavity liner; (2) the instruments emerge horizontally into the front cell area through the cavity liner from the high-temperature concrete; (3) the instruments emerge horizontally into the vault from the high-temperature concrete; (4) the instrument thimbles emerge vertically into the cell from the high-temperature concrete.

Case 1 requires a neutron window in the shield structure. Case 2 requires the thimbles to penetrate the containment liner and imposes containment considerations upon the thimbles design. Case 3 imposes operational restrictions since maintenance within the vault is difficult and time-consuming. Case 4 imposes severe remote handling and maintenance problems. In each case, it appears as though some cooling of the thimbles may be required.

2. Safety Analysis

A study has been made of the dynamic behavior of FARET during scram, based on an analog computer study at ANL. The results indicated that (1) reactor scram leads to no excessive temperatures anywhere in the system, (2) the rate of change of the coolant temperature leaving the reactor vessel is large enough to require thermal baffling, (3) the temperature-time profiles are essentially independent of the initial system temperature levels.

3. Reactor Vessel

a. Design. The basic design of the reactor vessel, including the core support structure, the vessel extension, and the vessel head, has been completed (see Figure 9). The procurement package has been compiled and delivered to prospective bidders. Proposals have been requested by November 30, 1964.

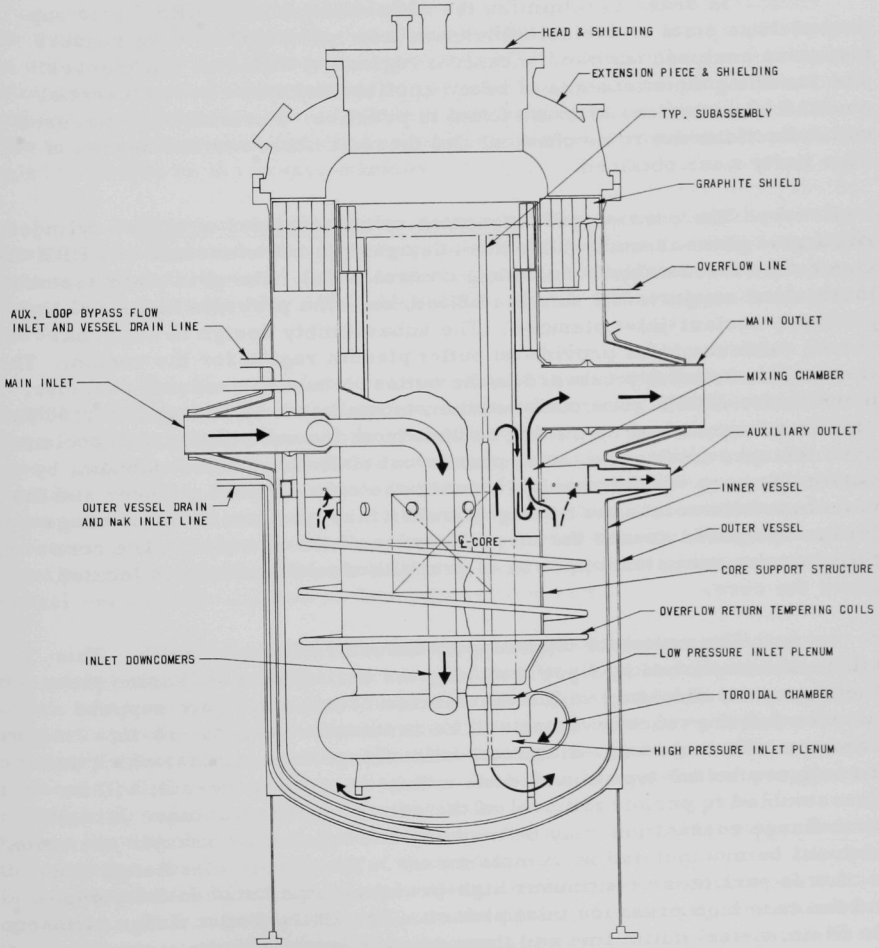


Figure 9. Reactor Vessel for FARET

The reactor vessel is comprised of a double-walled vessel assembly, supported from the bottom through the outer wall of the vessel. The inner wall of the vessel is suspended and supported from the outer wall at the point of junction of the walls above the inlet and outlet nozzles. The annulus between the vessel walls is normally filled with NaK, which serves to equilibrate temperatures and to provide a heatup system for bringing the vessel to sodium-loading temperature.

In order to minimize the deflections of the FARET grid support plate, a plate of variable thickness was investigated. The support plate was analyzed for two concentric regions of different thicknesses. The resulting equations are of broad application; they can represent almost all distributions of loads found in practice. Formulae for stresses and deflections due to mechanical and thermal loads and any degree of edge fixity were obtained.

The core support structure, which consists of a core cylinder and a grid plate assembly, has been designed to accommodate 433 EBR-II-type core subassemblies (including control rods). The grid plate assembly locates and supports the subassemblies, and also provides high- and low-pressure coolant-inlet plenums. The subassembly design is such that nested subassemblies provide an outlet plenum region for the coolant. The coolant flows radially outward in the outlet plenum to a mixing chamber, in which the 1200°F core outlet sodium temperature is lowered to 1150°F. This is accomplished by mixing coolant from the core outlet with coolant from the core inlet. The latter passes out of the lower inlet plenum, bypasses the core via the annulus between the core support cylinder and the vessel, and flows into the mixing chamber through a series of openings uniformly spaced around the circumference of the chamber. The core cylinder also supports a portion of graphite shielding which is located above the core.

The complete core support structure is replaceable. This will be accomplished by first removing the seal-welded extension piece. Then, graphite shielding within the annulus between the core support cylinder and the reactor vessel will be removed. Next, the 14-in.-diameter inlet and 24-in.-diameter outlet flange connections, which are the only two bolted-type connections within the reactor vessel, will be disassembled to permit removal of the core support structure. Initially these flange connections may be made by hand, but after reactor operation they will be manipulated by remote means. The 14-in. inlet flange connection is part of the continuous high-pressure pipe between the pump and the core high pressure inlet plenum. The 24-in. outlet flange connects the 24-in. vessel outlet line and the pipe extension from the core support structure.

The reactor vessel extension, which contains the nozzles for in-core instrumentation lead penetrations, has been changed from a conical to an ellipsoidal shape. This shape provides more space within the head and permits the head shielding to be accommodated internally. This will reduce neutron activation of the extension piece. Internal shielding also provides more available space in the cell area, and a cleaner, less cluttered area around the extension piece.

The reactor vessel head is a flat type, designed to support the necessary shielding sections at the vessel opening. Steel balls may be used to fill the shield sections of the head. The head flange sealing arrangement is a double-gasketed pressure-seal system. The control rod drive mechanisms are attached to and supported on the vessel head. The drive mechanisms and head assembly are removed remotely as a unit for access to the vessel interior.

b. Thermal and Hydraulic Analysis. The thermal and hydraulic work necessary for the design requirements of the basic reactor vessel has been completed. Several significant changes in the hydraulic design (see Progress Report for May 1964, ANL-6904, pp. 58-9) have been made as follows:

1) The top of the reactor vessel is no longer cooled by the main bypass flow since this flow now enters the mixing chamber of the core support cylinder through holes which are lower than the main outlet pipe. Cooling of the top of the reactor vessel is accomplished by the overflow-makeup system, which continuously removes 100 gpm of sodium from near the free surface, cools the sodium to the reactor inlet temperature, and returns the sodium into the reactor vessel. This arrangement provides for adequate cooling of the upper portion of the reactor vessel even at low and not-so-low bypass flow rates.

2) The auxiliary outlet is no longer directly connected to the mixing chamber. Rather, it is connected to a circumferential header which takes suction from the annulus between the vessel and the core support cylinder. Thus, when the main system is shut down and the auxiliary system is operative, the flow through the mixing chamber holes reverses. Under these conditions, the core flow leaves the core support cylinder through the mixing chamber holes and joins the bypass flow before leaving the reactor vessel through the auxiliary outlet pipe. In this manner, the heat capacity of the sodium in the reactor vessel annulus is used to absorb heat immediately after a scram with auxiliary system operation. This significantly reduces the heat-removal requirements of the auxiliary system. During normal operation, the auxiliary system is kept on the line under low-flow conditions by using the reactor vessel drain line to return this flow to the reactor vessel.

4. Cell Components

a. Cell Containment. Criteria were established and basic analysis was carried out for the plastic design of the cell roof to withstand the missile impact of the reactor vessel cover. All parties have agreed to proceed on the basis of the ANL plastic design proposal for the analysis and design of the FARET cell.

b. Cell Lighting. Since the 1000-W mercury vapor lamp appears to offer the most favorable combination of high lumens per watt and unit volume, long service life, and reasonable price, the FARET cell lighting design has proceeded on the basis that this light source will be used. The present effort is directed toward optimum utilization of the type of luminaire now used for the Fuel Cycle Facility of EBR-II. This luminaire was specifically designed for remote replacement by the operating manipulator. In addition, it was contoured to give optimum lighting when wall-mounted at a height of $9\frac{1}{2}$ to $10\frac{1}{2}$ ft on walls opposite to shielding windows in a cell 15 to 16 ft wide. To obtain satisfactory lighting in the center of a cell 20 ft wide, the mounting height should be increased.

The maximum feasible height for location of lights in the FARET core appears to be $17\frac{1}{2}$ ft above the cell floor. Thirty lamps spaced as uniformly as possible on the walls, with some necessary deviation in height to accommodate existing wall penetrations, should afford illumination down the center of the cell length of about 210 ft-candles and at a distance of 5 ft out from the walls of about 215 ft-candles. Figure 10 shows calculated values of illumination at various

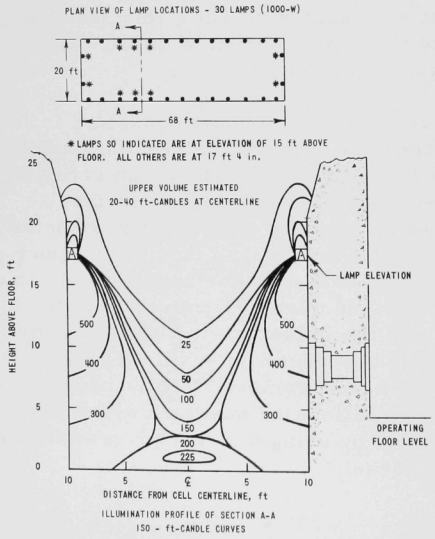


Figure 10

FARET Cell Lighting

heights above the floor. In order to be able to concentrate lighting when necessary, it is recommended that about ten (10) spare wall support brackets be installed at a height of $9\frac{1}{2}$ ft above the cell floor to accept luminaires. To limit the heat load of fixed cell lighting to 30 kW, the number of lamps will not exceed 30, but luminaires may be transferred from upper locations to lower ones if circumstances so dictate. It is planned to utilize the vertically telescoping TV camera boom to remove and replace luminaires. It is further planned that four (4) additional 1000-W wall mounts be furnished wired to 125-V DC emergency power.

c. Cell Shielding Windows. In order to have reasonable control over the mechanical fit of window components into their liners, it is planned that both the windows and the liners be furnished by one vendor. The preliminary shielding window design has been completed, including all requirements and design criteria. A cross section through the window is shown in Figure 11.

The window will consist of two dry units removable from inside the cell, and an oil- and glass-filled tank unit removable from the operator's side of the cell wall. In such a tank unit, the oil volume is minimal, its only purpose being to reduce reflectance losses between the numerous glass slabs.

The primary gas seal will be accomplished with the B slab assembly gasketed to the steel liner which is to withstand a cell pressure of 30 psig. Glass slab B-2 will be seated on the gasket with pressure supplied by its frame which is bolted to the window liner.

The tank unit will be the secondary gas seal. The annular space (about 1/2 in.) between the tank and the liner will be bridged by a continuous sheet gasket around the tank periphery at the outside cell face. It is designed to withstand 30 psig. The two glass cover plates for the tank, each 4 in. thick, will be sealed in a manner to withstand oil and gas pressures of 30 psig. Mechanical restraint of the tank itself in the liner is independent of the peripheral gasket. The two cover plate glass slabs are restrained by the recess in the liner and by the framing bars bolted to the tank around the periphery of the openings at either open end.

The volume between the tank and the liner will normally be pressurized to about 1 psig of argon gas. A low-capacity flow indicator will be used to monitor for any leakage of seals.

In addition, the "A" slab assembly will be gasketed to the steel frame of the "B"slab assembly, with glass slab A-2 sealing on the gasket. Sealing force is provided by bolting the hinged frame to the steel liner.

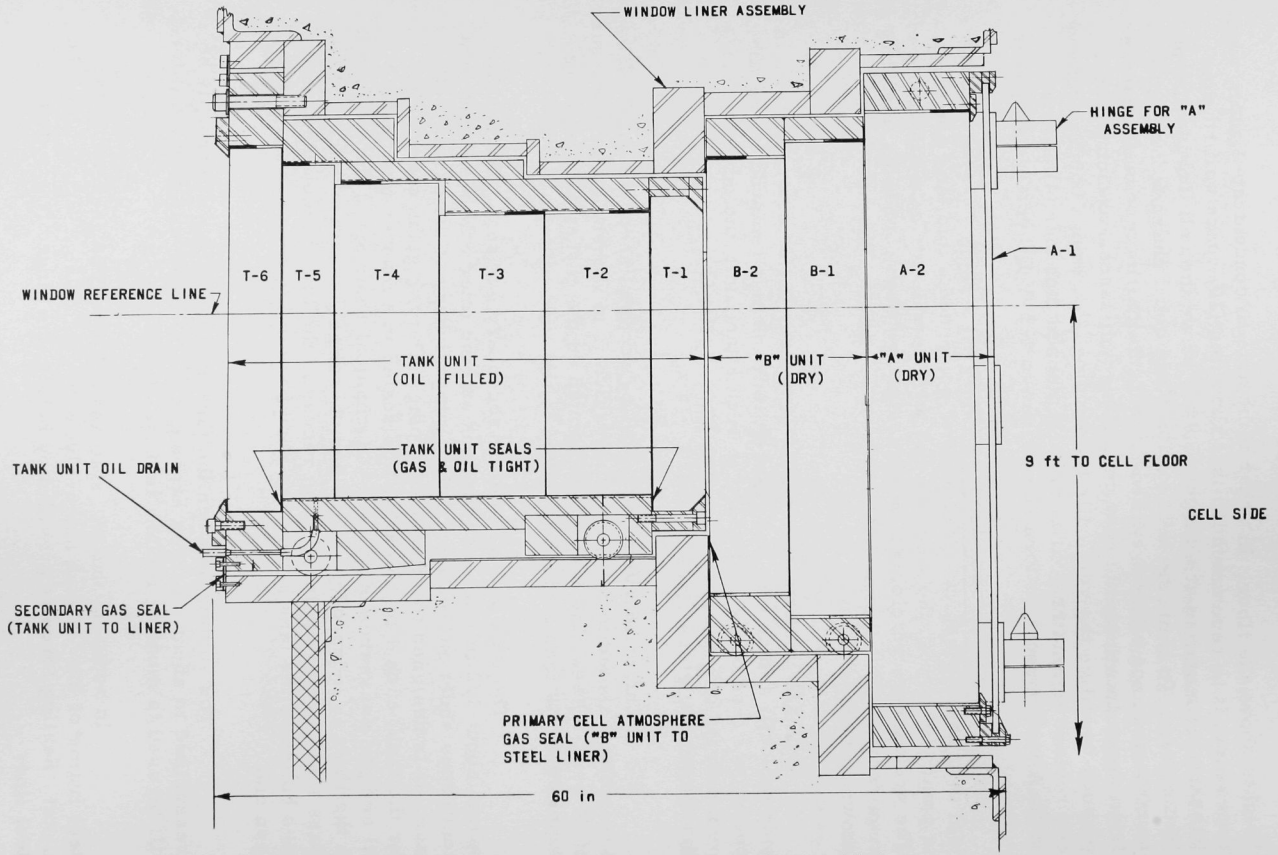


Figure 11. Vertical Section through FARET Cell Shielding Window

Window liner details have been provided to the Architect-Engineer for consideration of mounting provisions, for support in the cell wall, and details of leak-tight joining of the liner to the inner steel shell of the cell. Minor modification to the liner design as may be necessitated by these considerations will then be incorporated, after which the complete window specifications will be readied for bidding.

Table X shows the general viewing and glass-slab requirements for the window design.

Table X. General Window Data

| Glass Slab | Density (g/cc) | Thickness (in.) | Framed Weight (approx) (lb) |
|---|---|---|---|
| A1 | 2.7 | 1/2 | 3,200 |
| A2 | 3.3 | 8 | |
| B-1 | 3.3 | 6 | 3,000 |
| B-2 | 3.3 | 6 | |
| T1 | 3.3 | 4 | |
| T2, 3, 4 | 3.3 | 24 (3 x 8) | |
| T5 | 3.3 | 4 | 7,500 |
| T6 | 3.3 | 4 | |
| | Total | $56\frac{1}{2}$ | 13,700 |

Angle of View (Maximum):
Upward, 45°
Downward, 66°
Sidewards, 53°

Light transmittance expected: from 17 to 20%.

d. Cell Penetrations. A mockup of a typical cell stepped penetration with internal equipment using submarine cable has been constructed. Tools required to install and change the cable have been developed. Cable-changing operations have been successfully performed. A pressure test was made at 30 psig on the total assembled penetration. There were no leaks of the welded components, mechanical end seals, or cable-sealing gland. The sample cable, however, leaked (0.08 scfm). The bonding agent between the insulation of the individual conductors and the total cable insulation was found to be defective. The manufacturer is replacing the defective cable. A new sample is now enroute.

The leak tests were performed by pressurizing the mockup with nitrogen. Accurate leak measurements could not be made. A "standard leak" for a Freon leak detector will be purchased for the use in making more reliable leak measurements.

## 5. Core Instrumentation

It has been reported (see Progress Report for May 1964, ANL-6904, p. 58) that to have a standard deviation of less than 5% assigned to the average fuel temperature of the test zone of the zoned core, about 15 sensors should be placed at each of 12 r,z positions in the test zone. (Each of the 15 sensors is at a different $\theta$ position.) In order to meet this requirement, almost every subassembly in the test zone would require an instrument lead, and almost every one of the subassemblies would have its sensors in different positions. Because these conditions are exceedingly difficult and costly to attain, consideration has been given to the possibility of reducing the number of sensors. On the same basis as used previously, if only 10 sensors at each of 8 r,z positions are used, the standard deviation assigned to the average fuel temperature would increase from a value of 5 to 8 percent. (Twenty percent sensor failures are assumed in each case.) This requirement can be met by providing instrument leads to 12 subassemblies instead of to 36. In addition, the sensor position can be the same in each of these subassemblies.

## 6. Fuel Slip-fit Experiment

The heat transducer for the FARET slip-fit experiment has been checked out for the best method for calibration. Before the heater burned out, it appeared that the heat output can be determined to within ±100 W at 4200 W. The temperature change indicated by the transducer was not constant with time, but the signal with its erratic amplitude and frequency, could be averaged out with time and an integrator. The results can be duplicated by this means.

The heater burned out because of a weld failure, which allowed water to enter into the heater, burning out the lead wire. A new heater is being prepared. The hardware for the experiment is ready. The pressure tube and transducer is assembled and the transducer will be calibrated as soon as the heater is ready.

## 7. Fuel Assembly Sodium Flow Test Facility

Rework on the dump tank for the Flow Test Loop was delayed because of the use of improper material for a welded 2-in. tee. A replacement has been ordered.

The fittings for the pressure vessel have been received by the fabricator. Delivery of this unit may be made in the middle of November.

Pipe-system fabrication continues to be held up since the 20 stainless steel 304 pipe fittings replacing those made of 304L stainless steel have not yet been received.

The manufacturers' drawings which include required changes by the Laboratory for the 800-gpm pump have been approved for fabrication. The changes were made to the welded pump casing to insure the reliability of the pump for operation up to 1200°F.

The interim pump case has been re-radiographed; all welds are satisfactory. The final closure weld is being made. This will complete all of the work.

Experimentation continues on the electric-input requirements for the pipe heaters. Currently, a 4-in. schedule 10-304 SS pipe, about 8 ft long with two 5/16-in. Calrod heaters in place, is used. A shell of 0.010-in. stainless steel, a 2-in.-thick inner layer of Kaylo 20 insulation and a 2-in.-thick outer layer of Kaylo insulation are placed over the Calrod heaters.

# II. GENERAL REACTOR TECHNOLOGY

## A. Experimental Reactor and Nuclear Physics

### 1. Solid-state Neutron Spectrometer

To gain some information about the neutron spectrum, a hydrogenous film (irradiator) backed by a solid-state detector was used to measure spectra of recoil protons, both at the center of Assembly No. 2, ZPR-VI, and also in a beam of fast neutrons produced by a converter plate at beam hole No. 4 of the JUGGERNAUT. The principles underlying the conversion of a proton spectrum to a neutron spectrum are described by Bennett.[4] The chief advantage of this method is that wall effects which are troublesome in a proportional counter for neutrons of higher energy are reduced, if not eliminated, by this technique. The chief disadvantage is that gammas and perhaps fast neutrons produce a high background. The pulse-height discrimination between gamma rays and protons used in proportional counters is not possible at the present time in solid-state detectors.

The experimental arrangement of irradiator and detector is shown in Figure 12. The hydrogenous film was 500-$\mu g/cm^2$ rubber hydrochloride. Two surface-barrier solid-state detectors were used: one (designated as A) had a depletion depth of 750 $\mu$ at a bias voltage of 100 V (this device was free of hydrogenous material) and the other (designated as B) had a depletion depth of 290 $\mu$ at 100-V bias (this device was not free of hydrogenous material). The presence of hydrogenous material in the structural components of a detector is undesirable because such materials contribute to the background. Detector A was used in ZPR-VI Assembly No. 2. Detector B was used in the beam produced by a converter plate at the JUGGERNAUT because Detector A broke down prior to the measurement at the JUGGERNAUT. The arrangement of the converter plate and detector at the JUGGERNAUT is shown in Figure 13.

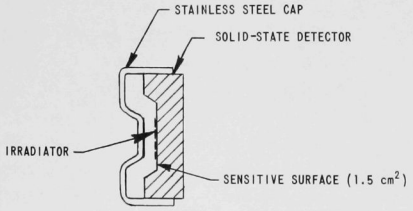


Figure 12
Arrangement of Detector and Irradiator

[4] E. F. Bennett, Proportional Counter Proton-Recoil Spectrometer with Gamma Discrimination, Rev. Sci. Instr. 33, 1153-1160 (1962); A Study of the 1/E Slowing-down Neutron Spectrum Using 4π-Recoil Proportional Counter, ANL-6897, to be issued.

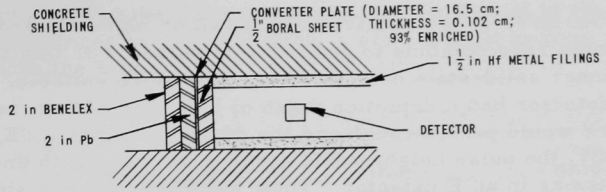


Figure 13. Arrangement of Converter Plate and Detector

Two runs were taken in each case: One run with the irradiator in place and one run without the irradiator. The difference between the two runs was considered as the recoil proton spectrum. The ratio of signal to background was about 15% at the lower end of the spectrum; this ratio was only 3%-4% at the higher end. Figure 14 shows the neutron spectrum obtained at the center of ZPR-VI Assembly No. 2. The fission rate of $U^{238}$ calculated from this spectrum was found to be $3.1 \times 10^5$ fissions/g/min. The measured fission rate[5] of $U^{238}$ was $4.3 \times 10^5$ fissions/g/min. It should be stated that the calculated fission rate is based on the fraction of the spectrum shown in Figure 14. The calculated fission rate from the spectrum obtained at JUGGERNAUT and the measured fission rate of $U^{238}$ were $1.31 \times 10^4$ fissions/g/sec and $1.15 \times 10^4$ fissions/g/sec, respectively.

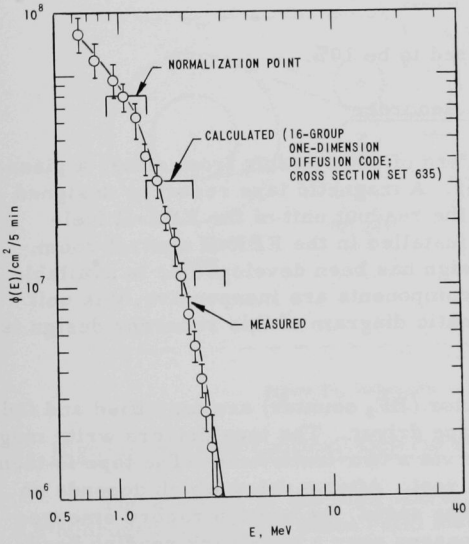


Figure 14

Neutron Spectrum Taken at Center of Assembly No. 2, ZPR VI

It should be stated first that the results reported here are preliminary in nature. The problem of background is not fully understood. It was thought that the gamma-ray background would not be appreciable above 100 keV; however, this was not the case. The gamma background seemed to be quite

[5] Dearnalley, G., and Whitehead, A. B., The Semiconductor Surface Barrier for Nuclear Particle Detection, Nucl. Instr. and Methods, 12, 205-226 (1961).

high up to 500 keV. It is conceivable that two or more electrons "knocked off" by gamma rays combine to produce one pulse. For this type of phenomena thinner solid-state detectors would be more suitable. On the other hand, if a detector had a depletion depth of less than 300 $\mu$, recoil protons above 6 MeV would pass through and the device becomes a dE/dX detector. Consequently, the pulse height would not be proportional to energy in the same manner as in an E detector. Thus, the simple conversion from proton-recoil pulse-height spectrum to neutron spectrum would be complicated considerably. The background above 500 keV is also higher than expected from fast-neutron interactions with the detector materials. The signal-to-background ratio in detector A was lower than that of detector B even though detector B had some hydrogen material in the form of epoxy in its structural material. This seems to indicate that gamma rays are the major contributor to the background.

The resolution was considered to be 10%.

2. Design of Excursion Alarm and Recorder

It is desirable to have a record of neutron flux from either a planned or accidental excursion in a reactor. A magnetic tape recorder designed for this purpose is patterned after the readout unit of the EBR-II fuel-element-failure monitor presently installed in the EBR-II control room. All the circuitry utilized in this design has been developed or is available from stock. Since the mechanical components are inexpensive, this unit can be readily fabricated. A schematic diagram of this recorder design is shown in Figure 15.

Pulses from a neutron detector ($BF_3$ counter) are amplified and fed to a discriminator and then into a tape driver. The tape drivers write magnetization reversals on 1/4-in. tape via a two-track head. The tape is then spooled onto a continuous loop-type reel. After a delay which depends on the size of the reel, as well as on tape speed, the written record emerges from the inner rim of the reel and passes over a two-track reading head.

The direct output is monitored by a count-rate meter having an adjustable trigger level, which shuts down the unit to preserve the record in case of an excursion. After passing the readout head, the tape runs through a short delay and then passes over an erase head just ahead of the writing head. Thus, count-rate information is continuously written onto the tape, stored for a certain period of time, and then automatically erased. A count-rate meter and trigger circuit may also be connected to the tape input so as to furnish a warning or reactor shutdown signal.

The system is designed so that the whole tape or interesting sections of the tape can be played into the kicksorter memory at any desirable rate. The memory may, in turn, be displayed on a CRT and photographed, plotted,

or punched into paper tape. If some portion of the record in the direct channel was overtaxed by the excursion, a scaled-down channel may be used to examine the tape.

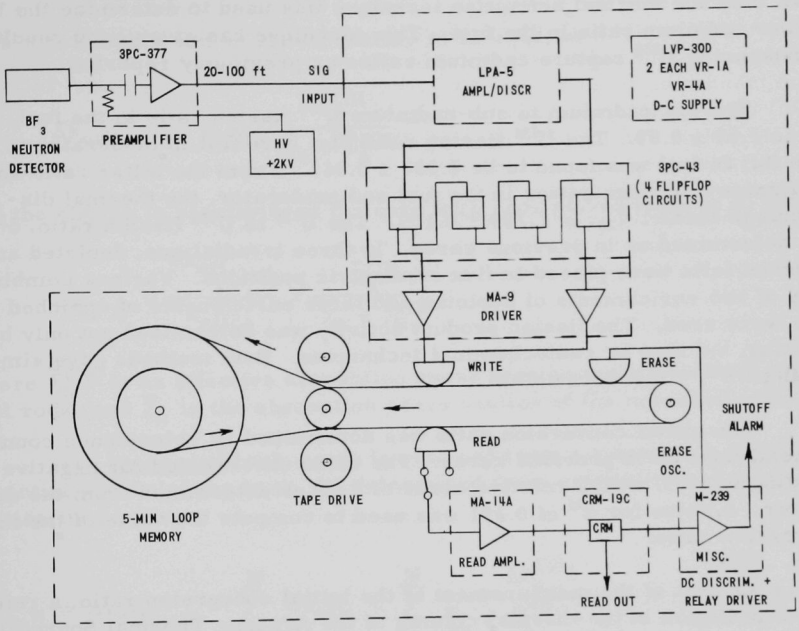


Figure 15. Schematic of Excursion Recorder

## 3. High-conversion Critical Experiment

The analysis of the microparameter measurements made in the 0.5 hydrogen to one $U^{238}$ atom ratio loading in the central zone core (see Progress Report for August 1964, ANL-6936, p. 43) has been completed. This core consisted of a central zone of stainless steel-clad Hi-C fuel rods in the most densely packed arrangement possible. The system was made critical by loading an annulus of less densely packed aluminum-clad fuel pins (higher hydrogen to $U^{238}$ atom ratio) around the central zone and reflecting the core with $H_2O$.

The values obtained for the $U^{235}$ fission cadmium ratio in the fuel and in the moderator were as follows:

in the fuel: $1.59 \pm 0.03$;

in the moderator: $1.69 \pm 0.09$.

These cadmium ratios were corrected for thermal self-shielding and extrapolated to zero mass of cadmium, as with previous cores. Because of the close packing of the fuel and the expected low value for the fuel-cadmium ratio, only the thermal activation technique was used to determine the $U^{235}$ fission-cadmium ratio in the fuel. This technique has given good results in measuring $U^{238}$ capture cadmium ratios as previously reported.

The epi-cadmium to sub-cadmium $U^{235}$ fission ratio in the fuel, $\rho_f^{25}$, is 1.69 ± 0.09. The $U^{235}$ fission ratio of a bare foil in moderator to a bare foil in fuel was found to be 1.081 ± 0.041. From the latter ratio and the fission-cadmium ratios in the fuel and moderator, the thermal disadvantage factor, $\zeta_{25}$, is 1.189 ± 0.109. The $U^{238}$ to $U^{235}$ fission ratio, $\delta^{28}$, was determined as in previous cores. In three irradiations, depleted and enriched foils were placed in flux symmetric positions. Various combinations of two enrichments of depleted and three enrichments of enriched foils were used. The fission product activity was determined not only by counting, but also by radiochemical techniques. Both methods gave similar results: $\delta^{28}$ = 0.2622 ± 0.0036.

The initial conversion ratio was determined by coincidence counting of metal foils as in previous cores. The value uncorrected for negative buckling is 1.45, with a relative error of $4\frac{1}{2}\%$ as determined from the data scatter. A value for $\alpha^{25}$ of 0.391 was used to compute the value of the initial conversion ratio.

As part of the measurement of the initial conversion ratio, a reference irradiation in the thermal column of the Argonne Thermal Source Reactor (ATSR) was necessary. When the initial conversion ratio was measured in the 1.24-cm square stainless steel zone core, a slight difference in weight normalized $U^{238}$ capture was noted between metal foils and various sizes of oxide fuel pellets. After several runs in the thermal column of the ATSR it was determined that foils and oxide pellets irradiated in the ATSR should be corrected for thermal self-shielding and epi-cadmium activity. All of the previous initial conversion ratio results will be corrected for these effects.

A final report on the completed phases of the Hi-C program is being prepared.

## B. Theoretical Reactor Physics

### 1. Control Rod Evaluation

On the basis of current definitions of control rod worths, the calculated worth for a bank of rods will be greater than the measured value, obtained by "Period Runs," by a factor equal to the $k_{eff}$ of the core with all rods out. This is shown below.

The calculated worth of a bank may be defined as

$$k_{eff}(\text{rods out}) - k_{eff}(\text{rods in}) = \Delta k_{eff_{(o-I)}}.$$

This relationship can be shown readily to be equal to

$$\Delta k_{eff_{(o-I)}} = k_{eff_{(o)}} \frac{\bar{\Sigma}_a^{CR}}{\bar{\Sigma}_a + \bar{\Sigma}_a^{CR}}, \tag{1}$$

and the change in reactivity of the core with rods moved from in to out as

$$\Delta\rho_{(o-I)} = \frac{\Delta k_{eff_{(o-I)}}}{k_{eff_{(o)}}} = \frac{\bar{\Sigma}_a^{CR}}{\bar{\Sigma}_a + \bar{\Sigma}_a^{CR}}, \tag{2}$$

where $\bar{\Sigma}_a^{CR}$ is an effective absorption cross section associated with the control rods, and $\bar{\Sigma}_a$ is the absorption cross section of the unrodded core.

The measured bank worth is obtained from a summation of "N" differential worths of the bank, all determined from criticality and near criticality readings:

$$\Delta\rho_{(o-I)} = \Delta k_{eff_{(o-I)}} = \sum_{i=1}^{N} \Delta k_{eff_i} = \sum_{i=1}^{N} \frac{\Delta\Sigma_a^{CR_i}}{\bar{\Sigma}_a + \bar{\Sigma}_a^{CR_i} + \Sigma_a^{B_i}} = \frac{\bar{\Sigma}_a^{CR}}{\bar{\Sigma}_a + \bar{\Sigma}_a^{CR}}, \tag{3}$$

where $\Sigma_a^{B_i}$ refers to variable poison (such as $H_3BO_3$) used in calibrating the rods. It follows from Eqs. (2) and (3) that

$$\Delta k_{eff_{(o-I)}}^{\text{calculated}} = k_{eff_{(o)}} \Delta k_{eff_{(o-I)}}^{\text{measured}}.$$

2. Resonance Interference

a. Improved Estimate of Escape Probability. The use of the Wigner rational approximation for the probability of escape of neutrons from a lump leads to the well-known equivalence theorem in resonance absorption, that is, under appropriate weak assumptions, resonance absorption in a heterogeneous system may be represented as that in a homogeneous system of the same average composition, but with added potential scattering. The shortcomings of this proposal resides in the fact that the Wigner rational approximation seriously underestimates the escape probability over much of the range. Various ad hoc proposals have been made to remedy this

situation by altering the effective mean chord length of the lump, either uniformly for all resonances[6,7] or resonance by resonance.[8]

By means of the latter technique it has been shown that a simple weighting procedure produces an estimate of the effective mean chord length, $\ell_e$, which will preserve the value of the resonance integral. The representation is given in terms of an iterative scheme based on the equations

$$\ell_e^{-1} = \frac{1}{n}\left[\frac{1}{2}(\ell_0^{-1} + \ell_n^{-1}) + \sum_{i=1}^{n-1} \ell_i^{-1}\right];$$

$$\ell_i = \ell[\Sigma(\theta_i)] \text{ with } i=0,1,2,\ldots,n;$$

$$\theta = \tan^{-1} x\,[1 + (\Sigma_0/\Sigma_m)]^{-1/2};$$

$$\Sigma = \frac{\Sigma_0}{1 + x^2} + \Sigma_p;$$

$$\Sigma_m = \Sigma_m(\ell_e).$$

Here $\theta_0 = 0$, $\theta_n = \pi/2$, and the $\theta_i$ are determined by

$$\int_{\theta_{i-1}}^{\theta_i} \cos^2\theta \, d\theta = \frac{\pi}{4}\frac{1}{n} \text{ with } i = 1,\ldots,n-1.$$

The quantity $\ell[\Sigma(\theta)]$ has been given a convenient numerical representation by Otter.[9] The dependence of $\Sigma_m$ on $\ell_e$ and the potential scattering $\Sigma_p$ makes the process an iterative one. Starting with $\ell_e = \ell$, the actual mean chord length, the first iteration is often sufficient.

b. A Simple Estimate of the Effects of Resonance Interference. When two resonance absorbers are present in a medium but one level predominates by reason of level parameters or nuclide abundance, the absorption in the second level or isotope may be calculated by assuming the flux to be determined by the first resonance. Assuming the two levels to be close, using the intermediate resonance approximation, and neglecting interference scattering, we obtain the resonance integral (RI) for the second resonance as

---

[6] M. M. Levine, Resonance Integral Calculations for $U^{238}$ Lattices, Nucl. Sci. and Eng. 16, 271-279 (1963).

[7] G. I. Bell, Theory of Effective Cross Sections, LA-2327 (1959).

[8] J. M. Otter, Escape Probability Approximations in Lumped Absorbers, NAA-SR-9744 (Aug 1, 1964).

$$RI_2 = \frac{I_{0,2}}{\beta_\lambda} \frac{\Gamma_1}{\Gamma_2} \frac{E_2}{E_1} \left[ 1 - \frac{(\Gamma_1^2 - \Gamma_2^2)\beta_\lambda + 4(E_2 - E_1)^2}{\Gamma_2^2(1+\beta_\lambda)} \right].$$

Here $I_{0,2}$ is the infinite dilution resonance integral for level 2, $\Gamma_i$ is the total width, $E_i$ the resonant energy, and $\beta_\lambda$ is given by

$$\beta_\lambda^2 = 1 + \frac{\sigma_{01}}{s_1 + \lambda\sigma_{p_1}} \frac{\Gamma_{1\gamma} + \lambda\Gamma_{1_n}}{\Gamma_1},$$

where $\lambda$ is an intermediate parameter; $\sigma_{01}$ the peak cross section for isotope 1; $\Gamma_{1\gamma}$, $\Gamma_{1n}$, $\Gamma$ are the gamma, neutron, and total widths of resonance 1; $s_1$ is the excess scattering per atom of isotope 1; and $\sigma_{p_1}$ is the potential scattering. This formula must not be used if $E_1 - E_2 \gg {}^1\Gamma_2$; a more generally applicable formula is

$$RI_2 = I_{0,2} \frac{E_2}{E_1} \left[ 1 + (1 - \beta_\lambda^2) \frac{\Gamma_1}{\beta_\lambda} \frac{(\Gamma_2 + \beta_\lambda\Gamma_1)}{(\Gamma_2 + \beta_\lambda\Gamma_1)^2 + 4(E_2 - E_1)^2} \right].$$

3. Total Neutron Cross Sections

The total cross section for two purely scattering $\ell = 0$ resonances was calculated both as the sum of the cross sections of two single-level resonances and also by use of a multilevel formula for two resonances. A Fortran code was written for the CDC 160A computer to perform the computations. In the calculations, values of A (atomic weight) and $r_0$ (nuclear radius) were chosen to give a phase shift of 45° at the one resonance energy, $E_1 = 750$ keV, which was held fixed in all problems. The values of the widths $\Gamma_1$ and $\Gamma_2$ were taken to be equal, and the values of $E_2$ differing from $E_1$ by $n\Gamma$, with n varying from 1 to 5, were used.

Cross sections calculated from use of the multilevel formula showed minima of zero on the low-energy sides of each resonance, and maxima of $4\pi/k^2$ on the high-energy sides. Cross sections calculated from the single-level formula actually became negative over a certain range of energy on the low-energy side of the resonance with the lower value of $E_i$. Also, the cross sections become greater than $4\pi/k^2$ over an energy range on the high-energy side of the resonance with the larger $E_i$. The shapes of the single-level and multilevel curves became progressively more different as the resonances moved closer together, and were drastically different when the resonance energies differed only by $\Gamma$.

## 4. ZPR-VII Data Analysis

The two-region version of the cylindrical lattice collision probability codes[9] has been programmed for the CDC 3600. An analytical approximation was used for the $K_{i3}$ functions, rather than numerical integration as in the IBM-704 version. Results of test problems were in exact agreement with the corresponding 704 problems.

## 5. Correction for Resolution Losses of Radiation-counting Equipment

A description of a means of comparing various formulas for resolution-loss correction was reported in Progress Report for December 1961, ANL-6485, p. 43. Further work has produced a new technique for measuring resolution losses; an improved theory which is relatively independent of equipment characteristics; and methods for determining equipment characteristics by analysis of calibration data.

a. Formulas for Resolution-loss Correction. Older methods for resolution losses are shown to accommodate no more than first-order measured corrections; however, they include various arbitrary higher-ordered terms. The older formulas have been expressed in power series for the convenience of comparison and evaluation.

In the following equation, the relation of a corrected count rate N is given as a function of the observed count rate n. The term N is also a function of radiation source activity S and counter efficiency E, i.e., $N = SE$, as well as source decay constant $\lambda$, since, typically, $S = S_0 \exp(-\lambda t)$.

$$N = n(C_0 + C_1 n + C_2 n^2 + C_3 n^3 \ldots). \qquad (1)$$

The coefficients $C_0$, $C_1$, $C_2$, ... may be solved by determinants applied to a series of measurements of the ratio $N/n$ when using different source intensities. The intensities should typically be decade multiples. The number of coefficients obtainable is known to be one less than the number of measurements made, because of mathematical restrictions. However, $C_0$ is seen to be unity.

The equation may be rewritten for the case involving only a knowledge of the relative source intensities $R_2$, $R_3$, ..., $R_j = N_j/N_1$, and the measured count rates $n_1$, $n_2$, $n_3$, ..., $n_j$. The relation between the two sets of coefficients is

$$C_i = C_i' N_1/n_1 = C_i'/C_0', \quad \text{and } C_i \geq C_i';$$

$$(n_1/n_j)\, R_j = C_0' + C_1' n_j + C_2' n_j^2 + C_3' n_j^3 + \ldots . \qquad (2)$$

---

[9] E. M. Pennington, Cylindrical Lattice Collision Probability Codes, B692/RP, ANL-6836, (Feb 1964).

Equation (1) is conveniently rewritten with $C_0 = 1$ and $C_1 = \tau$, the resolving time. The coefficients are redefined as $c_i = C_i/\tau^i$.

$$N = n[1 + c_1 n\tau + c_2(n\tau)^2 + c_3(n\tau)^3 + \ldots]. \qquad (3)$$

Equation (3) serves as an interpolation formula between calibration points obtained with known relative source intensities and fixed geometry, or with fewer sources and varied geometry. All coefficients may be determined analytically by means of Eq. (1) or (2). Interestingly, the established formulas for resolving loss correction all yield the same series expansion as Eq. (3), but with differing values of the coefficients $c_i$. These were obtained by simple methods, including iteration and reversion of series, with results shown in Table XI.

Table XI. Power Series Coefficients of Resolving Loss Formulas

| Formula for N | $c_1$ | $c_2$ | $c_3$ | $c_4$ |
|---|---|---|---|---|
| $\frac{n}{1 - n\tau}$ | 1 | 1 | 1 | 1 |
| $\frac{n}{1 - N\tau}$ | 1 | 2 | 5 | 14 |
| $n \exp(N\tau)$ | 1 | 3/2 | 8/3 | 125/24 |
| $n \exp(n\tau)$ | 1 | 1/2 | 1/3! | 1/4! |
| $\int_t^\infty N dt = \int_t^\infty n \exp(N\tau) dt$ | $\lambda/2$ | $\lambda^2/3$ | $\lambda^3/3$ | $\lambda^4/5$ |

The values of $c_2$, $c_3$, and $c_4$ are to be arbitrary in the formulas of Table XI, thus affecting all terms beyond the first-order correction. Measurement of these coefficients avoids arbitrary assumptions and extends the range in which accurate data corrections may be made, as well as providing a basis for evaluation of equipment characteristics.

b. Formulas Showing Equipment Characteristics. The fitted values of the $c_i$ terms may be related to equipment characteristics by comparison with like coefficients of a suitable derived formula. The following formulas apply to a particular type of counting device and include explicit terms for certain characteristics as described in the derivation. A typical counting device scales at a rate n. However, some fraction $F_1$ of the observed counts consists of single resolved events, which occur at a rate $P_1 = nF_1$, and other fractions $F_2$, $F_3$, $F_4$, ... consist of unresolved pairs of events ($F_2$), and longer sequences. For such equipment the following equations apply:

$$n = \sum_{i=1}^{\infty} P_i = n \sum_{i=1}^{\infty} F_i;$$

$$N = \sum_{i=1}^{\infty} iP_i = n \sum_{i=1}^{\infty} iF_i;$$

$$N = n + \sum_{i=2}^{\infty} (i-1)P_i = n(1 + F_2 + 2F_3 + 3F_4 + \ldots). \tag{4}$$

If a scaled event is accompanied by an average interval $\tau$ during which resolution cannot occur, and events occur randomly at an average rate N, then the probability that a scaled event will be followed by an unresolved event is approximately the following:

$$N\tau \doteq F_2 + F_3 + F_4 + \ldots = \sum_{i=2}^{\infty} F_i.$$

Elementary statistical considerations indicate that each of these events occurs before expiration of the interval $\tau$ and that a more precise statement may be written in which $b_1 \doteq 1/2$, $d_1 \doteq 1/4$, etc., since each event in an unresolved sequence cuts short the pre-existing interval by about one-half. Thus,

$$N\tau(1 - b_1 N\tau - d_1 N^2\tau^2 - \ldots) = \sum_{i=2}^{\infty} F_i.$$

If the $i^{th}$ event of each unresolved sequence of i events is followed by an average interval $B_i\tau$ during which resolution cannot occur, the following general term can be written, which is substituted into Eq. (4) with a new coefficient $A_i = B_i(1 - b_{i-1}B_{i-1} - d_{i-2}B_{i-2} - \ldots - X_1B_1)$:

$$B_i N^i \tau^i (1 - b_i B_{i-1} N\tau - \ldots) = F_{i+1} + F_{i+2} + \ldots = \sum_{j=i+1}^{\infty} F_j;$$

$$N = n(1 + N\tau + A_2 N^2\tau^2 + A_3 N^3\tau^3 + \ldots).$$

Reversion of this equation by iteration produces Eq. (5) having like coefficients with Eq. (3):

$$N = n[1 + n\tau + (A_2+1)n^2\tau^2 + (A_3+3A_2+1)n^3\tau^3$$

$$+ (A_4+4A_3+2A_2^2+6A_2+1)n^4\tau^4$$

$$+ (A_5+5A_4+10A_3+5A_3\,A_2+10A_2^2+10A_2+1)n^5\tau^5 + \ldots]. \qquad (5)$$

This equation corresponds with the first and second formulas of Table XI: the first having the property that $0 = A_2 = A_3 = \ldots$ ; and the second that $1 = A_2 = A_3 = \ldots$ .

If the statistical consideration is introduced that $b_i \doteq 1/2$, $d_i \doteq 1/4$, ... , and if $1 = B_1 = B_2 = \ldots$ , then $A_2 \doteq 1/2$, $A_3 \doteq 1/4$, $A_4 \doteq 1/8$, ... , and the higher terms of the $A_i$ sequence are inconsequential in Eq. (5). The appearance of smaller values of the $A_i$ terms indicates heavy dependence on scaled events and little dependence on unresolved events. The appearance of a sequence where $A_i \doteq A_{i-1}/2$ indicates a heavy dependence on the terminal event, regardless of the length of an unresolved sequence (i.e., systems with relatively short memories). The $c_i$ terms obtained for such systems should be nearly identical to those shown for the Poisson approximation, in Table XI. Larger $A_i$ values indicate increased dependence on length of unresolved sequences, or systems having relatively long memories.

c. Formula for Measurement of Rapidly Decaying Activities.

(i) Counting Intervals of Several Half-lives Duration. The preceding formulas apply to steady count rates. In counting rapidly decaying activities, the count rate may vary significantly during the counting interval.

The corrected count S during a counting interval t, and the measured count s were related by the following derivation which utilizes the Poisson approximation to relate N to n:

$$S = \int_0^t N\,dt = \frac{-1}{\lambda}[N_t - N_0] = \frac{N_0}{\lambda}[1 - \exp(-\lambda t)];$$

$$s = \int_0^t n\,dt = \int_0^t N \exp(-N\tau)dt = \frac{1}{\lambda\tau}[\exp(-N_t\tau) - \exp(-N_0\tau)].$$

As t becomes infinite, N decays to zero, and the terms $S_\infty$ and $s_\infty$ for long counting intervals are easily related by the common factor $N_0$, yielding the fifth equation indicated in Table XI.

$$S_\infty = \frac{N_0}{\lambda} = s_\infty[1 + \frac{1}{2}(s_\infty\lambda\tau) + \frac{1}{3}(s_\infty\lambda\tau)^2 + \ldots + \frac{1}{j}(s_\infty\lambda\tau)^{j-1}]. \qquad (6)$$

(ii) Counting Intervals of Half-life or Longer Duration. For variable counting intervals polynomial solutions may be derived; however, an exact series, Eq. (7) below, is not convenient to use and approximations are limited to restricted ranges of $\lambda t$:

$$F_j = \frac{(-1)^{j-1}}{j!} \frac{[1 - \exp(-j\lambda t)]}{[1 - \exp(-\lambda t)]^j} = \frac{(-1)^{j-1} [(j\lambda t) + \frac{1}{2!}(j\lambda t)^2 + \ldots]}{j! \quad [(\lambda t) + \frac{1}{2!}(\lambda t)^2 + \ldots]^j}.$$

For large values of $(\lambda t)$,

$$F_j \doteq \frac{(-1)^{j-1}}{j!},$$

and

$$S = s[1 - F_2(s\lambda\tau) + (2F_2^2 - F_3)(s\lambda\tau)^2 - (5F_2^3 - 5F_2F_3 + F_4)(s\lambda\tau)^3 + (14F_2^4 - 21F_2^2F_3 + 3F_3^2 + 6F_2F_4 - F_5)(s\lambda\tau)^4 + \ldots]. \quad (7)$$

(iii) Counting Intervals of Half-life or Shorter. Another series was derived for use with small values of $\lambda\tau$.

Defining

$$G = \frac{1 + \exp(-\lambda t)}{1 - \exp(-\lambda t)},$$

we obtain

$$S = s\left\{1 + s\lambda\tau\left(\frac{G}{2}\right) + \frac{3}{2}(s\lambda\tau)^2\left[\left(\frac{G}{2}\right)^2 - \frac{1}{96}\right] + \frac{8}{3}(s\lambda\tau)^3\left[\left(\frac{G}{2}\right)^3 - \frac{1}{16}\left(\frac{G}{2}\right)\right] + \ldots\right\}. \quad (8)$$

Since

$$s\lambda\tau\left(\frac{G}{2}\right) \rightarrow \frac{s}{t}\tau = n\tau \text{ as } t \rightarrow 0,$$

this series corresponds almost identically term-by-term with those of the Poisson approximation for short-counting intervals.

Although some discretion may be required in applying these results to other equations, it appears that the substitution of the F and G terms should apply reasonably accurate corrections into series having coefficients similar to those of Table XI.

(iv) Effect of Correction for Length of Counting Interval. As may be seen by comparison of Eqs. (6) and (8), the first-order correction may vary radically if counting intervals vary between long and short. Since the correction depends on the second power of $\lambda t$, the correction is negligible with short counting intervals. The following approximations indicate the nature of this correction:

$$s\lambda\left(\frac{G}{2}\right) = \frac{s}{t}\left(1 + \frac{\lambda^2 t^2}{12} - \frac{\lambda^4 t^4}{720} + \frac{\lambda^6 t^6}{30{,}240} + \ldots\right);$$

$$S \doteq s\left\{1 + \left(\frac{s\tau}{t}\right)\left(1 + \frac{\lambda^2 t^2}{12}\right) + \frac{3}{2}\left(\frac{s\tau}{t}\right)^2\left(\frac{95}{96}\right)\left(1 + \frac{\lambda^2 t^2}{12}\right)^2 + \ldots\right\}.$$

d. Limitations of Formulas for Resolving-loss Correction.

(i) Poisson Approximation. The Poisson approximation indicates a maximum at $n\tau \doteq 0.37$, or $N\tau = 1.0$, since $dn/dN = 0$. Obviously a small variation of n near that region, such as is inherent in counting statistics, results in a variation proportional to $dN/dn$ in the estimate of N. Series approximations converge slowly, and iteration requires essentially an equal number of operations, if $n\tau > 0.25$. The series generally produce only a single estimate of N for a single n although the Poisson approximation is double-valued, and is satisfied by either a small or a large estimate of N for any value of $n\tau < \exp(-1)$.

(ii) Interpolation Formula. Although a set of calibration data may be fitted by an interpolation formula, the comments relative to the Poisson formula apply in the vicinity of any maximum in n. The other possibility is that the equipment may saturate, so that $dn/dN$ approaches zero asymptotically as N increases. The region where $dn/dN$ is small ( or $dN/dn$ is large) may require least-squares fit if extension into this region is considered necessary.

## 6. An Analytical Method for Optimizing Reflector Located Control Vane Thickness

The thickness of the poison region of a reflector located control drum will usually have an optimum thickness in terms of its control effectiveness. This is partially due to the fact that as thickness of the poison region increases, the average distance over which the poison is moved between the most and least reactive configurations becomes smaller. The poison self-shielding effect is the other significant aspect. Reflector composition and geometry also have significant bearing on the study.

By considering only the geometrical effect of decreasing distance of poison movement, it was determined analytically that the optimum vane

thickness is 1/3 of the control drum radius. This result does not take into account the important self-shielding effect which, by decreasing the effectiveness of the lumped poison, results in small optimum vane thicknesses. An analytical method was devised which uses the perturbed real and adjoint fluxes of a radial DSN calculation with a perturbation code written for this purpose in CDC 160-A Fortran. The code uses the product of the perturbed adjoint and real fluxes by fitting them through a least-square approximation to various reflector vane thicknesses. That product is then weighted by the capture cross section of the absorber and integrated over the reflector for the "in" and "out" positions of the control drums. The optimum control vane thickness is the one which produces the maximum difference for the in and out control position integrals.

Preliminary calculations for an $Al_2O_3$ reflector that is 20 cm thick with a 20-cm diameter imbedded drum show that the optimum vane thickness is ~2.7 cm.

## C. High-temperature Materials Development

### 1. Ceramics

Among the fertile and fissile materials being studied or developed for reactor use at a maximum temperature in the range from 750 to 2000°C are the ceramic compounds of uranium, of plutonium, and of thorium, and various mixtures or solid solutions of these compounds. Some of the binary compounds have melting temperatures of about 3000°C. Although most of the work on ceramic fuels has been on the oxides and the carbides, the sulfides, phosphides, and such combinations as UP-US, UC-US, PuS-US, and PuP-UP are receiving considerable attention. The arsenides, antimonides, and tellurides will eventually be investigated.

Some of the more important considerations, besides melting point, are thermal, chemical and irradiative stability, fabricability, composition control, the effects of impurities, compatibility with cladding materials, mechanical and elastic properties, volatility, thermal conductivity and thermal expansion. No one of the binary compounds has all the desired characteristics in sufficient degree, but no one of the compounds is beyond the possibility of improvement through certain modifications and combinations of compounds. Considerable emphasis is therefore being given to preparing these ceramics and studying their properties.

a. Anelasticity of Some Group V and VI Uranium Compounds. The four bars of $UO_2$ of rectangular cross section (see Progress Report for September 1964, ANL-6944, p. 61) could not be successfully surface ground. In order to surmount this problem a technique involving lapping was worked out. The results were encouraging. A specimen was prepared in which the faces were kept flat and parallel within four mils.

In order to check some of the results obtained previously, pellets with different amounts of $Nb_2O_5$ were prepared and sintered at 1750°C and 1450°C. The densities of the batch sintered at 1750°C agreed fairly well with those obtained previously (see Progress Report for July 1964, ANL-6923, p. 53), although the decrease of density in the pellets with more than 0.4% $Nb_2O_5$ addition is less marked than previously observed. Density was determined by the Archimedes displacement method, with $CCl_4$ as the medium.

b. Thermal Stability. All phases of the thermal stability of ceramic materials have become of increased importance as a result of interest in higher operational temperatures and special operating conditions of nuclear reactors. The need for the prolonged maintenance of high fuel-center temperatures requires that more information be had, especially rate data, concerning the volatility of fuel materials, migration of fuels, compatibility, and reactions of fuels with gaseous and solid contaminants and coolants. The same need is present for nonfuel reactor ceramics.

An apparatus has been constructed for the study of evaporation rates of ceramic materials as affected by variations in the operating environment of temperature, pressure, and atmosphere. Total weight change and rate of weight change during testing are determined in different environments. The apparatus can be used to 2500°C in the pressure range from $5 \times 10^{-6}$ Torr to 1.5 atm of an inert gas or hydrogen. The balance can determine a weight change of 0.1 mg.

Preliminary and calibration tests are being made with polycrystalline MgO as the reference material. Observations have been made of evaporation rates in vacuum at temperatures in the range from 1700 to 2050°C. Complete characterization of the materials are being made, before and after testing, to determine changes in grain size, microstructure, density, and other properties which may correlate with the test results.

c. Measurements of Thermal Properties. The intermediate-temperature furnace was put into operation, and a thermocouple pickup was used to obtain diffusivity values of Armco iron between room temperature and 1000°C. The data obtained, shown in Figure 16, are in fairly good agreement with results obtained at the U. S. Naval Radiological Defense Laboratory.

Considerably more experimentation is needed to extend the capability of this system to the measurement of heat capacities of all substances and of the thermal diffusivity of nonmetals. An increase in the energy transferred from the flashtube to the specimens in the furnace is required. In the case of the intermediate-temperature furnace an additional capacitor is being installed to effect the increase. In the case of the tantalum-heater high-temperature furnace a laser will probably be necessary to accomplish the transfer of the energy flash to the specimen

efficiently enough to raise the sample temperature adequately. Work is proceeding on the high-temperature furnace and optical detection and amplification devices.

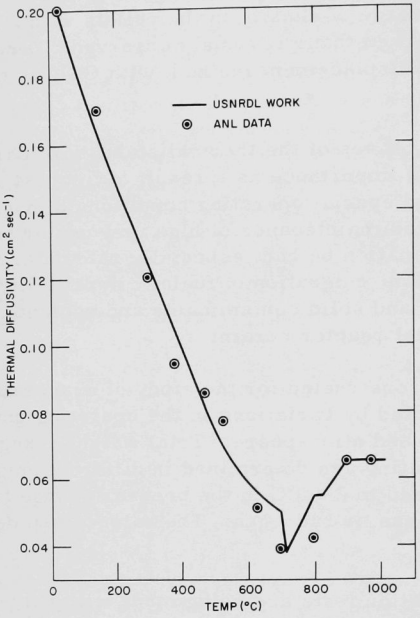


Figure 16

Thermal Diffusivity of Armco Iron

d. Mechanical Properties of Uranium Compounds. Fracture tests have been carried out with specimens of $UO_2$, prepared in batches from a bulk sample of powder and mainly at room temperature. Results are expressed in Table XII.

Table XII. Fracture Test Data for $UO_2$

| Batch Number of Samples | Density, gm/cc | | Modulus of Rupture kg/cm² | | Load Rate, lb/sec | (g/sec) | Temp, °C |
|---|---|---|---|---|---|---|---|
| | Mean Value | Standard Deviation σ | Mean Value | σ | | | |
| 5 | 10.58 | 0.009 | 841 | 128 | 0.15 | (68) | R.T. |
| 5 | 10.44 | 0.07 | 599 | 37 | 0.15 | (68) | R.T. |
| 5 | 10.26 | 0.025 | 944 | 18 | 1.50 | (680) | R.T. |
| 2 | 10.47 | 0.07 | 1128 | 53 | 1.50 | (680) | 1020 |

Density measurements on the fractured test pieces revealed a decrease of from 1.0 to 2.1%. Checks on unbroken samples, and by techniques other than the normal suspension weighings in air and in a liquid, confirmed that the changes were real. Specimens tested at slow rates, 68 g/sec (0.15 lb/sec), showed drops in density from 1.0 to 1.4%, those tested at a higher rate, 680 g/sec (1.5 lb/sec), a drop of 1.4 to 2.1%. This can only result from the production of internal voids or vacant lattice sites. Microscopic examination does not indicate any great enlargement of the pores, except close to the fracture itself, so that vacancies may be mainly responsible. The results are of the order previously found in cubic lattices where vacancies have been formed by quenching. Vacancies of such order would indicate some considerable slip taking place in the $UO_2$ during stressing, probably by cross slip. These points may be resolved by electron microscopy.

The high-temperature furnace has only recently been recommissioned after repair, and has functioned very well. Pressures as low as $2 \times 10^{-6}$ mm Hg have been obtained at room temperature, and $6 \times 10^{-6}$ mm at 1500°C over a period of 75 min. Temperatures have been taken to 1960°C with no difficulty.

## 2. Corrosion by Liquid Metals

The development of fuels and materials for reactor service at high temperatures is invariably associated with problems of corrosion. One corrosive medium of some concern is eutectic bismuth-tin alloy, which has been used as a fusible sealant, but is being investigated primarily as part of an attempt to correlate absolute corrosion rates with critical parameters. The dissolution kinetics of Type 304 stainless steel in Bi-42 w/o Sn, a eutectic alloy, is being studied as part of the investigation. Preliminary values of the overall heats of solution of Fe, Cr, Ni, and Mn from the stainless steel have been determined from equilibrium solubility data obtained in the temperature range from 450 to 985°C.

A dissolution run has been made at a rotational speed near the transition from a process that is controlled by liquid diffusion to one that is surface controlled. The results of chemical analyses of metal samples are awaited. An additional run at 1000°C and 10 rpm is needed to confirm the temperature dependence of the dissolution process under liquid-diffusion control at lower rotational speeds.

## 3. Throium-base Fuels

a. Potential Cladding Materials for Thorium-Uranium-Plutonium Alloys. Thorium is of outstanding promise for use in fuel alloys for power production. Not only is thorium the most abundant potential source of fuel but - quite aside from its breeder potentialities - thorium shows promise

of being a useful and economical base for alloying with uranium and plutonium to form a stable, compatible fuel capable of operating at reasonably high temperatures.

A study of thorium-uranium-plutonium alloys has been undertaken to determine the usefulness of these alloys as nuclear fuels from a metallurgical point of view. One program is concerned with the structure of these alloys, phase diagrams, transformation kinetics, and heat treatment; another is concerned with engineering properties. Considerable progress has been made in studying the phase diagram and in determining properties and fabricating characteristics, but information was lacking on the compatibility of thorium-base fuel alloys with potential cladding materials.

Stainless steel was considered as a cladding for the thorium-uranium-plutonium alloys because of its availability in tubular form, its known technology, and its excellent resistance to molten sodium. Compatibility tests in a manner described by Walter,[10] as applied to uranium-fissium alloys, were carried out with Type 304 stainless steel in contact with each of the following three alloys: Th-4 w/o U; Th-4 w/o U-10 w/o Pu, and Th-4 w/o U-20 w/o Pu. The penetrations of the stainless steel into the fuel and of the fuel into the stainless steel were determined metallographically after 7, 17, 42, and 51 days, respectively, at a temperature of 650°C. The results are shown in Figure 17. The penetration of the fuel into the cladding is large enough to eliminate this type of stainless steel, and possibly also all other types, from consideration as high-temperature cladding materials for thorium-uranium-plutonium alloys. The penetration of the cladding into the fuel is even greater. The penetration is only slightly greater for the plutonium-bearing alloys than for the binary thorium-uranium alloy. The diffusion follows the parabolic rate law.

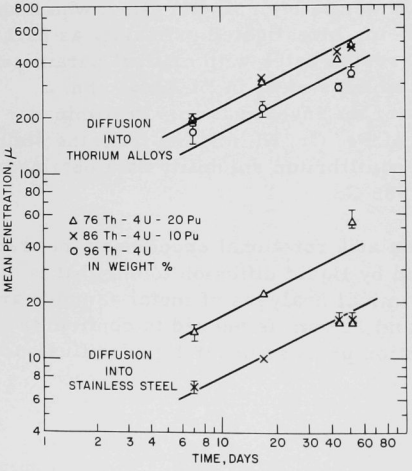


Figure 17. Interdiffusion of Type 304 Stainless Steel and Thorium-Uranium-Plutonium Alloys at 650°C

A single microprobe analysis of a section of the 76-4-20 alloy carried out at the Mound Laboratory showed that the iron and nickel component of the stainless steel diffused farthest into the fuel in agreement with the metallographic observations of the band width. The depth of the chromium diffusion was very small.

[10] Walter, C. M., Interdiffusion between Uranium-5 w/o Fissium Alloy and Type 304 Stainless Steel, ANL-6816 (March 1964).

On the other hand, neither thorium nor uranium penetrated into the stainless steel, but plutonium did.

These results suggested that pure chromium metal might be a satisfactory cladding for plutonium-bearing alloys. A few spot checks, the results of which are shown in Table XIII, were then carried out for 17 days at a temperature of 650°C with Th-10 w/o U-10 w/o Pu and with Th-20 w/o U-10 w/o Pu, selected as a result of a parallel investigation of the ternary thorium-uranium-plutonium phase diagram. In these spot checks the compatibility of these alloys with ductile chromium metal of rather low purity was compared with the compatibility of the alloys with pure nickel, with a nickel-20 w/o chromium alloy, and with a vanadium-20 w/o titanium alloy. Initially, we had difficulties in creating a good bond between the chromium and the fuel. We succeeded, however, in several experiments and, for the test conditions mentioned, the chromium metal showed the lowest penetration rate of the materials investigated.

Table XIII. Interdiffusion of Thorium-Uranium-Plutonium Alloys and Some Cladding Materials for 17 Days at 650°C

| | Fuel | | | |
|---|---|---|---|---|
| | 80 w/o Th-10 w/o U-10 w/o Pu | | 70 w/o Th-20 w/o U-10 w/o Pu | |
| | Penetration ($cm^{-4}$) | | | |
| Cladding Material | Into Cladding | Into Fuel | Into Cladding | Into Fuel |
| V-20 w/o Ti | - | 10[a] | - | 9[a] |
| Ni | -[b] | -[b] | -[c] | 265 |
| Ni-20 w/o Cr | 8 | 116 | 11 | 108 |
| Cr | - | 2.5[a] | - | 2.3[a] |

[a] Total band width in cladding and fuel. No separate bands are discernible.
[b] Did not bond.
[c] Broke apart at band-cladding interface.

## D. Other Reactor Fuels and Materials Development

### 1. Nondestructive Testing

a. Determination of Elastic Moduli of High-temperature Materials by Ultrasonics. Transit times and delay times in a bar of TV-20 alloy (V-20 w/o Ti) have been measured at various temperatures from room temperature to 950°C. Only one temperature run was used to determine both longitudinal-wave and shear-wave velocities. Even though the data have not been fully reduced and the final results have not been calculated, the run seems to be successful.

A scheme of using a thin mica sheet as an insulator between the specimen and a heater coil in direct contact with the sheet did not reduce the thermal gradient in the specimens because the tantalum wire reacted with the mica, and the wire melted.

Another approach to insulating the heater from the specimen was tried. With a plasma torch, a layer of alumina was sprayed on the proper section of a stainless steel specimen, which first had to be sand blasted to get a surface upon which the ceramic would adhere. The tantalum heater wire was then wound over the coated section of the sample. First experiments with this scheme appeared successful. Work was halted on this problem when the TV-20 sample became available; no attempt was made to control the gradient in the TV-20 sample. More work will be done on the gradient problem.

b. Ultrasonic Imaging. A one-megacycle ultrasonic imaging system operating with a 10-cm-diameter $BaTiO_3$ receiving transducer on an ultrasound television camera has been placed in operation. Although the larger useful image area is in one sense an advantage over the 5-cm-diameter, 2-Mc system, the decreased resolution capability of the lower-frequency system is a definite disadvantage for most testing applications. No advantage has been observed on using the 1-Mc system for inspecting fuel plates of the prototype for type $A^2R^2$. The new fuel-plate samples are appreciably more uniform in fuel distribution than those previously tested, and acceptable inspection results can be obtained on using the 2-Mc system. For this particular application, the improved resolution capability of the higher-frequency system is desirable.

c. Development of a Neutron-image-intensification System. The scattering characteristics of the neutron-imaging system, as they might influence either an image intensifier or radiographic detector, have been considered. Some preliminary measurements of the relative scatter intensity for several inspection sample materials and thicknesses have been obtained. These will be compared with similar measurements made with an imaging system containing a radiographic grid between the inspection sample and the detector, and comparisons will also be made by using radiographic quality as a criterion. The neutron radiographic grid, to be made of a series of boron-coated aluminum strips, is now under construction. The aluminum will transmit the desired direct imaging neutron beam while the intervening boron layers will absorb scattered neutrons arriving at the detector at angles of incidence off normal.

d. Correlation of Heat Transfer and Bond Quality. Measurements of thermal diffusivity $\alpha$ and conductivity K have been completed on six roll-bonded specimens prepared from BORAX fuel plates. Data reduction has not as yet been completed.

As a result of an error in the calibration of the system, the values reported for Type 304 stainless steel and the BORAX standard (see Progress Report for July 1964, ANL-6923, Table XXII, p. 60) are incorrect. The correct values are:

| | $\alpha(cm^2/sec)$ | $K(cal\text{-}cm/cm^2\text{-}sec°C)$ |
|---|---|---|
| Type 304 stainless steel | 0.033 ± 0.003 | 0.038 ± 0.004 |
| BORAX standard | 0.028 ± 0.003 | 0.032 ± 0.003 |

e. Infrared Systems for Nondestructive Testing. Work on infrared sensing instrumentation has been renewed. A pair of high-speed scanning mirrors has been constructed that scan a vertical or horizontal line or an area at the rate of 30 to 50 lines/sec. This high scanning rate will give a stationary pattern on an oscilloscope so that the thermal image can be continually observed visually.

2. Polarization Studies in Liquid Metal Environment

A variety of materials have been tested in highly oxygenated sodium at up to 650°C in a search for materials appropriate for electrodes therein. The most appropriate sample materials appear to be zirconium and zirconium alloys such as Zr-3 w/o Ni-0.5 w/o Fe and Zr-1 w/o Cu-1 w/o Fe, which form dark, adherent corrosion-product films that are insulators at room temperature.

Substantial loss of zirconium corrosion product in the oxygenated sodium at 650°C makes simple measurement of weight changes unsuitable for corrosion evaluation unless all of the remaining corrosion product can be stripped from a specimen before the final weighing. Attempts are being made to determine the film thickness either by weighing, stripping and reweighing or by other methods.

a. Method of Evaluation of Film Thickness. In the absence of a well-developed corrosion film-stripping method, a technique for measuring film capacitance has been developed to obtain estimates of relative film thicknesses on corroded zirconium electrodes after polarization experiments in oxygenated sodium. Because of the possibility of film loss during the sodium exposure, weight-change data are open to some question.

To obtain a capacitance measurement, a sample electrode (previously exposed to the sodium) is first anodized to 50-V equivalent film thickness in 80% saturated boric acid solution at room temperature for 100 sec, to eliminate film short circuits that otherwise would interfere with capacitance measurement. The area of the shorted regions being small, their effect on the result is relatively small when anodizing is done in this

manner. The anodizing is followed by careful water washing and vacuum drying. The capacitance is then determined at room temperature with an impedance bridge with a 1000-cps current, which is measured between the electrode metal and a liquid-metal solution of mercury-30 w/o Woods metal in which the corroded region is immersed. The meniscus effect of this solution is virtually absent. The value obtained is frequency-sensitive, and the 1000-cps null values are chosen.

Parallel capacitance values are derived in order to include the effect of dissipation factor, also observed with the bridge. Capacitances were not completely stable, but useful indications of relative film thickness were obtained. Among nine sample electrodes exposed to the oxygenated sodium at 540°C for 20 to 67.5 hr at various polarization currents, the capacitances varied from 4 to 28.5 $m\mu fd/cm^2$. A plot of 1/C versus weight gain suffered from excessive point scatter, due in part perhaps to the large effect of film loss on weight-gain data compared with its effect on capacitance (or on apparent film thickness). A plot of 1/C versus polarizing current gave a result containing substantial point scatter, but which implied maximum thickness at zero polarizing current and decreasing thickness with increasing current of either polarity, in the range from 4 to 22 $mA/cm^2$. A larger number of exposures would be required to verify or disprove this unexpected result. Error due to averaging of total polarization current over the exposed area, where evidence of irregular film shorting exists, may well have contributed to the data scatter.

Concurrently, a technique of film stripping in sodium saturated with calcium at 600°C (see Progress Report for August 1964, ANL-6936, p. 56) is being investigated. Metallographic examination of a sample cross section has verified the existence of a layer of metal, presumably reduced from the corrosion product, on the outer surface of a Zr-1 w/o Cu-1 w/o Fe sample prefilmed in steam and exposed overnight to Na-Ca at 600°C in a stainless steel autoclave. Spectroanalysis obtained by sparking directly to the outer metallic layer showed 10-100% Zr, 0.1-10% Fe, 0.01-1% Ca, 0.01-0.1% Cr, 0.001-0.1% Na, 0.0001-0.001% Ni, and no copper. The lack of copper suggests that the base metal did not interfere with the analysis; however, possibility of a contribution from the unreduced corrosion product has not been ruled out.

Currently attention is centered on corroded, unalloyed zirconium samples. Methods of removing the reduced layer to permit further reduction are being tested. The use of aqua regia as an etchant is being investigated since, owing perhaps to the disperse form of the layer, it attacks the base metal only slowly and appears to dissolve the reduced layer relatively rapidly. This stripping method is in a preliminary stage and requires a substantial amount of further development.

b. Polarization Curves. A form of anodic polarization curve has been measured for several unalloyed zirconium electrodes during polarization in oxygenated sodium at 540°C. The curve is a plot of cell voltage versus time at constant anodizing current, in the range from 4 to 22 $mA/cm^2$. Characteristically, the curves rise to 20 to 40 mV (and occasionally higher) from an unpolarized value of about 4 mV, levels that are presumably related to film thickness. The cell potential is frequently reduced instantaneously, and the potential as a rule rises gradually thereafter nearly to the previous value. Such cycling is interpreted as due to occasional cracking and gradual repair of the corrosion film. No cathodic curves have been obtained.

The emf measured at the beginning and end of a cathodic polarization run at 21.5 $mA/cm^2$ (averaged over surface) was only slightly below that of the unpolarized value. Momentary cathodization, as previously shown, reduces the resistance to subsequent anodizing current to a low value. It thus appears that the techniques of polarization are applicable to the study of the corrosion in this system and that phenomena such as film cracking may be observed more readily here than in other media.

## E. Remote Control Engineering Development

### 1. Electric Master-Slave Manipulator Mark E4

Work has continued on various aspects of this 50-lb-capacity manipulator. The configuration under design has a 30-in. long upper arm and a 40-in. lower arm. This upper arm extension is intended to improve the manipulator capacity to work around large equipment where the access is difficult. A pair of manipulator slave arms are connected to a single grouping of servo drive units to save space and to simplify cooling.

Considerable effort was required to achieve compact design of the shoulder joint between the upper and lower arms for the slave unit. The best shoulder joint, of the several designs studied in detail, is about 17 in. wide. In this joint, the mechanical cables for the servo motions are routed on either side of the counterweights. This arrangement, together with a tight grouping of cables, allows the "Z" motion to move through ±90° without excessive change in cable length. The use of cables, as compared with tapes, on the slave arms permits easier remote repair. Of course, cables have greater friction than tapes.

The design for the master manipulator arms will be modified from the slave design to achieve a more desirable configuration for the operator. Also, to reduce friction, the master will use tapes for all motions except "X," "Y," and "Z," which will be accomplished by direct gear drives. Consideration is being given to enclosing all gearing for these drives on both the master and slave arms in a dust-tight manner.

Sixteen servo amplifiers have been completed. Each has been tested in a breadboard servo mockup. In addition, one of the 3-phase, 1000-cycle-supply amplifiers for the synchros is now complete and has been tested with a 3-phase delta-connected load. The wiring of the amplifier console has been started.

Eight gearboxes have been assembled, except for the synchro drives which are on order. These gearboxes, together with the servo control, will be used to test the independent motions of the manipulator and will be subsequently incorporated into the prototype manipulator.

2. Studies of Higher Force Feedback

Studies are continuing on methods of developing manipulators having a greater degree of static and dynamic force feedback. None of several approaches that are likely to give good results are very simple. Putting pickup transducer between the tongs and the wrist joint and between the handle and the wrist joint still looks like a reasonably good approach even though the total system is quite complicated.

## F. Heat Engineering

1. Two-phase Flow Studies

a. Void Fraction - Pressure-drop Facility. This experimental facility is designed to investigate the two-phase flow characteristics of boiling sodium in forced convection; it is desired to obtain experimental information pertinent to the vapor volume fraction and two-phase frictional losses in an adiabatic test section. The loop is constructed of Type 316 stainless steel and is limited to short-term operation up to approximately atmospheric pressure and about 1630°F.

The flowmeter calibrations at 1000°F have been completed. The eddy-current liquid-level gauges in the differential pressure pots showed a long-term drift effect and have been recalibrated after repairs to the oscillator circuit. Some difficulty was encountered with subcooling control because of low heat losses and inadequate power control to the homogeneous boiler section. The cleanup apparatus for the argon control system started to plug after approximately 1000 hr of intermittent operation; this system was dismantled and recharged with fresh sodium with low oxide concentration and also a new supply of magnesium perchlorate for removal of water vapor.

During the preceding events, the loop logged approximately 750 hr of continuous operation at 1000°F, with two short excursions to 1200°F. As soon as the subcooling control is revised, low-pressure boiling runs will be effected at approximately 1450°F.

2. Boiling Liquid Metal Technology

a. Niobium-1% Zirconium Loop. The design of the Nb-1% Zr loop has been completed and is ready for purchase.

Some work has been started on the design of the support structure for the electromagnetic sodium pump stator and on the layout of the auxiliary equipment.

The vacuum chamber vendor is continuing efforts to seal the defective chamber cooling-water lines. Repair of lines located adjacent to the upper vessel reinforcement ring has proven exceedingly difficult and has not yet been accomplished. Some consideration is being given to the possibility of shipping and beginning installation (at ANL) of the lower portion of the chamber and the vacuum pumping system to avoid further delays in the schedule. The vacuum chamber walkway has been delivered but requires some minor modifications. The possibility of connecting the various vacuum-system cooling-water circuits to a canal water line to be installed in the building has been investigated and found feasible. This would relieve a considerable future drain on the domestic cold-water-supply system. On the other hand no simple way has yet been found to drain cooling water to the storm sewer to ease future loading of the laboratory drain system.

Specifications are being written for several types of equipment for supplying liquid nitrogen to the cryogenic baffle on the chamber. The possibilities include (1) several relatively small transportable tanks manifolded together and closely coupled to the baffle, (2) a large remote (outdoor) stationary storage vessel, (3) a combination of one small and one large mobile tank, and (4) a Stirling-cycle refrigerator. Each of these systems has technical advantages and disadvantages for this application. Cost estimates are necessary.

b. Heater Experiments

(i) Thermal Radiation Heater Experiment. The thermal-radiation-heated, forced-convection loop has operated for 300 hr. NaK temperatures ranging up to 1300°F and flow rates ranging up to 1 gpm have been obtained. The tantalum thermal radiation heater has supplied heat fluxes up to 62,000 Btu/hr-ft$^2$ to the NaK flowing inside a 1/2-in-OD, 0.035-in.-wall, Type 316 SS tube. The information gained from the thermal-radiation-heated section and forced-convection loop is being utilized in the design of the Nb-1% Zr loop and heated section.

(ii) Electron-bombardment-heating Experiment. Assembly of the electron-bombardment-heated sodium pool boiling experiment is progressing. Installation of the thoriated-tungsten wire which will be used as the cathode and the high-voltage wiring have been completed. The present effort is being directed to the installation of the gas system, sodium fill system, and readout equipment.

3. General Heat Transfer

a. Heat Transfer in Double-pipe Heat Exchangers.

(i) Liquid Metal Cocurrent Turbulent Flow. Fabrication and thorough cleaning of the mercury heat transfer loop (see Progress Report for April 1964, ANL-6885, p. 54) has been completed. Calibration of the flow orifices, which will be used in turn to calibrate the electromagnetic flowmeters, has also been completed. Fabrication of the initial nickel test section is in progress. Initial loop operation with mercury will use the stainless steel dummy test section now in place.

(ii) The Counter-current Flow Exchanger. It was reported previously (see Progress Report for August 1964, ANL-6936, p. 61) that a formal analytical solution for the general counter-current flow heat exchanger has been obtained, and as a result useful detailed analyses of counter-current flow cases now appear feasible. It has been learned since that researchers at Syracuse University have also obtained analytical solutions for counter-current flow cases, although their work, supported mainly by the Office of Saline Water, relates more to mass transfer processes than to heat transfer.

The ANL and Syracuse University formulations are nearly the same; both involve equivalent difficulties in theory and application which appear to be at least unusual if not unique in the field of applied mathematics. The ANL formulation is somewhat more general, however, and the method of application presently planned for exploration appears to be different. Further discussion and collaboration are planned.

Separation of variables applied to the general counter-current flow heat-exchanger problem leads to consideration of a "two-region" Sturm-Liouville system for which there exists an infinite set of real eigenvalues extending from $-\infty$ to $+\infty$. The existence of the negative eigenvalues extending to $-\infty$ is the first unusual feature of the mathematics as applied to a physical problem.

Use of an appropriate orthogonality condition for the purpose of expanding the exchanger inlet temperature distributions as an infinite series of eigenfunctions leads to the second unusual feature. Since, with a counter-current flow exchanger, inlet temperatures must be specified for each fluid at opposite ends of the exchanger, the expansion cannot be developed as an initial-value problem. Instead, an infinite set of integral relations result in which the outlet temperature distributions for each fluid occur as unknown functions. Each of the integral relations corresponds to a particular eigenvalue; the "zeroth" member of the set is equivalent to the exchanger overall heat balance.

During the past two months investigations have concentrated on attempts to demonstrate that the infinite set of integral relations are sufficient to determine the outlet temperature distributions, and can be used as a basis for actual computations. Present indications, although based largely on heuristic arguments, are sufficiently convincing to warrent proceeding with detailed numerical machine calculations.

There are other aspects of the problem that deserve to be mentioned at this time. The present form of solution appears to be convenient and practical for the purpose of computing the overall heat exchange effectiveness. Computation of detailed temperature distributions and local heat fluxes, however, do not appear practical except along the central regions of the exchanger. This difficulty is analogous to those usually associated with the practical use of eigenfunction solutions of diffusion-type equations in that sufficiently large values of the "timelike" variable are required. In the counter-current flow heat-exchanger problem small values of the "timelike" variable correspond to regions near both ends of the exchanger. As a result, and as to be expected from physical considerations, fully developed heat transfer conditions, if obtained at all, will occur only along a central region of the exchanger.

4. ANL-AMU Program

Other heat engineering experiments, performed as part of a joint program (not supported by the Division of Reactor Development) between the Laboratory and the Associated Midwest Universities (AMU), are described below.

a. Two-phase Flow Characteristics during the Complete Vaporization of a Fluid. The forced-circulation loop was pressurized with a mixture of Freon and nitrogen to pressures in excess of 800 psia at room temperature. A halogen leak detector unit was employed to locate leaks in the system. Leakage through the packing of several valves was noted and the packing replaced. Very low leakage was found around the sealing couplings for the heater units in the large preheater. It appears that a small amount of leakage around these connections can be tolerated, thereby eliminating the necessity of a major modification in the preheater. The system was vacuum checked and a quantity of Freon 11 distilled into the loop. (It had been previously found that the commercial refrigerant contained a small amount of oil which would probably have deposited on the heating surfaces under high heat flux conditions. Thus all Freon is distilled into the system at a slow rate and the oil thus removed.)

A leak check of the loop under elevated temperatures was instituted by employing the preheaters to increase both the temperature and the system pressure which was increased due to the density change. In actual test operations, the total quantity of Freon in the loop will be varied for the

range of test pressures by adding or bleeding off Freon in an accumulator unit. The centrifugal pump was tested. The suction pressure must be maintained at approximately 50 psia in order to prevent cavitation in the pump.

During the check-out of the preheater units, one of the small heaters underwent a burnout which subsequently contaminated the system. An alcohol-soluble deposit was found on the surfaces of the system. The loop was filled with alcohol which was then circulated and subsequently dumped. Freon was distilled into the loop to remove any remaining alcohol. The Freon was then forced out of the system by pressurizing the loop with nitrogen. The 2-kW heater that was destroyed was not replaced, since remaining heating facilities appear to be adequate.

The inlet and exit sections for the loop, fabricated in England, have been received, and completion of these portions of the loop is imminent. Final shop work on the gamma-ray unit and its installation is expected shortly.

The two-color photography technique to be employed has been checked on an air-water loop. The inversion of color for drops and bubbles was easily distinguished. Only single-sheet color photographs with strobe-lighting have been taken at present. The use of a Fastex camera for the photography will be made in order to check the lighting arrangements.

It is now expected that the Freon flow loop will undergo preliminary operations during the next reporting period.

b. Propagation of Void Waves in an Air-Water System. Before any reliable test data could be taken for investigating the behavior of void waves in an air-water system, a few more preliminary experiments were performed (see Progress Report for August, 1964, ANL-6936, p. 62).

One of the most critical parameters of the main experiment is the length of a test run. The number of cycles, or in this case, the number of void perturbations, for each run must be determined. This number determines how many times a particular experiment is repeated. The analysis of the test data is based on the average values of each of these experiments. It is obvious that increasing the number of cycles will result in a better statistical average; however, an optimum value must be reached. This value was obtained by analyzing runs of various lengths (varying the number of cycles) and calculating the standard deviation of the average void fraction. It was found that runs of length 500 cycles would be the most satisfactory.

Since data-taking for each run is done over a long period of time, it is necessary that the probe measurements be stable during this time. No significant change in void fraction was detected during a 4-hr period.

During the test runs, void fraction measurements will be taken simultaneously with five different probes. All five probes must behave similarly. In reproducibility checks, the largest deviation of any probe from the median was less than 4%.

c. Inception of Hydrodynamic Instability in a Natural-circulation Loop. One of the aims of this study is to compare the experimental results with predictions from available theoretical models. A digital program is now nearly complete to enable obtaining predictions from the Jones' model.[11] The other models under consideration are due to Jahnberg[12] and Solberg.[13]

The analysis of data recorded on charts is time-consuming, and it does not appear feasible to have enough samples for each run for correlation studies. Therefore, it was decided that for most runs, root-mean-square values be plotted against power to obtain the thresholds of instability. Later, some runs will be analyzed to obtain auto- and cross-correlations. Among other things, these correlations will demonstrate whether the hydrodynamic instability is a periodic behavior and, if so, the basic frequency of oscillation will be calculated.

d. Power-to-Void Transfer Functions. The experimental investigation of the transient behavior of steam voids in a reactor coolant channel as heat production in the fuel varies, commonly referred to as the power-to-void transfer function, has been continued at 400 psia. Previous results are contained in Progress Reports for July 1964, ANL-6923, p. 67, and ANL-6936, August 1964, p. 62.

Figure 18 gives the void amplitude response at 400 psia obtained by use of the "one-shot" gamma attenuation technique. The theoretical curve was again obtained by means of the Marchaterre-Hoglund correlation[14] in a digital computer program. The experimental data lie above the theoretical curve in the low-frequency range (0.01-0.30 cps); this might be due to omission of the subcooled boiling region effects in the channel. Figure 19 gives the void phase response under the same experimental conditions as for Figure 18; here the agreement is good between the theoretical prediction and experimental data.

---

[11] Jones, A. B., Hydrodynamic Stability of a Boiling Channel, KAPL-2170.

[12] Jahnberg, S., A one-dimensional Model for Calculation of Non-steady Two-phase Flow, EAES-Symposium, Studsvik, Sweden, Oct 1963.

[13] Solberg, K. O., The 'Kjeller Model' for the Dynamics of Coolant Channels in Boiling Water Reactors, EAES-Symposium, Studsvik, Sweden, Oct 1963.

[14] Marchaterre, J. F., and Hoglund, B. M., Correlation for Two-phase Flow, Nucleonics, 20 (8) (1962).

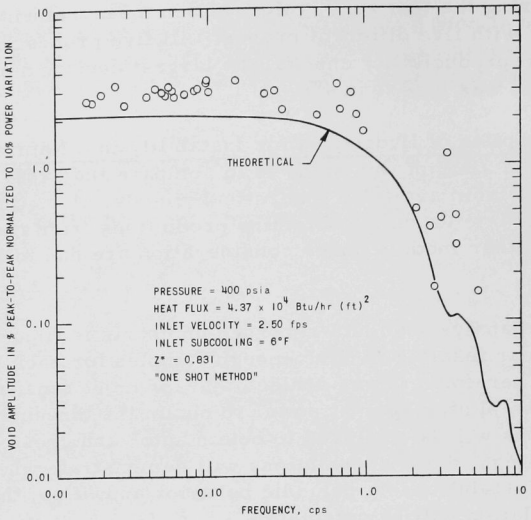


Figure 18. Transient Void Amplitude vs. Frequency by One-shot Gamma-attenuation Technique

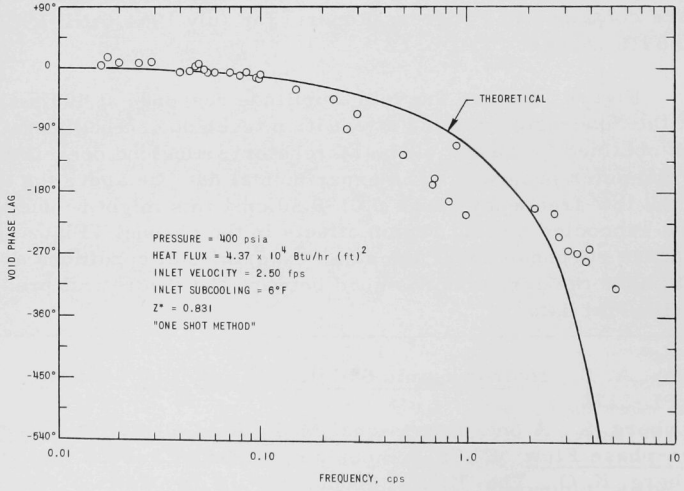


Figure 19. Transient Void Phase-lag Response vs. Frequency by One-shot Gamma-attenuation Technique

Figure 20 gives the transient void amplitude as a function of frequency at various transverse positions which were obtained using a 1/32-in. window in the gamma-attenuation technique. As in the 300-psia results (ANL-6936) a slight two-dimensional effect is evident in that the void amplitude response is higher at the centerline than near the test section wall for the frequency range from 0.01 to 0.10 cps. However, there was no discernible difference in the transient void phase response at each transverse position under the same conditions or with the void phase response obtained using the one-shot method (see Figure 19).

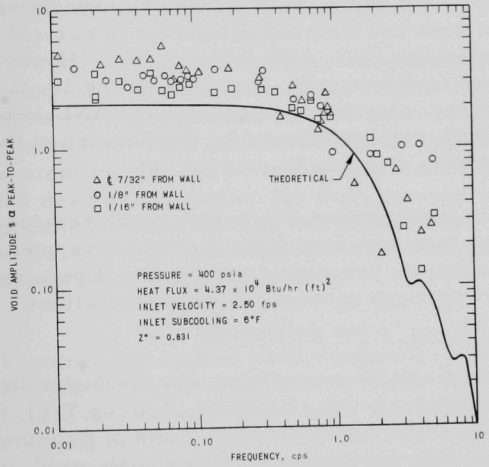


Figure 20

Transient Void Amplitude Response vs. Frequency by Gamma-attenuation Technique with 1/32-in. Window

The linear range of void response to power modulation was obtained at 400 psia employing the one-shot technique (see Figure 21). These results indicate that the response is linear up to at least 20% power modulation peak-to-peak.

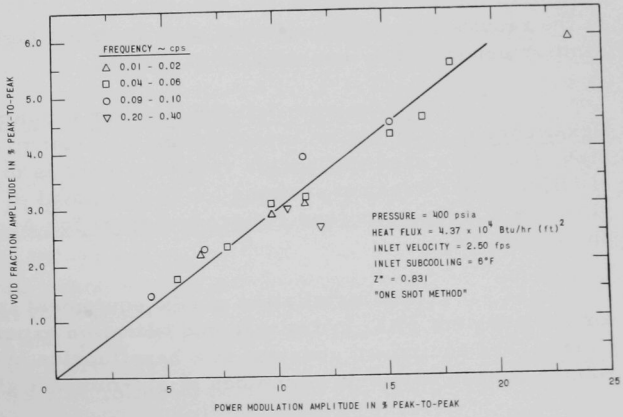


Figure 21

Linearity Range of Void Response to Power Modulation

## G. Chemical Separations

### 1. Fluidization and Volatility Separation Processes

#### a. Recovery of Uranium from Low-enrichment Ceramic Fuels

(i) Laboratory Support Work. The installation of a second fluid-bed reactor (of 2-in. dia) for carrying out laboratory work in support of a fluid-bed fluoride volatility process has been completed. The new reactor will provide greater flexibility for performing laboratory experiments than is possible in the $1\frac{1}{2}$-in.-dia fluid-bed fluorinator reactor in current use (see Progress Report for September 1964, ANL-6944, p. 68). (However, research on process steps will also continue to be conducted in the $1\frac{1}{2}$-in.-dia reactor.) In the 2-in.-dia reactor, chemical decladding (see ANL-6944, p. 69) of unirradiated, clad $UO_2$-$PuO_2$ pellets followed by fluorination of the material resulting from the decladding step can be carried out.

Shakedown runs in which unclad $UO_2$ pellets were reacted first with HF-oxygen mixtures and then with elemental fluorine have been made to test the fluid-bed reactor and its associated equipment. Operation of the equipment was satisfactory, although several minor modifications were indicated.

In other laboratory work, an experiment was conducted in the $1\frac{1}{2}$-in.-dia fluid-bed reactor to evaluate the suitability of Alcoa T-61 alumina for use as the inert fluidized-bed material. This form of alumina is less expensive than the Type RR high-purity alumina previously used. The reaction charge containing $PuO_2$ and fission products mixed with the T-61 alumina bed material was contained in the fluid-bed reactor at the start of the fluorination. The fluorination reaction was conducted with 100% fluorine at three temperatures: 5 hr at 450°C, 5 hr at 500°C, followed by 10 hr at 550°C. At the end of the run, the residual plutonium concentration in the T-61 alumina bed amounted to $<0.007$ w/o, which corresponds to the results previously obtained with Type RR high-purity alumina in similar experiments (see ANL-6944, p. 69).

(ii) Cleanup of Cell Exhaust Air Contaminated with Plutonium Hexafluoride. A program investigating the cleanup of exhaust air from alpha facilities used in fluoride volatility work is directed toward the design of efficient gas-cleanup systems for the removal of $UF_6$ and $PuF_6$ from glovebox atmospheres (see Progress Report for August 1964, ANL-6936, pp. 67-68).

The installation of new equipment in a glovebox facility, for carrying out $PuF_6$ hydrolysis and filtration experiments, has been completed. The equipment consists of a hexafluoride hydrolyzer ($1\frac{1}{2}$-in.-dia column packed with 3-in.-deep bed of 3.2-mm-dia glass spheres) and

auxiliaries which are designed to simulate the conditions of leakage of dilute hexafluoride gas streams into ambient cell air. This equipment replaces older, similar apparatus designed for experiments with $UF_6$ containing no $PuF_6$.

Two tests in which air was diluent have been completed in the new apparatus, one with $UF_6$ and the other with $PuF_6$. The results of the first agree with a test performed in the older apparatus within the range of experimental error. This would suggest that the diluent gas has no effect on the hydrolysis rates.

Preliminary results from the $PuF_6$ test indicate that the behavior of $PuF_6$ is similar to that of $UF_6$. The hydrolysis rates of $PuF_6$ were not higher than twice the rates of hydrolysis of $UF_6$ under similar conditions. This indicated that (1) the design of the exhaust air cleanup system may be based on the data for the hydrolysis of $UF_6$, and (2) most of the design information for $PuF_6$ cleanup systems may be obtained with experiments utilizing $UF_6$, which are less expensive to conduct than those utilizing $PuF_6$. Experiments with $PuF_6$ are being continued to verify and amplify the preliminary data.

(iii) Decladding and Fluorination of Uranium Dioxide Fuels. Development studies have continued on the decladding and fluorination of low-enriched uranium dioxide fuels. Previous work at Oak Ridge, Brookhaven, and Argonne has shown that chemical destruction of stainless steel cladding can be achieved by the high-temperature reaction with oxygen in the presence of hydrogen fluoride (see Progress Report for September 1964, ANL-6944, pp. 69-70). The uranium dioxide fuel is converted to fine particles of uranyl fluoride and a small quantity of $U_3O_8$ and $UF_4$ in the decladding step. Current experimental studies are directed toward establishing operating conditions for the recovery of uranium as uranium hexafluoride by direct fluorination of uranyl fluoride.

A test was performed in a 3-in.-diameter fluid-bed reactor to demonstrate the pulverization of $UO_2$ pellets in a hydrogen fluoride-oxygen atmosphere and the subsequent fluorination of the $UO_2F_2$ to recover $UF_6$. This test represented the processing of $UO_2$ pellets after a Zircaloy cladding had been removed as volatile chlorides in a hydrochlorination step. Approximately 4.5 kg of $UO_2$ pellets and 7.7 kg of alumina grain as the inert fluid-bed material were charged to the reactor. The pellets were pulverized by contacting at 400°C with a gas containing 5 v/o HF, 7 v/o $O_2$, and 88 v/o $N_2$ for one hour, and 43 v/o HF-57 v/o $O_2$ for 3 hr. Screen analysis of the bed material at the end of the reaction step indicated that 75 w/o of the $UO_2$ had been pulverized and that the remainder of the pellets appeared as small lumps containing $UO_2F_2$ and $U_3O_8$. The entire bed was subsequently contacted with fluorine using a processing sequence involving 10 v/o fluorine in nitrogen at 400°C for 5.5 hr followed by 4 hr at 550°C in which the $F_2$

concentration was increased to 90 v/o. The overall fluorine-utilization efficiency based on the conversion of $UO_2F_2$ was 32.5%. The average $UF_6$ production rate over the 9.5-hr fluorination period was 27.7 lb/(sq ft)(hr). The quality of fluidization throughout both the pulverization and fluorination reactions was good, and the fluid bed after fluorination was free-flowing. Development work is continuing to establish process conditions which will result in increased $UF_6$ production rates and fluorine-utilization efficiencies.

(iv) Engineering-scale Alpha Facility. An engineering-scale alpha facility is being installed to permit demonstration of the major steps of the fluid-bed fluoride volatility process for the recovery of uranium and plutonium from ceramic oxide fuels. Shakedown testing of the fluorinator system was temporarily postponed while the off-gas equipment was modified to accommodate hydrogen fluoride and oxygen mixtures which will be used in the processing of stainless steel-clad fuel (see Progress Report for September 1964, ANL-6944, pp. 69-70). Mechanical installation work has continued on the converter system in which mixed uranium-plutonium hexafluoride products from the fluorinator will be converted to oxides. The process piping and instrument piping are now complete. Installation of the piping for the off-gas scrubber located in the small alpha box is in progress, while electrical work in the large alpha box is continuing.

In addition to installation work on the fluorinator and converter systems, testing of the general facilities and developing of special operating procedures are in progress. Procedures are being established for the vertical transfer of objects into and out of the gloveboxes. Tests are being performed on the ventilation controls and alarm system including the emergency air compressor system.

b. Recovery of Plutonium from Rocky Flat Plant Scrap Materials. At the request of the Rocky Flats Division, Dow Chemical Company, a laboratory-scale examination of the applicability of fluoride volatility methods to the recovery of plutonium from scrap materials generated in their plant was carried out. Interest stemmed from the potential savings which may be attained by using a simple, direct method of plutonium separation in which the plutonium would be fluorinated to volatile plutonium hexafluoride with elemental fluorine. For testing purposes, three types of plutonium-bearing scrap materials were submitted: (1) a skull oxide (87.13 w/o Pu) which is relatively pure $PuO_2$, (2) an incinerator ash (11.6 w/o Pu) which contains a number of impurities including C, Ca, Cu, K, Na, Pd, Al, Fe, and Mg, and (3) sweepings (58.8 w/o Pu) composed mainly of $PuO_2$, but also containing, as impurities, C, Si, Ni, Ti, Al, Fe, and Mg. The samples of incinerator ash and sweeping samples were oxidized and hydrofluorinated at Rocky Flats prior to shipment because of their high initial carbon and silicon content.

Samples (2 to 4 g) of the scrap materials, in nickel boat reaction vessels, were heated in a furnace and exposed to elemental fluorine (200 ml/min, except for one experiment at 100 ml/min) for periods of 5 and 10 hr at 500°C or 550°C. The $PuF_6$ produced was collected in cold traps. After fluorination, the sample and boat were dissolved in 4 N $HNO_3$ containing $Al(NO_3)_3$ and a trace of HF, and the residual plutonium determined by alpha counting. Data on the rate of reaction for the skull oxide were also obtained by weighing the $PuF_6$ collected during successive intervals of time.

Except for one fluorination experiment on incinerator ash, plutonium removals of 99% or better were achieved (see Table XIV). When this experiment was repeated, a satisfactory plutonium removal was obtained (98.8% as compared with 82.8%). No explanation for the low result can be offered at this time.

Table XIV. Plutonium Removal from Rocky Flats Scrap Materials with Fluorine in a Boat Reaction

| Scrap Material[a] | Sample Weight, g | Reaction Time, hr | Temp, °C | Fluorine Flow, ml/min | Plutonium in Residue, g | Plutonium Removal, % |
|---|---|---|---|---|---|---|
| Skull Oxide | 2.0795 | 9 | 500[b] | 100[b] | 0.0034 | 99.8 |
| Skull Oxide | 4.1120 | 10 | 500 | 200 | 0.0255 | 99.3 |
| Skull Oxide | 3.6811 | 5 | 550 | 200 | 0.0353 | 98.9 |
| Incinerator Ash | 2.2087 | 5 | 550 | 200 | 0.0455 | 82.2 |
| Incinerator Ash | 2.2103 | 10 | 550 | 200 | 0.0017 | 99.3 |
| Sweepings | 2.151 | 5 | 550 | 200 | 0.0006 | 99.9 |
| Sweepings | 2.1365 | 10 | 550 | 200 | 0.0004 | 99.9 |
| Incinerator Ash | 2.2677 | 5 | 550 | 200 | 0.0004 | 98.8 |

[a]On the basis of Rocky Flats analysis, the plutonium content per gram of scrap material is as follows: skull oxide, 0.8713 g; incinerator ash, 0.116 g; sweepings, 0.588 g.

[b]Temperature from 370°C to 510°C first hour, $F_2$ flow-100 ml/min; temperature from 510°C next 4 hr, $F_2$ flow - 100 ml/min; temperature from 490°C next 4 hr, $F_2$ flow-500 ml/min.

The results of the exploratory experiments appear encouraging. It has been suggested that a recovery process utilizing fluid-bed reactors might be developed which would yield purified plutonium tetrafluoride as a product. Although several areas of research and development will need to be explored in detail before such a process will be fully developed, no further work on this problem is to be done at this Laboratory.

## 2. General Chemistry and Chemical Engineering

a. Preparation of Plutonium Carbide-Uranium Carbide Solid Solution. Studies are being performed to develop a procedure for the preparation of a solid solution of the monocarbides of plutonium and uranium, $\left[U_xPu_{(1-x)}\right]C$. One of the methods investigated is the reaction of

magnesium sesquicarbide with a molten chloride salt containing uranium and plutonium halides. By this reaction the carbides of the heavy metals were formed and the salt phase removed from the carbides by a vacuum distillation at 850°C. The plutonium-to-uranium ratio in the carbide product was approximately the same as in the original salt phase. X-ray diffraction analysis of the carbide product indicated the presence of

(i) a component with a face-centered cubic structure having a lattice parameter of 4.96 Å, which is the value to be expected for solid solutions of plutonium-uranium carbide containing up to 15 a/o plutonium, and

(ii) a component with a body-centered cubic structure having a lattice parameter of 8.09 Å.

Both $Pu_2C_3$ and $U_2C_3$ have body-centered cubic structures with lattice parameters of 8.129 Å and 8.088 Å, respectively, and the product of this experiment is thus seen to contain a sesquicarbide phase in addition to the monocarbide phase. Because of these discouraging results and previously encountered problems, work on the above method for the preparation of a solid solution of uranium and plutonium monocarbide has been discontinued.

b. Preparation of Uranium Mononitride. Uranium turnings (90 g) were reacted directly with nitrogen at 200 to 400 mm Hg pressure and at a temperature which was varied from 1050°C (for $2\frac{1}{2}$ hr at the beginning of nitriding) to 1300°C for the final 45 min. The product, which was dark gray and had the form of the original uranium turnings, was easily ground into a coarse powder (+80 mesh). X-ray analysis of a sample of the nitride product indicated the major phase to be uranium nitride with a minor amount of $U_2N_3$ present. The lattice constant for the UN phase was 4.890 Å, which is in good agreement with recent literature.[15]

The bulk density of the UN powder was 8.0 g/cc, which is higher than any value found in the literature for uncompacted UN powder. Because of these favorable results, apparatus is being prepared to experiment with preparation of UN on a scale of several kilograms per batch. This material will be used in the UN-Na paste studies for fast-reactor, mobile blankets.

The above method produced a more dense product than the standard literature procedures for UN preparation in which a mixture of $U_2N_3$ and $UN_2$ is first prepared by one of the following reactions: (1) direct reaction of uranium with nitrogen at 800-1000°C, (2) reaction of $UH_3$ with nitrogen at 250-350°C, (3) reaction of $UH_3$ with $NH_3$ at 200°C, or (4) reaction of nitrogen with $UCl_4$ dissolved in NaCl at 700-1000°C. The product of these preparations is then decomposed to UN and nitrogen, under reduced pressure, by heating to 1300°C. A typical UN product obtained by by procedure (1) above consisted of powder which could be vibratory-compacted to a density ranging from 5 to 7 g/cc.

---

[15] Evans, P. E., and Davies, T. J., Uranium Nitrides, J. Nucl. Materials, 10, 43 (1963).

c. Thermal Conductivity of Uranium Nitride-liquid Metal Pastes. Knowledge of the thermal conductivity of uranium nitride-liquid metal pastes is required in order to evaluate these pastes as fast reactor blanket materials. It is envisioned that blanket pastes would be moved through tubes in the blanket section of a reactor.

The thermal conductivities of UN-50 v/o Na paste and of UN-50 v/o Bi/Pb eutectic (44.5% Pb, 55.5% Bi) paste has been calculated (for 1500°F) to be 0.086 and 0.042 cal/(sec)(cm)(°C), respectively. The rate of heat generation in blanket pastes would limit the size of tubing for containing a blanket paste with a thermal conductivity of this order of magnitude to diameters only slightly larger than are now contemplated for tubing containing solid blanket elements.

d. Preparation of Uranium Monocarbide. In the preparation of uranium monocarbide (UC) by a fluid-bed process, uranium is hydrided at a temperature of 250°C for about 2 hr to form particles suitable for fluidization. The bed is then fluidized with a hydrocarbon gas and hydrogen to convert the uranium particles to UC at a temperature of 500-600°C.

One run on a scale of 100 g of $UH_3$ has been made in a stainless steel column with a $C_3H_8$-$H_2$ gas mixture, a fluidizing gas velocity of 0.50 ft/sec, a temperature of 600°C, and a run time of $5\frac{3}{4}$ hr. Satisfactory fluidization was obtained, and the low fluidizing gas velocity helped to prevent entrainment of the fine hydride particles in the off-gas stream. The total carbon content of the product was 2.83 w/o, and there was partial sintering of the product.

A more recent run in the same column utilized approximately the same process conditions, except that the fluidizing gas velocity was 0.75 ft/sec during the initial 15 min. There was no sintering. The total carbon analysis for the product from this run is not yet available.

3. Chemical-Metallurgical Process Studies

a. Chemistry of Liquid Metals

(i) Neodymium-Cadmium Galvanic Cell Studies. The thermodynamic properties of the neodymium-cadmium system are being studied by means of the galvanic cell

$$Nd/NdCl_3,\ LiCl\text{-}KCl\ (eutectic),\ LiF/Nd\text{-}Cd\ (2\text{-}phase\ alloy).$$

The emf of the cell has been measured as a function of temperature between 352 and 567°C. A preliminary value for the free energy of formation of $NdCd_{11}$ at 400°C is -37.6 kcal/mole. The activity coefficient of neodymium in the saturated solution ($x_{Nd} = 1.5 \times 10^{-3}$) at 400°C is $4.5 \times 10^{-10}$.

4. Calorimetry

A series of eight calorimetric combustions of holmium in fluorine have been carried out. Calculation of the heat of formation of $HoF_3$ is in progress. Calorimetric combustions of phosphorus in fluorine are being conducted. The value of the enthalpy of formation of phosphorus pentafluoride obtained from this study will ultimately be used in the planned study of the enthalpy of formation of uranium monophosphide.

Eight calorimetric combustions of beta silicon carbide in fluorine have been completed, using samples from two sources. Standard-state calculations have been completed. The combustion results for beta silicon carbide, combined with enthalpy of formation data for $SiF_4$ (-386.0 kcal $mole^{-1}$)[16] and $CF_4$ (-221 kcal $mole^{-1}$),[17] yield a value of -15.5 kcal $mole^{-1}$ for the enthalpy of formation of beta silicon carbide. The major uncertainty in this result is the estimated ±1 kcal $mole^{-1}$ in the enthalpy of formation of $CF_4$. Combustions of alpha silicon carbide are in progress.

## H. Plutonium Recycle Program

### 1. EBWR Plutonium Recycle Experiment

The EBWR 6-in. and 10-in. forced-circulation valve weld radiographs were reviewed. All welds were sound and acceptable, following repairs.

### 2. Plutonium Recycle Vessel Surveillance

a. Irradiation Capsule. An irradiation capsule has been designed to irradiate modified Charpy vee-notch bars of SA-212B vessel steel in the four irradiation thimbles within the EBWR vessel.

Five capsules will be fabricated: two for irradiation within the boron-stainless steel-shielded thimbles; two for irradiation within the bare thimbles; one control capsule in the steam dome. Each capsule will contain 15 impact bars arranged in 5 layers of 3 each. The capsules will be filled with helium to 500 psi, at room temperature, to transfer gamma heat from the steel specimens to the downcomer coolant.

The centerline of the irradiation capsule will be approximately 4 in. below the centerline of a 48-in.-long core which places the irradiation surveillance specimens in a region of maximum flux. This region of maximum flux has been determined to be below the centerline of the core.

b. Charpy Vee-notch Irradiation Specimens. The standard Charpy vee-notch impact surveillance bars would not fit into the 1-in.-ID capsule

[16] Wise, S. S., Margrave, J. L., Feder, H. M., and Hubbard, W. N., J. Phys. Chem. 67, 815 (1963).

[17] This value is currently being adopted by the U. S. National Bureau of Standards for a revision of NBS Circular 500.

in the desired 3-group layer unless two of the sharp corners were chamfered 0.015 to 0.020 in. In the absence of data on geometry effects on impact strength, three groups (of 12 each) of test bars were prepared from the center portion of a 4-in. plate of SA-212B steel to determine the effects of chamfering of the corners. The three groups tested were:

(i) standard square cornered bars;

(ii) front chamfered bars, i.e., faces in contact with anvil;

(iii) back chamfered bars, i.e., face contacted by impact pendulum hammer.

All tests were conducted with a Schnadt impact test machine calibrated, at an earlier date, against Watertown Arsenal bar standards. The results revealed that neither the placement of the chamfer, front or back, nor the presence or absence of the chamfer was significant. The scatter in the data was normal for tests of this type.

The 4-in. EBWR plate material is being prepared into irradiation surveillance impact bars. Inasmuch as the EBWR SA-212B steel is a different heat of material than that utilized in these tests, the effects of chamfering will also be determined prior to the irradiation.

3. Plutonium Recycle Fuel

A total of 810 central-type Plutonium Recycle fuel rods have been delivered to ANL from Hanford for loading into fuel elements. An additional quantity of 525 rods are through final inspection at Hanford ready for shipment to ANL. The remaining 175 fuel rods are in process.

In addition to the regular $PuO_2$-$UO_2$ fuel for the central zone, Hanford is preparing material and loading the following 25 additional test fuel rods, which will be used for physics measurements on the core:

(a) five rods containing Al-3.35 w/o Pu alloy fuel jacketed in Zircaloy-2 tubes; the plutonium has an isotopic content of 8% $Pu^{240}$;

(b) five similar rods in which the plutonium has an isotopic content of 26% $Pu^{240}$;

(c) five rods containing natural $UO_2$ fuel;

(d) five rods containing regular Nupac and Vipac $UO_2$-1.5 w/o $PuO_2$, in which the plutonium has an isotopic content of 20% $Pu^{240}$;

(e) five similar rods in which the plutonium has an isotopic content of 26% $Pu^{240}$.

All of the components and hardware needed by United Nuclear Corporation for the enriched and natural fuel element loadings has been received. Approximately 90% of the Zircaloy-2 jacket tubing has been processed through the final inspection and accepted for loading. One lot of tubing, 253 m (1000 ft) long, was rejected as a result of an inner surface crack-type defect found in the 2% sampling for overcheck inspection by ANL. This lot of tubing was returned to the subcontractor for reinspection. Approximately 366 m (1200 ft) of tubing fabricated by the subcontractor for United Nuclear was diverted by the subcontractor for another order. Fabrication of additional tubing to replace this material is nearly completed.

4. Plutonium Recycle Control Rods

Eight new control rods and one spare central oscillator rod (see Progress Report for September 1964, ANL-6944, p. 73) have been fabricated.

5. Nondestructive Tests of Components

a. Inspection of Zircaloy-2 Tubing. Ultrasonic evaluation of both loaded and unloaded Plutonium Recycle tubing has continued. The detection of an inner-surface longitudinal defect in Lot 28 of unloaded tubing last month (see Progress Report for September 1964, ANL-6944, p. 74) resulted in a rejection of that lot and in a 50% sampling of Lot 29 instead of the normal (four tubes)/(lot) procedure. No defects, either transverse or longitudinal, were found in Lot 29.

6. Physics Calculations

The problem of preparation of cross sections for the SAMPLE code (see Progress Report for September 1964, ANL-6944, pp. 75-76) is being examined by the THERMOS code.[18] To increase the flexibility and speed of THERMOS, a CDC 3600 version has been compiled which allows 50 speed points and 25 materials in the problem and edit. The original IBM 704 version was limited to 30 speed points and 10 materials. In addition, the CDC 3600 version allows both speed integration limits to be specified, and prints out point fluxes as well as neutron densities. A 30-group problem which would require about 45 min of IBM 704 time has been run in less than 3 min on the CDC 3600. The short running time suggests the use of THERMOS as a subroutine of SAMPLE so that cross sections can be generated by the code as burnup proceeds.

THERMOS has been used to examine the influence of lattice composition on fuel-rod cross sections. Three problems were run. The first

[18] Honeck, H. C., A Thermalization Theory Code for Reactor Lattice Calculations, BNL-5826 (Sept 1961).

was a cell calculation for the standard EBWR $PuO_2$-$UO_2$ fuel pin having 0.12 w/o $Pu^{240}$ and 1.38 w/o $Pu^{239}$. The second was a cell calculation for a Pu-Al fuel pin having 3.35 w/o plutonium which was 71.9 w/o $Pu^{239}$, 26 w/o $Pu^{240}$, and 2.1 w/o $Pu^{241}$. The third problem involved the same Pu-Al fuel pin as in the second problem, but a thick outer region, based on the homogenized result of problem 1 was used. Thus the third problem most closely corresponds to the case of a single Pu-Al pin imbedded in the standard EBWR lattice. Table XV shows a comparison of some of the average cross sections from the three problems for the fuel pin region. It can be seen that the cross sections in the Pu-Al pin are considerably influenced by the surrounding lattice composition.

Table XV. Average Cross Sections (b) in the Fuel-pin Region (0-0.532 eV)

| Problem | $Pu^{239}$ | $Pu^{239}$ | $Pu^{240}$ | $Pu^{241}$ | $Pu^{241}$ | $Pu^{235}$ | $Pu^{235}$ |
|---|---|---|---|---|---|---|---|
| EBWR Cell | 1152.3 | 722.8 | 186.0 | 1075.0 | 734.6 | 332.8 | 281.7 |
| Pu-Al Cell | 1144.1 | 724.2 | 190.0 | 1123.6 | 766.1 | 358.7 | 303.9 |
| Pu-Al Pin in EBWR Lattice | 1169.6 | 733.4 | 186.7 | 1086.1 | 742.6 | 336.1 | 284.5 |

# III. ADVANCED SYSTEMS RESEARCH AND DEVELOPMENT

## A. Argonne Advanced Research Reactor (AARR)

### 1. Core Physics

a. The Reactivity Worth of Boric Acid in Solution in the Reference Graded-fuel System. The effective multiplication factor $k_{eff}$ has been calculated as a function of the concentration of $H_3B^{10}O_3$ in the reactor water. It was assumed that no water was displaced by the solution of fully enriched boric acid. The coefficient of reactivity is approximately 1% per gram of $H_3B^{10}O_3$ per gallon of water at zero concentration. This coefficient is essentially a function of the boric acid concentration only and would be little affected by the presence of lumped burnable poisons. However, its absolute magnitude decreases rapidly with increasing concentration because of the accompanying reduction in the low-energy neutron flux in the internal thermal column.

Approximately 7.5 g/gal are required for a reactivity reduction of 5% and approximately 22 g/gal for a reduction of 10%.

The calculation is for information purposes only at this time. The use of boric acid for reactivity control would be limited as an auxiliary shutdown mechanism under very special conditions.

Since the current design concept requires approximately 20,000 gal of water in the primary coolant system, a total of 120 g of natural $H_3BO_3$ per gallon or more than 5000 lb would be required for 10% control in a recirculating cooling system.

b. Heating Rates in the Beryllium Reflector. Calculations have been made for the case of a prompt shutdown to a decay power of 7% of the equilibrium power level to estimate the heating rates in the beryllium reflector. The total power in the reflector is then approximately 0.5 MWt per 100 MWt of equilibrium power level.

A comparison with the operating case has been provided by modifying results supplied by the United Nuclear Corporation. Approximately 2 MWt are developed in the reflector for 100 MWt of total reactor power during operation. This comparison indicates that the coolant flow rate is determined by the cooling requirements of the fuel zone during operation and by the requirements of the reflector after shutdown.

The peak heating rates are approximately 20 W/g of beryllium per 100 MWt during operation and approximately 5 W/g immediately after shutdown to very low power. These rates apply to the beryllium at the outer edge of the reactor core. The ratio of axial maximum to average reactor power has been assumed to be 1.3.

## 2. Critical Experiment

a. First Critical Loading. Initial criticality was obtained with the AARR critical experiment on October 7, 1964. Excess reactivity was 0.4% as measured by rising periods. The $U^{235}$ content of the core was 16 kg, loaded in the form of 315 uranium metal fuel strips, 93% enriched, weighing 54.7 g each, and 0.01 x 5.7 x 45.7 cm in dimensions.

The fuel loading had been chosen with consideration of a nominal goal of 15 kg $U^{235}$ plus sufficient additional fuel to obtain a value of $k_{ex}$ in the range from 0.1 to 0.5. A uniform distribution of 7 fuel strips in each of the 45 fuel assemblies offered the simplest and most appropriate loading pattern, since this provided a spacing of three dummy positions (loaded with stainless steel strips) between positions loaded with fuel. This pattern produced the 315-strip loading.

Core dimensions are as follows: The $H_2O$-filled axial flux trap is hexagonal in cross section, with 6-cm sides. The fuel region is also hexagonal in shape with approximately 6-cm sides on the inner boundary and approximately 25 cm on the periphery. The radial reflector is 90% beryllium and 10% Plexiglass by volume. There are six hafnium safety blades with 0.5-cm-thick aluminum followers separating the fuel region from the beryllium reflector, plus six hafnium control blades inside the fuel region.

The fuel region has a metal-to-water volume ratio of approximately unity, since the fuel plates and dummy plates are each 0.1-cm thick and the $H_2O$-filled coolant channels are of the same thickness.

Reproducibility of criticality was carefully checked. The major cause of variability was the source contribution from fission products, because of the related $(\gamma,n)$ reaction in the beryllium reflector. The critical position reproduced at all flux levels from $10^4$ to $10^8$ nv after decay reduced the fission product concentration to negligible amounts. Otherwise a stable critical position may be obtained by operating at a sufficiently high flux to result in an equilibrium level of fission products.

Reactivity drift because of air entrapment in the fuel assemblies was detectable but nearly negligible. The variability during steady operation is believed to be less than 0.05% per hour with no significant trend. Consecutive runs during a single day produced greater variations than steady operation for an equivalent time. The first runs on consecutive days generally reproduced within approximately 0.05%.

Calibration of control blades is not complete; however, the worth of an individual blade is roughly 2% in reactivity. Slightly more than one-third of a blade remained inserted at criticality and controlled the excess reactivity of 0.4%. The twelve safety and control blades yield four

subgroups of three blades each, having similar critical positions. The subgroups are related to adjacent fuel locations as well as to radial distance from the center of the reactor and orientation.

Measurements to determine the prompt-neutron lifetime (Rossi-alpha determination) are being analyzed. Preliminary measurements of the flux distribution have been made. Reactor instrumentation is also being tested and adjusted to avoid a tendency to scram at different levels for the various ranges.

Work still to be done with this core loading includes measurements of the reactivity worth of various core components (fuel, moderator, control materials, and poisons), completion of flux distribution measurements, and measurement of activation ratios of selected materials.

It is expected that enough fuel will be available to permit reloading with approximately 40 kg of enriched uranium in the core during December.

b. Analysis of the First Critical Loading. A 16-group diffusion-theory calculation of the initial system yields a value of 1.02 for the effective multiplication factor $k_{eff}$, using the approximation of a uniform homogeneous fuel zone. This system containing 16 kg of $U^{235}$ in 315 fuel foils is described in Section a above.

Sixteen-group DSN cell calculations have been performed to estimate the magnitude of the error in the calculated $k_{eff}$ arising from the approximation of homogeneity. The heterogeneity of the fuel loading, consisting of one enveloped foil per four plates, causes a reactivity loss of approximately 3%. This, with the assumption of a 5% void in the coolant in the fuel zone, yields a net calculated $k_{eff}$ value of 0.99.

3. Heat Transfer

a. Studies of Flow Instability. It was reported (see Progress Report for June 1964, ANL-6912, p. 87) that the STDY-3 Code[19] was being used to compare the ATR (Avanced Test Reactor) burnout heat transfer data[20] with the code calculations for flow-instability conditions. The comparison was made since the AARR could be limited by flow instability, and an estimate of the accuracy of the STDY-3 Code for predicting flow instability was needed. The results of the STDY-3 analysis as applied

---

[19] Pyle, R. S., STDY-3. A Program for the Thermal Analysis of a Pressurized Water Nuclear Reactor during Steady State Operation, WAPD-TM-213 (June 1960).

[20] Croft, M. W., Advanced Test Reactor Burnout Heat Transfer Tests, ATR-FE-102 (Jan 1964).

to corresponding ATR data are presented in Table XVI. The problem number in Table XVI includes the initial channel spacing (mils) as used in the ATR tests followed by the test number. The column of ATR Burnout Test Conditions includes a listing of the actual conditions in the test shortly before burnout was indicated in a test section with a 1.4 peak-to-average axial chopped cosine heat flux. The underlined quantities were the final values of the quantity being changed in the tests.

Table XVI. Comparison of ATR Burnout Test Data with STDY-3 Calculations

| | ATR Burnout Test Conditions | | | | | STDY-3 Calculated Limiting Conditions | | | | |
|---|---|---|---|---|---|---|---|---|---|---|
| Problem Number | Inlet Temp, °F | Exit Pressure, psia | Mass Velocity, lb/hr-ft$^2$ $10^6$ | Average Heat flux, B/hr-ft$^2$ $10^6$ | Type of Test[a] | Inlet Temp, °F | Exit Pressure, psia | Mass Velocity, lb/hr-ft$^2$ $10^6$ | Average Heat flux, B/hr-ft$^2$ $10^6$ | Deviation of STDY-3 with Data, Percent |
| 54-1 | 130 | 226 | 7.46 | 1.270 | P.I. | | | | 1.04 | 18 |
| 54-2 | 131 | 227 | 7.91 | 1.285 | P.I. | | | | 1.115 | 13 |
| 54-3 | 131 | 85 | 8.13 | 0.915 | P.D. | | 143 | | | 21.4[c] |
| 54-4 | 126 | 85 | 8.01 | 0.922 | P.D. | | 122 | | | 14.2[c] |
| 54-5 | 131 | 227 | 5.49 | 0.930 | F.D. | | | 6.6 | | 20.2 |
| 54-6 | 131 | 233 | 12.62 | 1.995 | P.I. | | | | 1.80 | 9.8 |
| 54-7 | 239 | 227 | 6.92 | 0.678 | T.I. | 210 | | | | 18.3[c] |
| 54-8 | 132 | 227 | 7.14 | 1.142 | P.I. | | | | 0.985 | 13.7 |
| 72-1 | 128 | 227 | 9.34 | 2.030 | P.I. | | | | 1.70 | 16.3 |
| 72-2 | 128 | 227 | 9.46 | 2.060 | P.I. | | | | 1.70 | 17.5 |
| 72-3 | 133 | 86 | 9.75 | 1.470 | P.D. | | 150 | | | 23.2[c] |
| 72-4 | 131 | 83.5 | 9.75 | 1.470 | P.D. | | 150 | | | 24.4[c] |
| 72-5 | 136 | 227 | 7.15 | 1.465 | F.D. | | | 8.8 | | 23 |
| 72-6 | 125 | 227 | 6.74 | 1.465 | F.D. | | | 8.25 | | 22.4 |
| 72-7 | 132 | 227 | 12.84 | 2.60 | P.I. | | | | 2.2[b] | 15.3 |
| 72-8 | 131.5 | 225 | 12.76 | 2.610 | P.I. | | | | 2.22[b] | 14.9 |
| 72-9 | 132 | 252 | 9.11 | 2.010 | P.I. | | | | 1.65 | 17.9 |
| 72-10 | 132.5 | 252 | 9.42 | 2.040 | P.I. | | | | 1.67 | 18.1 |
| 72-11 | 101 | 227 | 9.55 | 2.240 | P.I. | | | | 1.92 | 16.7 |
| 72-12 | 230 | 227 | 9.34 | 1.285 | T.I. | 175[b] | | | | 32.8[c] |
| 94-1 | 130 | 227 | 10.34 | 2.77 | P.I. | | | | 2.32 | 16.2 |
| 94-2 | 132 | 82 | 9.41 | 1.99 | P.D. | | 160 | | | 28.4[c] |
| 94-3 | 129 | 95 | 9.59 | 1.98 | P.D. | | 167 | | | 17.7[c] |
| 94-4 | 131 | 83 | 9.59 | 1.98 | P.D. | | 137 | | | 20.7[c] |
| 94-5 | 130 | 227 | 7.28 | 1.99 | F.D. | | | 7.90 | | 8.5 |
| 94-6 | 124 | 227 | 6.88 | 1.99 | F.D. | | | 7.55 | | 9.7 |
| 94-7 | 123 | 230 | 7.38 | 1.98 | F.D. | | | 7.80 | | 5.7 |
| 94-8 | 137 | 227 | 7.75 | 1.99 | F.D. | | | 8.10 | | 4.5 |
| 94-9 | 132 | 110 | 10.1 | 1.99 | P.D. | | 108 | | | -0.6[c] |
| 94-10 | 136 | 97 | 10.1 | 1.99 | P.D. | | 108 | | | 1.0[c] |

[a]These abbreviations indicate the way burnout conditions were achieved:

P.I. - Power Increase
P.D. - Pressure Decrease
F.D. - Flow Decrease
T.I. - Inlet Temperature Increase

[b]These values were obtained by extrapolation.

[c]The deviation is based on enthalpy change.

The value of the quantity undergoing the change as calculated by the application of the STDY-3 Code is listed under the same specific heading on the right hand side of Table XV. These values should be compared with the underlined quantities on the left.

The results show good agreement for all the tests, even though several parameters, including channel spacing, were varied. In general, for tests conducted with increasing power, the average heat flux value required for burnout was predicted at 10% to 18% below the actual average heat flux value at burnout. Test results with decreasing flow predicted a

flow rate about 4.5% to 23% above the actual flow rate values at burnout. Tests conducted by decreasing the pressure were conservatively estimated in every case except one (94-9), but the discrepancy for that case was only 0.6%. In tests in which the inlet temperature was allowed to rise, burnout was predicted conservatively, since failure was estimated at a lower inlet water temperature than was actually encountered in the tests.

Comparison of HFIR and ATR data with the STDY-3 Code has established confidence in the code. Speculation that the reason for good agreement between the code and the data may be related to critical flow phenomena has led to changes in the AARR heat transfer test instrumentation to detect critical flow phenomena. The study of the HFIR and ATR data will continue, with emphasis on the agreement between burnout correlations and the HFIR and ATR data.

b. Heat Transfer Studies. A steady-state analysis of the effect of a linear variation of the volumetric heat generation rate across the 0.030-in. fuel region in an AARR fuel plate has been performed. The ratio $q_2/q_1$ of the volumetric heat-generation rates on the high to the low side (front-to-back ratio) is believed to be as high as 1.15. The purpose of the study was: 1) to calculate the magnitude of the heat fluxes passing through the heat transfer surface on each side of the fuel plate, 2) to calculate the temperature distribution in the fuel plate for thermal-stress determinations, and 3) to estimate the effect of the front-to-back ratio on hot channel and hot spot conditions.

The analysis showed that $q_2/q_1$ varied from about 1.02 when equal film coefficients are used on each side of the fuel plate to 1.145 when local boiling occurs on each side and a clad thickness of 0.004 in. is assumed on the high heat generation side. As a result of this study, the local heat flux is being increased in the AARR steady-state and transient heat transfer analysis. The results are regarded as preliminary since a detailed check has not been made of the analysis and because the effect of time-dependent conditions on $q_2/q_1$ have not been determined.

A parametric, steady-state, heat transfer study of the AARR has been initiated in order to bring certain design aspects, such as axial heat flux distribution, channel spacing, and effect of operating conditions, into focus. The study, which is being written for computer solution, will be used to investigate the influence of channel spacing, velocity, pressure, inlet temperature, and core metal-to-water ratio.

4. Hydraulic Test Loop

A hydraulic test loop is being provided for experimental flow studies of AARR fuel sections. Verification of theoretical studies and influence of parameters which cannot be demonstrated theoretically will be supplied through the use of this loop.

Construction drawings have been completed and are under review for final approval.

A wide variation of flow between the temperature extremes of 100 to 500°F is possible.

These wide ranges in flow and temperature are made possible by combining two identical main pumps and three heat exchangers of different capacities. The range of variability is being verified by a computer study to insure that the complete temperature range is guaranteed by alternate heat exchanger arrangements over the full test-section range for water velocity.

The construction of the loop is being evaluated by PERT.[21]

## B. Magnetohydrodynamics (MHD)

### 1. MHD Power Generation - Jet Pump Studies

The necessary operating conditions of temperature and pressure required for a realistic MHD jet pump system have been evaluated. An evaluation made of some of the experimental findings in operation of a jet pump emphasized the necessity of a combiner design to maximize efficiency. A program was suggested to expedite the attainment of results pertinent to the MHD program.

A tentative design was prepared for the variable aspect ratio jet pump to allow determination of the optimum geometry for the device.

## C. Regenerative Emf Cells

### 1. Bimetallic Cells

a. Sodium-Bismuth Cells. The ternary eutectic NaI-NaCl-NaF, being studied for possible use as the electrolyte for the sodium-bismuth cell, is attractive for several reasons: 1) the melting point is lower than that of any of the sodium halide binaries, and 2) the presence of fluoride is expected to aid in the prevention of metal dispersions in the electrolyte. Preliminary values for the composition and melting point of the ternary eutectic were reported in the Progress Report for August 1964, ANL-6936, p. 76. Further study of the ternary system by thermal analysis has established the composition of the eutectic as 53.2 m/o NaI, 31.6 m/o NaCl, and 15.2 m/o NaF, and the melting point at 529.4°C.

---

[21] Pearlman, J., Engineering Program Planning and Control through the Use of PERT, IRE Trans. Engineering Management, EM-7 (Dec 1960), p. 125-134.

The solubility of $Na_3Bi$ in the ternary eutectic is being determined so that the possible sodium losses resulting from an irreversible sodium transfer from anode to cathode may be estimated. The results of a similar study of the solubility of sodium metal in the eutectic were reported previously (see Progress Report for August 1964, ANL-6936, p. 76). Preliminary experiments indicate a solubility of $Na_3Bi$ in the NaI-NaCl-NaF eutectic of the order of a few mole percent in the temperature range from 550 to 750°C. However, these results may be high because of sampling difficulties. An attempt will be made to obtain filtered samples of the melt.

b. Engineering Material Study. In connection with the sodium-bismuth cell studies, a series of dynamic corrosion tests is being conducted to determine the effect of liquid bismuth at various temperatures on low carbon steel. For the high-temperature tests, thermal convection loops of low carbon steel were externally coated with stainless steel for protection against air oxidation.

In initial tests conducted at a hot leg temperature of 800°C with a temperature difference of about 100°C, the circulation of the bismuth in the loop ceased after 24 hr of operation. Sectioning of the loop revealed that plugs had formed at the two corners which were boundaries between the hot and cold legs of the loop. The deposited material was identified as a residual mill scale left at the weld joints.

Recent work has been directed toward finding an effective descaling procedure. Acid-and-solvent methods and mechanical treatments did not remove the scale completely. Electrolytic descaling was considered inapplicable because of the geometry of the loop. Satisfactory descaling has been accomplished by circulating molten NaOH-1% NaH in the loop.

The loop, containing bismuth, is now in operation with the hot leg temperature at 850°C and a temperature difference of 400°C.

# IV. NUCLEAR SAFETY

## A. Thermal Reactor Safety Studies

### 1. Metal-Water Reactions

a. Laser-beam Heating Applications. Additional experiments were performed by the laser-beam heating method to determine the effect of pressure on the aluminum-water reaction. Previously (see Progress Report for August 1964, ANL-6936, p. 77), 2 x 2 x 0.025-mm foils were exposed to laser beams in two types of experiments: 1) submerged in room-temperature water with an overpressure of 1 atm of argon, and 2) submerged in water heated to 100°C with an overpressure of 1 atm of steam. The values for the extent of metal-water reaction in the first type experiment were about 15%. The values for the extent of metal-water reaction in heated water averaged about 42%, but varied widely because of variable break-up of the foils into small metal spheres. In the present studies, smaller aluminum foils (1 x 1 x 0.025 mm), submerged in water at 25°C and at 100°C (with an overpressure of 1 atm of steam), were exposed to laser beams of varied energies.

In each experiment, the foil was converted to a single sphere with a diameter of about 360 $\mu$. In room-temperature water, the values for the extent of metal-water reaction for 10 experiments varied from 6 to 11%, independent of laser beam energy in the range 10 to 48 J. In water heated to 100°C, the extent of reaction appeared to be dependent on the laser beam energy. In the energy range from 16 to 35 J, no significant metal-water reaction occurred (5 experiments); in the range from 45 to 49 J, 97 to 100% metal-water reaction occurred (3 experiments). In a single experiment at an energy of 44 J, the extent of metal-water reaction was 13%.

During each experiment, dark-field, high-speed motion pictures were taken of the heated aluminum specimen with no light sources except the laser beam and the luminous particles. Measurements were made of the time of persistence of light emission from the particle, i.e., the time required for the particle to cool to 1500°C. Reaction times of about 170 msec were observed for experiments in which 97 to 100% reaction occurred; reaction times of 10 to 16 msec were observed for experiments in which the extent of reaction was $<13\%$. The fact that a relatively long time is required for the reaction to go to completion suggests that the reaction rate in heated water is not necessarily faster, but merely longer. Apparently, once ignition occurs, the post-ignition consumption reaction is able to continue to completion only in heated water.

The ignition reaction observed in the laser experiments is markedly different from that observed in the levitation experiments with

larger pellets of aluminum (see Progress Report for May 1964, ANL-6904, pp. 102-104). In the levitation experiments the reaction product was very finely divided aluminum oxide resulting from vapor phase burning; in the laser experiments the product of a completely reacted particle appears to be a single transparent crystal of alumina.

b. Studies in TREAT of Uranium Dioxide Fuel. Experiments were continued in TREAT to investigate the safety problems associated with the behavior of unclad $UO_2$ fuel specimens under conditions simulating a power excursion. Results of similar studies with Zircaloy-2-clad oxide-core fuel pins were summarized in the June 1964 Progress Report (ANL-6912, pp. 90-94), and results with 304 stainless steel-clad oxide-core pins in the September 1964 Progress Report (ANL-6944, pp. 82-84). As in previous studies, the unclad $UO_2$ specimens were exposed to TREAT transients while submerged in water at room temperature. The objectives of the studies were to determine: 1) the extent of reaction of $UO_2$ with water at temperatures in the range from 2000 to 3300°C, and 2) the degree of fragmentation of $UO_2$, in the absence of metal cladding, as a function of the integrated power of the reactor excursion to which the $UO_2$ was subjected. The results with unclad $UO_2$ fuel specimens are summarized in Table XVII. Included are the results of one experiment, CEN-188, which was reported previously (see Progress Report for August 1964, ANL-6936, p. 77).

Table XVII. Results of TREAT Experiments with Unclad $UO_2$ Fuel Pellets

(Water initially at room temperature; initial helium overpressure of 20 psia; fuel pellets were pure $UO_2$, 11.2% enriched, 3/8 in. in dia, 1/2 in. long)

| Fission Energy Input (cal/g) | Adiabatic Core Temp (°C) | CEN Run No. | TREAT Characteristics | | Appearance of Specimen after Transient | Mean Particle Diameter (mils) | Hydrogen Generated (ml at STP/g $UO_2$) |
|---|---|---|---|---|---|---|---|
| | | | Period (msec) | Integrated Power (MW-sec) | | | |
| 223 | 2700 | 189 | 78 | 248 | Fragmented | 127 | 5.7 |
| 409 | 3300[a] | 188 | 74 | 327 | Particles | 14 | 17.7 |
| 775 | 3300[a] | 191 | 43 | 861 | Fine particles | 6 | 16.9 |

[a]Vaporization temperature

The extent of reaction of $UO_2$ with water was computed from the amount of hydrogen evolved, as determined mass spectrometrically. A transient which caused partial melting of $UO_2$ (at 2700°C) produced about 6 ml $H_2$ (STP)/g $UO_2$, corresponding to a calculated average final composition of $UO_{2.07}$. More energetic transients which brought $UO_2$ into the vaporization region (3300°C) resulted in the evolution of about 17 ml $H_2$ (STP)/g $UO_2$ (calculated average composition, $UO_{2.19}$). X-ray diffraction analyses indicating final compositions of $UO_{2.12}$ to $UO_{2.17}$ support the hypothesis that $UO_2$ is reacting with water.

The results of the experiments with unclad $UO_2$ have led to a re-examination of the data from previous studies with Zircaloy-2-clad and stainless steel-clad $UO_2$-core specimens. At this time, it appears likely

that some of the hydrogen released in these experiments resulted from $UO_2$-water reaction rather than metal-water reaction. The extent of reaction of metal-clad $UO_2$ with water is difficult to assess because of differences in exposure of the $UO_2$ to water in the two types of experiments. In experiments with unclad $UO_2$, the specimens were in direct contact with water for extended periods of time prior to the TREAT transient. Breakup probably occurred early in these experiments, and contact with water was continuous throughout the transient. In the experiments with metal-clad specimens, the oxide core contacted water only after the cladding material failed during the transient; in cases where the cladding remained intact, there was no contact of $UO_2$ with water.

For purposes of evaluating the previously reported data, the experiments are divided into four general types, and the probable effect of the $UO_2$-water reaction on each type is discussed:

(i) For experiments at low energies, in which the cladding material remained intact, the $UO_2$-water reaction could not occur.

(ii) For experiments in which metal-clad $UO_2$-core specimens were heated into the melting region of $UO_2$ (2700°C), it appears that the $UO_2$-water reaction did not significantly influence metal-water reaction data. (Under these conditions, contact of $UO_2$ with water occurred only after cladding failure, and core breakup was incomplete.) This conclusion is supported by results of TREAT experiments with metal-clad, mixed oxide-core fuel pins heated to 2700°C. The mixed oxide core had the composition: 81.5 w/o $ZrO_2$, 9.1 w/o CaO, 8.7 w/o $U_3O_8$, 0.7 w/o $Al_2O_3$, and all of these materials are considered to be inert to steam. With metal-clad, mixed oxide-core pins, the extent of hydrogen evolution was comparable with that of metal-clad, $UO_2$-core specimens, indicating that little or no hydrogen was generated by reaction of $UO_2$ with water under these conditions.

(iii) For experiments in which metal-clad $UO_2$-core specimens were heated into the region of incipient $UO_2$ vaporization (about 400 cal/g $UO_2$), it appears that some $UO_2$-water reaction occurred. For stainless steel-clad specimens, the $UO_2$-water reaction may have been responsible for a maximum of about one-half of the amount of hydrogen evolved. For Zircaloy-2-clad specimens, the $UO_2$-water reaction was probably less than one-fourth of the total reaction.

(iv) For experiments in which the metal-clad $UO_2$-core fuel pins were heated to the region of extensive vaporization of $UO_2$ (700 cal/g $UO_2$), the $UO_2$-water reaction probably accounted for less than one-fourth of the hydrogen evolved from stainless steel-clad specimens and less than one-eighth from Zircaloy-2-clad specimens.

Although the $UO_2$-water reaction can, under some conditions, contribute to the amount of hydrogen generated in a reactor incident, it will not contribute significantly to the heat generated in the incident.

2. Metal Oxidation-Ignition Studies

a. Transient Boiling in Liquid Sodium. A study of transient heat transfer in liquid sodium under conditions relating to reactor safety problems for a fast breeder reactor is being undertaken. In order to clarify some of the problems involved, initial experiments will be conducted with water rather than sodium. Some experiments have been carried out to optimize conditions for the heating of an enclosed surface of copper by molten iron (formed from the ignition of a stoichiometric aluminum-iron oxide thermite). This method of heating was chosen for two reasons: (i) in water, surfaces with a high heat capacity can be heated without employing large electrical equipment, and (ii) in liquid sodium, surfaces can be heated without electrical shorting resulting from electrical conduction through sodium.

The experimental apparatus consisted of a two-chambered cell connected by a short copper tube. Ignition under vacuum of the aluminum-thermite mixture pressurized the upper chamber. A vacuum line in the lower chamber provided an exit for off-gases, and the pressure drop caused a flow of molten iron through the copper tube and into the lower chamber.

Heating rates of 2000 to 3000°C/sec were achieved for the copper tube, and the temperature rise continued uniformly through the melting point of the copper tube (1083°C). In previous experiments, in which the molten iron flowed through an orifice onto a copper plate in the lower chamber, the same heating rates were observed, but the maximum temperature reached was about 300°C.

## B. Fast Reactor Safety Studies

1. Systematics of Pressure Pulse Phenomena

Transient pressures and coolant flow are of interest to fast reactor safety analyses for two principal reasons: (a) they may affect fuel failure and movement during a meltdown accident, and (b) variations in coolant flow may produce significant increases in reactivity.

Experimental data are lacking on transient pressure phenomena for vaporizing liquid metal coolants in heated channels. Accordingly, a theoretical investigation of the effects of physical parameters on transient pressures and coolant expulsion, with detailed heat transfer phenomena phased into the study, is being undertaken.

As a test of the applicability of the basic theoretical model to an experimental situation, the approximate analytical description used for correlating computer solutions of pressure pulse problems (see Progress Report for December 1963, ANL-6810, pp. 53-4) has been used to correlate data from an extensive series of transient experiments in water using the

KEWB reactor.[22] Briefly, the experimental arrangement was as follows: the irradiation capsule contained an aluminum-clad U-10 w/o Mo disc immersed in water. Thermocouples were welded to the cladding surface. A piston in contact with the water was free to move as the system dilated due to thermal expansion and void growth in the coolant. Piston position was measured by means of a linear motion transducer. Piston mass could be varied to study the effects of different inertial loadings upon transient pressure or void generation. Pressure in the system was measured by use of an unbonded strain gage transducer. Data studied for correlation were the maximum pressure rise of the first pressure pulse* as a function of mass loading, reactor period, and the dependence upon mass loading of a maximum space-averaged velocity of water from the disc at the conclusion of the first pressure pulse.

The basic equation used was

$$\Delta P = K_1(q_1^2 Z/Ac^2 m_0)^{1/3},$$

where $\Delta P$ is pressure rise, $K_1$ is a numerical factor, $q_1$ is power (assumed to be constant for this version of the model), Z is the distance of expulsion, A is the effective area upon which $\Delta P$ is acting, $m_0$ is the mass loading, and c relates power to rate of pressure rise:

$$c = (m_H/m_0)\, c_H,$$

where $m_H$ is the heated mass whose temperature rise defines pressure, and $c_H$ is the ratio of specific heat of the $m_H$ material to the coolant saturation pressure rise per unit temperature rise of $m_H$.

For the series of experiments, an approximate scaling relationship was dervied consisting of

$$\Delta P = K_2(q_1^2 m_0)^{1/3}.$$

From the KEWB data, the ratio of pressure for the 30-g loading to that for 225-g loading in the middle of the range of reactor periods was approximately 2.17. The approximate scaling relationship predicts $7.5^{1/3} = 1.96$.

*Other pressure pulses occur at later times. Some have been identified with coolant rebounding against the fuel disc, others may be instrumental, or associated with details of experimental design.

[22] Wentz, L. B., Zivl, S. M., and Langmuir, D. B., Quarterly Progress Report for Period Ending June 30, 1964, Kinetic Studies of Heterogeneous Water Reactors, STL-372-6 (July 1964).

Since $q_1$ enters only to the 2/3 power, and heating (or pressure rise) is insignificant during the strictly exponential portion of the reactor power burst, the period dependence is estimated by replacing the actual power burst by one of constant power at a constant fraction of peak power. For the range of interest, peak reactor power varies approximately as the -1.63 power of the reactor period.[23] The curve fit to the KEWB data yielded a ratio of 13.8 for $\Delta P$ at a period of 1 msec to that at 10 msec. The approximate scaling relationship predicts a ratio of $10^{1.09} = 12.3$.

The values reported for maximum space-averaged coolant velocities (for the entire range of periods investigated) were 5.11 ± 1.13 cm/sec for the 30-g loading, 3.72 ± 2.38 cm/sec for the 124-g loading, and 2.75 ± 1.18 cm/sec for the 225-g loading. Experimental ratios of velocity were thus 1.86 for velocity at the 30-g loading to that for 225 g, and 1.35 for that at the 124-g loading to that for 225 g. The model predicts velocity proportional to $m^{-1/3}$, from which ratios of 1.96 and 1.61, respectively, can be computed.

2. Critical Constants of $UO_2$

In order to calculate the course of maximum accidents in which core material reaches excessively high temperatures, it is necessary to have equation of state data for high temperatures. The high-temperature properties of $UO_2$ have been evaluated to provide an estimate of the critical constants by means of a method described by Grosse.[24] The underlying assumption of this method is the applicability, to $UO_2$, of the "Rectlinear Diameter Law" of Cailletet and Mathias, which states that the average density (one-half the sum of the densities) of a saturated liquid and its saturated vapor decreases linearly with temperature, until the densities are equal at the critical point.

The density of solid $UO_2$, its melting point of 2800°C, and the density of molten $UO_2$ to 3100°C were taken from data reported by Christensen.[25] Density of the saturated vapor was calculated from measurements by

---

[23] Dunenfeld, M. S., and Stitt, R. K., Summary Review of the Kinetics Experiments on Water Boilers, NAA-SR-7087 (Feb 1963).

[24] Grosse, A. V., The Liquid Range of Metals and Some of Their Physical Properties at High Temperatures, TID Report NP-10795 (1960); The Temperature Range of Liquid Metals and an Estimate of Their Critical Constants, J. Inorg. and Nucl. Chem. 22, 23 (1961).

[25] Christensen, Thermal Expansion and Change in Volume on Melting for Uranium Dioxide, HW-75148 (1962); Quarterly Progress Report, HW-75914, 4.4 (1962).

Ackermann, Gilles, and Thorn.[26] The vapor was taken to have a molecular weight of 270 g/mole, on the basis of a report by Berkowitz, Chupka, and Inghram[27] that they were unable to find any dimer or higher polymer in $UO_2$ vapor at a concentration higher than one part in $10^7$. The vapor pressure extrapolation used was one derived from theoretical considerations and fitted to the lower temperature region of the experimental curve.[26]

By graphical means, the critical point was found to be 8970°K, with a critical volume of 180 $cm^3$/mole, and critical pressure of 1120 atm. The critical compressibility corresponding to these values was 0.27. Recent estimates of critical constants for $UO_2$ have been reported by Meyer and Wolfe,[28] based on a somewhat different vapor pressure relationship, a generalized correlation between entropy of vaporization and the ratio of temperature to critical temperature, and a generalized correlation between density at melting and critical density. A comparison of the two sets of constants is given in Table XVIII.

Table XVIII. Comparison of Critical Constant Estimates

| | Critical Temperature, °K | Critical Pressure, atm | Critical Volume, $cm^3$/mole |
|---|---|---|---|
| Meyer and Wolfe[28] | 8970 | 1120 | 180 |
| This work | 7300 | 1915 | 85 |

## C. TREAT

### 1. Large TREAT Loop

Design of the test section is reaching the final phase prior to submittal for bid on construction. The area which requires considerable design detail is concerned with the pressure transducers. A modification has been introduced in the form of a protection sleeve over the transducer housing to protect this region when the test section is handled in out-of-pile areas.

---

[26] Ackermann, R. J., Gilles, P. W., and Thorn, R. J., High Temperature Thermodynamic Properties of Uranium Dioxide, J. Chem. Phys. 25, 6, 1089 (1956).

[27] Berkowitz, J., Chupka, W. A., and Inghram, M. G., in Physics Division Summary Report, ANL-5754, p. 65 (1957).

[28] Meyer, R. A., and Wolfe, B. E., High Temperature Equations of State of Uranium Dioxide, Trans. Amer. Nuc. Soc. 7, 1, 111 (1964).

The sodium leak detectors have been designed and a cost estimate for the circuitry is being prepared.

The lifting mechanism on the cask has been tested satisfactorily with a load of 460 lb. Conditions similar to the unloading or loading of a test section were simulated.

Radiography has disclosed that the welds on all of the bellows delivered were faulty. These units are presently being corrected either by the ANL Central Shops or the manufacturer.

Selection of components for the gas system has been completed and a bill of material is being prepared. A number of the components, including the pressure regulator, pressure switch, and quick-disconnect coupling, have been ordered. These are all off-the-shelf items and are rated at 150 psi (minimum), which is twice the 75-psi nominal pressure rating of the replacement rupture discs in the sodium and gas systems. Gate-type, bellows-sealed, high-vacuum valves have been specified as shut-off valves in the inlet and outlet lines to the liquid-nitrogen-cooled charcoal cold trap and as control valves in the gas-system manifold. These valves, although designed primarily for high-vacuum service, are rated at 150 psi at room temperature.

# V. PUBLICATIONS

## Papers

THERMODYNAMICS OF BINARY ALLOYS. I. THE LITHIUM-BISMUTH SYSTEM
M. S. Foster, S. E. Wood, and C. E. Crouthamel
Inorg. Chem. 3, 1428-1431 (October 1964)

A FLUID-BED PROCESS FOR THE DIRECT CONVERSION OF URANIUM HEXAFLUORIDE TO URANIUM DIOXIDE
I. E. Knudsen, H. E. Hootman, and N. M. Levitz
Nucl. Sci. Eng. 20, 259-265 (November 1964)

FLUORINE BOMB CALORIMETRY. IX. THE HEAT OF FORMATION OF MAGNESIUM DIFLUORIDE
Edgars Rudzitis, H. M. Feder, and W. N. Hubbard
J. Phys. Chem. 68, 2978-2981 (October 1964)

CORROSION AND MATERIALS OF CONSTRUCTION IN CHEMICAL PROCESSING OF REACTOR FUELS
W. B. Seefeldt
Progress in Nuclear Energy, Series IV, Vol. V, C. M. Nicholls, Ed., Permagon Press, New York (1963), pp. 409-446

THERMOELECTRIC PROPERTIES OF URANIUM MONOSULFIDE, THORIUM MONOSULFIDE, AND US-ThS SOLID SOLUTIONS
Marvin Tetenbaum
J. Appl. Phys. 35, 2468-2472 (August 1964)

$CeCd_6$-TYPE RARE EARTH-CADMIUM ALLOYS
Irving Johnson, Robert Schablaske, Benjamin Tani, and Karl Anderson
Trans. Met. Soc. AIME 230, 1485-1486 (October 1964)

RECENT ADVANCES IN NONDESTRUCTIVE EXAMINATION OF IRRADIATED FUEL CAPSULES
W. N. Beck
Symposium on Problems in Irradiation Capsule Experiments Held at Germantown, Maryland, October 8-10, 1963. TID-7697, pp. 2.22.1-2.22.11 (March 1964).

RECENT OPERATING EXPERIENCES WITH CAPSULES USING VARIABLE GAS MIXTURES FOR TEMPERATURE CONTROL
C. C. Crothers
Symposium on Problems in Irradiation Capsule Experiments Held at Germantown, Maryland, October 8-10, 1963. TID-7697, pp. 4.11.1-4.11.10 (March 1964).

CORROSION OF STEELS AND NICKEL ALLOYS IN SUPERHEATED STEAM
W. E. Ruther and S. Greenberg
J. Electrochem. Soc. 111, 1116-1121 (October 1964)

CUTTING WHEEL RESIDUES OF PLUTONIUM WASTE CAUSES EXPLOSION
D. R. McFee and H. V. Rhude, Jr.
Health Phys. 10, 757-760 (October 1964)

COMMENTS ON TWO-PHASE MEASUREMENTS USING A RESISTIVE PROBE
T. T. Anderson
A.I.Ch.E. Journal 10, 776 (September 1964) Letter

$Be^{9}(d,n)B^{10}$ REACTION
S. G. Buccino and A. B. Smith
Bull. Am. Phys. Soc. 9, 628 (October 1964) Abstract

STUDY OF (d,n) REACTIONS ON $Fe^{54}$ AND $Ni^{58}$
D. S. Gemmell, L. L. Lee, Jr., J. P. Schiffer, and A. B. Smith
Bull. Am. Phys. Soc. 9, 676 (October 1964) Abstract

A SIMPLE COMPACT ROD DRIVE USING A STEPPING MOTOR
E. F. Groh and C. E. Cohn
Nucl. Sci. Eng. 20, 290-297 (November 1964)

ELECTRONIC DESIGN OF AN ABSOLUTE COUNTING SYSTEM FOR $Mn^{56}$
K. G. A. Porges, Alexander DeVolpi, and R. N. Larsen
Nucl. Inst. and Methods 29, 157-168 (September 1964)

FAST-NEUTRON TOTAL CROSS SECTIONS WITH AN AUTOMATED FACILITY
J. F. Whalen, R. R. Rogue, and A. B. Smith
Bull. Am. Phys. Soc. 9, 651 (October 1964) Abstract

## ANL Reports

ANL-6806 DEVELOPMENT OF TECHNIQUES FOR FABRICATION OF SMALL-DIAMETER THIN-WALL TUNGSTEN TUBING. Interim Progress Report Covering the Period from July 1, 1963 through December 31, 1963
W. R. Burt, Jr., H. C. Katiyar, and R. M. Mayfield

ANL-6838 DOPPLER EFFECT MEASUREMENTS, SODIUM VOID COEFFICIENTS, AND CRITICAL STUDIES OF A 5,000-LITER FAST POWER BREEDER REACTOR BY THE TWO-ZONE METHOD (ZPR-III Assembly 43)
J. M. Gasidlo, J. K. Long, and W. P. Keeney

ANL-6846 A SUMMARY REPORT ON NEUTRON RADIOGRAPHY
Harold Berger

ANL-6857 VAPOR CYCLE COOLANT REQUIREMENTS FOR NUCLEAR SPACE POWER PLANTS
Marion J. Janicke

ANL-6870 PERFORMANCE CHARACTERISTICS OF A LIQUID METAL MHD GENERATOR
Michael Petrick and Kung-You Lee

ANL-6921 DESIGN AND PERFORMANCE CHARACTERISTICS OF EBR-II CONTROL ROD DRIVE MECHANISMS
E. Hutter and G. Giorgis